# Lipid droplets regulate actin remodeling via prostaglandin signaling during Drosophila oogenesis

Michelle S. Giedt[*, 1], Jonathon M. Thomalla[*, 2], Matthew R. Johnson[2], Zon Weng Lai[3], Tina L. Tootle[#, 1], and Michael A. Welte[#, 2]

[*]equal contribution

[#]co-senior and co-corresponding authors, tina-tootle@uiowa.edu and michael.welte@rochester.edu

[1] Anatomy and Cell Biology, University of Iowa Carver College of Medicine, Iowa City, IA

[2] Department of Biology, University of Rochester, Rochester, NY

[3] Harvard T.H. Chan Advanced Multi-omics Platform, Harvard T.H. Chan School of Public Health, Boston, MA

Short Title: Lipid droplets regulate actin remodeling via prostaglandin signaling

Key words: actin cytoskeleton, lipid droplets, prostaglandin signaling, Drosophila, oogenesis

**Abstract**

To ensure fertility, it is paramount to understand the factors controlling oocyte quality. One incompletely characterized factor contributing to oocyte quality is lipids. In somatic cells, a key regulator of lipid metabolism is lipid droplets (LDs), the sites of intracellular fat storage. Yet the role of LDs in fertility is poorly understood. Here we use *Drosophila* oogenesis as a model for uncovering if and how LDs promote egg development. LD accumulation in nurse cells coincides with dynamic actin remodeling necessary for late-stage follicle morphogenesis and fertility. Loss of major LD proteins, including PLIN2, Jabba, and ATGL, disrupts both actin bundle formation and cortical actin integrity; this unusual phenotype is also seen when Pxt, the enzyme responsible for prostaglandin (PG) synthesis, is missing. Further, both pharmacologic and genetic loss of PG synthesis or loss of PLIN2 or Jabba impairs intracellular LD dispersal. These similar phenotypes suggest that PGs and LD proteins act in the same pathway. Dominant genetic interaction studies indicate that there are three actin regulatory pathways: PLIN2 regulates actin remodeling independent of PG signaling, whereas Jabba and ATGL act in two separate PG-dependent pathways to regulate actin remodeling. We find that neither Jabba nor ATGL modulate the levels of Pxt or its localization to the endoplasmic reticulum. As ATGL is a triglyceride lipase, we hypothesize that it may release arachidonic acid (AA), the substrate for PG production, from triglycerides stored in LDs. Indeed, lipidomic analysis reveals the presence of AA-containing triglycerides in ovaries. In addition, exogenous AA is toxic and reduction of ATGL ameliorates toxicity; these observations suggest that ATGL indeed generates free AA. Our studies provide the first evidence that LDs and their associated proteins regulate PG signaling to control actin remodeling. In particular, we propose that ATGL releases AA from LDs to drive PG synthesis necessary for follicle development. We speculate that the same pathways are conserved across organisms to regulate oocyte development and promote fertility.

## Introduction

Rates of infertility have increased globally between 1990 and 2017 [1], and combatting this increase is considered a public health priority [2]. Fertility requires the production of high-quality oocytes. It is becoming increasingly clear that among the key factors ensuring oocyte quality are the amount and types of lipids present during oogenesis [3, 4]. In mammalian follicles, for example, fatty acids (FAs) likely contribute a critical source of energy since inhibitors of FA oxidation impair oocyte maturation [5, 6]. In addition, lipid signaling molecules – from steroid hormones to eicosanoids – control diverse aspects of oocyte development and fertility [7]. Indeed, prostaglandins (PGs), a class of eicosanoids, regulate oocyte development, ovulation, fertilization, implantation, maintenance of pregnancy, and childbirth [8, 9]. Thus, control of lipid metabolism is likely central for oocyte development and fertility, yet only few of the underlying mechanisms have been elucidated.

Key regulatory steps in lipid metabolism are mediated by lipid droplets (LDs), the cellular organelles dedicated to the storage of neutral lipids [10]. For example, LDs store excess amounts of cholesterol and related sterols as sterol esters, and safely sequester toxic FAs in the form of triglycerides. Once such FAs are released by LD-bound lipases, they can then be shuttled to mitochondria for oxidative breakdown, used to generate various membrane precursors, or turned into signaling molecules [11]. Since both triglycerides and LDs are abundant in oocytes, LDs might perform similar regulatory roles during follicle development. Indeed, LD accumulation, composition, and localization are dynamic during oocyte maturation across organisms [3, 4, 12], and, in the context of obesity, oocytes display changes in LDs that are associated with infertility [13-15]. However, the functions of LDs in oogenesis remain largely undefined.

*Drosophila* oogenesis is a promising model for uncovering the roles of LDs in follicle development. Adult female flies have two ovaries, each comprised of ~15 ovarioles or chains of sequentially maturing follicles, also called egg chambers. Each follicle is made up of ~1000

epithelial cells termed follicle cells as well as 16 germline cells (15 nurse cells and one oocyte). Follicles develop over the course of ~10 days through 14 stages. Over just a few hours in mid-oogenesis, tens of thousands of LDs are newly formed and disperse throughout the nurse cells. Strikingly, failure to form LDs, due to loss of diacylglycerol O-acyl transferase 1 (DGAT1, *Drosophila* Midway), results in developmentally arrested follicles and an aberrant actin cytoskeleton [16]. These observations suggest that LDs may have a role in follicle development and directly or indirectly regulate actin.

Both LDs and the actin cytoskeleton undergo dramatic changes in mid-oogenesis (see Fig 1A-1I) [17]. Prior to Stage 8, only a few scattered LDs are found throughout the follicle, and the only obvious actin cytoskeletal structure in the nurse cells is F-actin (filamentous actin) at the cell cortex. In Stage 9, LD biogenesis is massively upregulated in the nurse cells, so that by Stage 10B, the nurse cell cytoplasm is full of uniformly sized LDs (~0.5 μm in diameter) [16, 18]. During Stage 10B, the actin cytoskeleton is also massively remodeled, parallel actin bundles extend from the plasma membrane to the nuclei to form a cage, and the cortical actin substantially thickens. Both of these actin structures are required during Stage 11 for the process of nurse cell dumping, during which the nurse cells squeeze their cytoplasmic contents into the oocyte via ring canals, intercellular bridges between the germline cells [19-21]; cortical actin provides the contractile force, and actin bundles prevent the nuclei from being pushed into and plugging the ring canals. Dumping also transfers the LDs from nurse cells to the oocyte. These LDs then provide the future embryo with stores of energy and specific proteins needed for embryo development; indeed, embryos with reduced numbers of LDs have reduced hatching probability [18, 22]. From Stage 12 onwards, oocyte LD content remains stable [23], and nurse cells undergo cell death [24].

The actin remodeling events during mid-oogenesis are regulated by lipid signaling via PGs. PGs are derived from arachidonic acid (AA) [8], a poly-unsaturated FA, which is converted first into $PGH_2$ and then into several types of bioactive PGs. These enzymatic steps are

mediated by cyclooxygenase (COX) enzymes and specific PG synthases, respectively. *Drosophila* has a single COX-like enzyme called Pxt, and its absence during oogenesis results in severe disruption in actin bundle formation, breakdown of cortical actin, and failure of nurse cell contraction, ultimately leading to severe defects in follicle development and female sterility [25, 26]. How PG production is temporally and spatially regulated during *Drosophila* oogenesis is unknown, but in many cells the release of AA from cellular lipids is the rate limiting step [8, 27]. Those precursor lipids are generally thought to be phospholipids in cellular membranes, but in mammalian immune cells neutral lipids are an essential source of AA for PG synthesis [28, 29].

Given the significance of lipid signals in actin remodeling during *Drosophila* oogenesis and the central role of LDs in lipid metabolism in other cells, we sought to determine if LDs contribute to *Drosophila* follicle development. We find that loss of each of three lipid droplet proteins – LSD2/PLIN2 (subsequently referred to as PLIN2), Jabba, or ATGL (*Drosophila* Brummer) – results in *pxt*-like actin remodeling defects during Stage 10B. Conversely, loss of Pxt or pharmacological inhibition of PG synthesis results in aberrant LD clustering during Stage 10B; LD clustering also occurs in *PLIN2* and *Jabba* mutants. The similar phenotypes led us to ask if LD proteins and Pxt function in the same pathway to regulate actin remodeling during *Drosophila* oogenesis. Dominant genetic interaction studies support that there are three actin regulatory pathways: PLIN2 regulates actin remodeling independent of PG signaling, whereas Jabba and ATGL act in two separate PG-dependent pathways. The connection between LD proteins and PG signaling is not due to Pxt localizing to LDs. Instead, our data support the model that ATGL is required to release AA to provide the substrate for PG production. Ultimately, these PGs control actin remodeling and thereby follicle development. Our studies thus have uncovered a role for LDs in regulating a critical developmental transition during oogenesis.

## Results

*DGAT1 functions suggest a link between LDs and actin organization during oogenesis*

During *Drosophila* oogenesis, both actin and LDs undergo dramatic changes over the course of just a few hours (Fig. 1A-I). F-actin present at the cortex of the nurse cells throughout early stages (Fig. 1 F, G) is dramatically strengthened during Stage 10B (Fig 1H); in addition, actin bundles form that hold the nurse cell nuclei in place (Fig. 1H-1J). LDs start to accumulate in Stage 9, fill the nurse cells by Stage 10B, and are transferred to the oocyte by Stage 12 (Fig. 1B-D).

**Fig 1. LD accumulation and actin cytoskeletal remodeling occur during mid-oogenesis. (A-D)** Single confocal slices of wild-type follicles of the indicated stages (E) stained for LDs (Nile red) in white and DNA (Hoechst) in cyan. **(E)** Schematic depicting the progression of LD accumulation and actin remodeling during oogenesis. **(F-I)** Single confocal slices of wild-type follicles of the indicated stages (E) stained for F-Actin (phalloidin) in white and DNA (Hoechst) in cyan. Note that all images and diagram in A-I are on top of a black box. **(J)** Single confocal slice of a Stage 10B nurse cell stained for F-Actin (phalloidin) in white and DNA (Hoechst) in cyan; actin bundles are indicated by the green arrowhead and cortical actin is indicated by the magenta arrowhead. Scale bars=50μm (A-I) or 10μm (J). **(K)** Thin layer chromatograph of whole-lipid extracts from late-stage follicles. **(L)** Quantitation of (K), in which the ratio of TAG to cholesterol intensity is plotted; error bars, SD. Few LDs are present in the nurse cells during early oogenesis, but begin to accumulate by Stage 9 (B). By Stage 10B, LDs are present in large numbers and evenly distributed throughout the nurse cell cytoplasm (C). The LDs are dumped into the oocyte during Stage 11 and are highly abundant in the ooplasm by Stage 12 (D). This temporal accumulation is also reflected by the increase in triglycerides and sterol esters (K, L), neutral lipids stored in LDs. Massive remodeling of the nurse cell actin cytoskeleton begins when LDs are highly abundant. During Stage 10B (H), cortical actin thickens (magenta arrowhead, J) and parallel actin bundles extend from the nurse cell membrane to the nucleus (green arrowhead, J). During Stage 11, the actin bundles hold the nurse cell nuclei in place while the cortical actin contracts, squeezing the nurse cell cytoplasm into the oocyte in a process termed nurse cell dumping. This process ultimately results in the nurse cells shrinking and the oocyte expanding (I). Cortical actin surrounds each nurse cell throughout oogenesis(F-I); during Stage 10B, actin bundles form (J) and support nurse cell dumping.

The main neutral lipids stored in LDs are triglycerides and/or sterol esters [10]. Using thin-layer chromatography on tissue extracts, we find that developing follicles accumulate both classes of neutral lipids, with a large predominance of triglycerides (Fig 1K-1L). The final step of triglyceride synthesis is mediated by DGATs, which catalyze the attachment of a third FA to

diacylglycerol. Like most animals, *Drosophila* encodes two such enzymes, DGAT1/Midway, and DGAT2 [30]. Genome-wide expression data indicate that DGAT1 predominates in most tissues, including in ovaries [31]. In *DGAT1* loss-of-function mutants, LDs fail to accumulate and follicles die by Stage 8/9 of oogenesis [16]. We confirmed that LDs in nurse cells and oocytes (though not follicle cells) are essentially abolished in follicles from *DGAT1* mutant animals and that mutant ovaries have massively reduced amounts of neutral lipids (Fig 2A-2D).

**Fig 2. DGAT1 is required for LD formation and actin cytoskeletal remodeling. (A-B)** Single confocal slices of Stage 9 follicles stained for LDs (Nile red) in white and DNA (Hoechst) in cyan. **(A)** WT, wild-type (Oregon R). **(B)** *DGAT1-/-* (*DGAT1*$^{QX25}$/*DGAT1*$^{RF48}$). **(C)** Thin layer chromatograph of whole-lipid extracts from whole ovary lysates of the indicated genotypes. **(D)** Graph of neutral lipid levels in the ovaries of the indicated genotypes normalized to cholesterol; TAG=triacylglycerol and SE=sterol esters. Error bars, SD. ***p=0.0028, *p=0.0234*, Sidák's multiple comparisons test. **(E-G)** Single confocal slices of *DGAT1 -/-* follicles of the indicated stages stained for F-Actin (phalloidin) in white and DNA (Hoechst) in cyan. **(H-I)** Single confocal slices of germline RNAi knockdown of *DGAT1* (mat-alpha4-Gal4-VP16>*DGAT1* RNAi (TRiP.HMC06242)); same follicle, different focal plane, stained for F-Actin (H, phalloidin) or LDs (I, Nile red) in white and DNA (Hoechst) in cyan. Magenta arrowheads indicate cortical actin defects, and green arrowheads indicate actin bundle defects. Scale bars=50μm. Loss of DGAT1 results in decreased lipid accumulation in the ovaries (C-D) and a loss of LDs in nurse cells and oocyte (B compared to A). Loss of DGAT1 also results in defects within the actin cytoskeleton. In early and mid-oogenesis, cortical actin breaks down (magenta arrowheads) and actin bundles form prematurely (green arrowheads) (E-F). Ultimately, *DGAT1-/-* follicles die at mid-oogenesis (G). Germline RNAi knockdown of *DGAT1* exhibits both actin remodeling defects (H) and decreased LD accumulation (I).

It had previously been reported that DGAT1 mutant follicles form premature actin bundles [16]. We also observe such bundles in the *DGAT1* mutant, *e.g.*, in Stage 9 (Fig 2F, green arrowhead); in the wild type, they only appear by Stage 10B (Fig 1J). In addition, we also detect defects in cortical actin, such as absence from the nurse cell periphery or aggregates around ring canals between neighboring nuclei (Fig 2E-2F, magenta arrowhead). DGAT1 is expressed throughout the adult fly, particularly in the fat body, the fly's adipose tissue [31]. Yet knocking down DGAT1 expression specifically in the germline via RNAi was sufficient to severely restrict LD accumulation and result in abnormal bundle formation and fractured cortical

actin (Fig 2H-2I). These tissue-autonomous actin defects suggest that DGAT1 and consequently LDs in nurse cells are linked to actin remodeling.

Because lack of DGAT1 results in follicle death, it is conceivable that the actin defects are a secondary consequence of the dramatic breakdown of cellular structures. This possibility seems unlikely since germline specific knockdown of DGAT1 allowed follicles to progress further, yet still resulted in fewer LDs and in actin defects (Fig 2H-2I). Nevertheless, to circumvent this problem, we next sought to disrupt specific LD functions without preventing LD accumulation or causing follicle death.

*Major lipid droplet proteins are required for actin remodeling in nurse cells*

In early Drosophila embryos, the two most abundant LD-specific proteins are PLIN2 and Jabba [32, 33]. PLIN2 is one of the two members of the perilipin family of LD proteins in flies and regulates lipid metabolism by protecting LDs from the lipolytic machinery [34-36]. Jabba anchors proteins from other cellular compartments to LDs [33, 37] and has been proposed to contribute to lipid metabolism during oogenesis [38].

Similar to germline knockdown of DGAT1 (Fig 3B), females lacking either Jabba or PLIN2 display two types of actin defects during oogenesis (Fig 3C-3D compared to 3A). First, actin bundles are aberrant. Specifically, some nurse cell membranes lack bundles, and the bundles that form are not uniformly distributed, shorter, and/or fail to project toward the nurse cell nuclei (Fig 3C-3D, green arrowheads). Second, cortical actin is broken down, leading to the appearance of multinucleate nurse cells (Fig 3C-3D, magenta arrowheads). Since in these mutants LDs are abundant [18, 33] (see also Fig 4) and because the frequency of dying follicles is similar to wild type (data not shown), we conclude that disruption of LD function indeed affects actin remodeling.

**Fig 3. LD proteins regulate actin bundling and cortical actin integrity in Stage 10B follicles. (A-F)** Maximum projections of three confocal slices of S10B follicles stained for F-Actin (phalloidin) in white, and DNA (DAPI) in cyan. Arrowheads indicate examples of defective actin bundling (green) and disrupted cortical actin (magenta). Images were brightened by 30% to increase clarity. Black boxes were placed behind channel labels to improve visualization. Scale bars=50μm. (**A)** WT, *wild-type* (*yw*). (**B)** *DGAT1 RNAi* (*osk3-GAL4>* TRiP.HMC06242/+). (**C)** *Jabba-/-* (*Jabba*$^{z101}$/*Jabba*$^{z101}$). (**D)** *PLIN2-/-* (*Lsd-2*$^{KG00149}$/*Lsd-2*$^{KG00149}$). **(E)** *ATGL-/-* (*bmm*$^{1}$/*bmm*$^{1}$). **(F)** *pxt-/-* (*pxt*$^{f01000}$/*pxt*$^{f01000}$). In wild-type late Stage 10B follicles, actin bundles extend from the nurse cell periphery to the nucleus, and the cortical actin is thickened relative to earlier stages (A). Actin bundles fail to form or form improperly, and cortical actin is disrupted upon RNAi knockdown of DGAT1 (B), or loss of Jabba (C), PLIN2 (D), or ATGL (E). These phenotypes resemble loss of the COX-like enzyme Pxt (F).

Most actin regulators impact either actin bundle formation or cortical actin, but not both [17, 21]. However, the same combination of phenotypes is observed when PG signaling is lost: lack of the COX-like enzyme Pxt causes delayed bundle development, collapsed, stunted or absent actin bundles, and cortical actin breakdown with a failure of nurse cell contraction (Fig 3F compared to 3A) [25, 26]. In most cases of actin bundling defects, nurse cell nuclei are pushed into the ring canals when the cortical actin contracts. However, this does not occur in *Pxt* [26, 39], *Jabba,* or *PLIN2* mutants (data not shown), suggesting that cortical actin contraction is also disrupted, presumably as result of the simultaneous breakdown of cortical actin. The fact that loss of all three proteins results in this unusual combination of phenotypes suggests a functional relationship between PGs and LD proteins in actin remodeling.

<u>*Both LD proteins and PG signaling control the intracellular distribution of LDs*</u>

The similarities between lack of PG signaling and lack of LD proteins extends to phenotypes beyond F-actin: *Jabba*, *PLIN2*, and *pxt* mutants all display altered spatial distribution of LDs. In wild-type Stage 10B follicles, LDs are dispersed throughout the entire nurse cell cytoplasm, with only minor variations in LD density (Fig 4A-4A'). In contrast, in all three mutants, some regions of the cytoplasm are depleted of LDs, while others have dense LD accumulation/clustering (Fig

194 4B-4D'). Clustering varies somewhat across the same follicle and between follicles. But when
195 Stage 10B follicles were scored as having either normal, mild, or severe LD clustering (see
196 Material and Methods for details), half or more of all follicles exhibited severe clustering in all
197 three mutants (Fig 4F).

**Fig 4. PG signaling and LD proteins promote LD dispersal. (A-E')** Single confocal slices of follicles of Stage 10B follicles stained for LDs (Nile red) in white and DNA (Hoechst) in cyan; A'-E' are zoomed in images of A-E. A black box was added under the channel labels in A' to aid in visualization. **(A)** WT, wild-type (Oregon R). **(B)** *pxt-/-* (*pxt*$^{f01000}$/*pxt*$^{f01000}$). **(C)** *Jabba-/-* (*Jabba*$^{DL}$/*Jabba*$^{DL}$). **(D)** *PLIN2-/-* (*LSD-2*$^{KG}$/*LSD-2*$^{KG}$). **(E)** *ATGL-/-* (*bmm*$^{1}$/*bmm*$^{1}$). **(F)** Quantification of LD clustering in Stage 10B follicles for the indicated genotypes. Follicles were classified as normal or as exhibiting moderate or severe clustering, and the percentage of each class was calculated. **(G)** Quantification of actin cytoskeletal and LD clustering defects in control versus 3mM aspirin-treated Stage 10B follicles. Dots represent the average of separate experiments; control n=49 and aspirin n=63. Error bars, SD. ****p=0.0001, ****=p<0.0001*, Sidák's multiple comparisons test. **(H-I'')** Single confocal slices of Stage 10B follicles treated with vehicle (control, EtOH or DMSO) or 3mM aspirin for 1 hour, and then stained for F-Actin (H, I, phalloidin) or LDs (H', I', Nile red) in white; H'' and I'' are zoomed in images of H' and (I'). Note that images in panels H-H' are on black box, and a black box was added under the I'' label to aid in visualization. Scale bars=50μm (A-E, H-H'. I-I') or 10μm (A'-E', H'', I''). Loss of Pxt or two LD proteins (Jabba and PLIN2) result in similar LD clustering/reorganization phenotypes. Similarly, treatment of Stage 10B follicles with 3mM aspirin, a COX inhibitor, for 1 hour results in both LD clustering (H'-H'' compared to I'-I'', and G) and actin cytoskeletal defects (H compared to I, and G).

198

199 To test whether clustering is caused by defective PG signaling within the follicle or some
200 as-yet uncharacterized function of Pxt, we pharmacologically inhibited Pxt to abolish PG
201 production [26]. Wild-type Stage 10B follicles were incubated *in vitro* for 1-1.5 hours in medium
202 containing either the solvent control or 3mM aspirin, an inhibitor of COX enzymes. Follicles were
203 then stained for both LDs and F-actin. Under control conditions, follicles maintain uniform LD
204 distribution and intact actin bundles and cortical actin, very similar to follicles without any
205 treatment (Fig 4G-4H''). In the aspirin treated samples, the actin cytoskeleton is disrupted, as
206 expected from previous studies (Fig 4G-4I) [26]. This treatment causes LD clustering (Fig 4G,
207 4I'-4I"). Such a rapid response supports the idea that PG signaling within the follicle not only
208 promotes actin remodeling but also maintains LD dispersal. Together, our observations indicate

209 that LDs and PG signaling may reciprocally influence each other. As the molecular mechanisms
210 underlying LD dispersal are not well understood, we focus the rest of the study on the actin
211 remodeling effects.
212
213 *Pxt functions in a linear pathway with Jabba, but not with PLIN2, to regulate actin remodeling*
214 The similar actin phenotypes in *pxt*, *PLIN2*, and *Jabba* mutants suggest these proteins act in the
215 same pathway to regulate actin remodeling. To test this hypothesis, we used a dominant
216 genetic interaction assay to assess actin remodeling defects. As the severity of actin disruption
217 can exhibit considerable variability within a given genotype, we developed a method to quantify
218 both actin bundle and cortical actin defects from confocal stacks of phalloidin-stained Stage 10B
219 follicles. Specifically, the degree of penetrance of actin bundle and cortical actin defects are
220 scored separately and summed to give an Actin Defect Index (ADI) that is used to classify each
221 follicle into three categories of defects: normal, mild, or severe (see the Material and Methods
222 and S1 Fig for details).

**S1 Fig. Examples and criteria used for scoring actin remodeling phenotypes.** Maximum projection of three confocal slices of representative Stage 10B follicles stained for F-Actin (phalloidin) in white, and DNA (DAPI) in cyan, and written definitions of the indicated actin bundle and cortical actin phenotypes. Actin bundle and cortical actin phenotypes were independently binned into four categories: Normal, Mild Defects, Moderate Defects, or Severe Defects. Images were brightened by 30% to increase clarity. Green arrowheads indicate examples of actin bundle defects, and magenta arrowheads indicate examples of cortical actin breakdown. Scale bar=50μm.

223
224 We expect heterozygosity for mutations in *pxt*, *PLIN2*, or *Jabba* alone to have little to no
225 effect on actin dynamics. If either PLIN2 and Pxt or Jabba and Pxt function in the same
226 pathway, then double heterozygotes for *PLIN2* and *pxt* or *Jabba* and *pxt* will exhibit severe actin
227 defects. Conversely, if they function in separate pathways, then actin defects in the double
228 heterozygotes will remain low or be additive of what is observed in the single heterozygotes.

As expected, there are few actin defects in single heterozygotes of PLIN2 (63% normal) and *pxt* (80% normal) (Fig 5A-5B, 5G). Co-reduction of both PLIN2 and Pxt (*PLIN2/+;;pxt/+*) does not significantly increase the frequency of actin defects (Fig 5C, 5G; 60% normal). This failure to exhibit a genetic interaction is not likely due to insufficient protein reduction as PLIN2 heterozygotes show a 40% reduction in PLIN2 protein level (S2 Fig), but instead suggests that Pxt and PLIN2 regulate actin remodeling via separate pathways.

**Fig 5. PLIN2 acts independently of Pxt, while Jabba acts in a linear pathway with Pxt to regulate actin remodeling. (A-F)** Maximum projections of three confocal slices of S10B follicles stained for F-Actin (phalloidin) in white, and DNA (DAPI) in cyan. Arrowheads indicate examples of defective actin bundling (green) and disrupted cortical actin (magenta). Images were brightened by 30% to increase clarity. Scale bars=50μm. **(A)** *PLIN2-/+* (*Lsd-2$^{KG00149}$-/+*). **(B)** *pxt-/+* (*pxt$^{f01000}$/+*). **(C)** *PLIN2-/+;; pxt-/+* (*Lsd-2$^{KG00149}$-/+;; pxt$^{f01000}$-/+*). **(D)** *Jabba-/+* (*Jabba$^{z101}$/+*). **(E)** *Jabba-/+; pxt-/+* (*Jabba$^{z101}$/+;pxt$^{f01000}$/+*). **(F)** *PLIN2-/+; Jabba-/+* (*Lsd-2$^{KG00149}$/+;Jabba$^{z101}$/+*). **(G-I)** Graphs of quantification of actin phenotypes. Data were from the following genotypes: *pxt-/+* = *pxt$^{f01000}$/+* and *pxt$^{EY03052}$/+; Jabba-/+* = *Jabba$^{z101}$/+* and *Jabba$^{DL}$/+*; *Jabba-/+; pxt-/+* = *Jabba$^{z101}$/+; pxt$^{f01000}$/+, Jabba$^{z101}$/+; pxt$^{EY03052}$/+, Jabba$^{DL}$/+; pxt$^{f01000}$/+,* and *Jabba$^{DL}$/+; pxt$^{EY03052}$/+; PLIN2-/+;; pxt-/+* = *Lsd-2$^{KG00149}$/+;; pxt$^{f01000}$/+* and *Lsd-2$^{KG00149}$/+;;pxt$^{EY03052}$/+*; and *PLIN2-/+; Jabba-/+* = *Lsd-2$^{KG00149}$/+;Jabba$^{z101}$/+*. Actin defects were quantified by scoring the penetrance of actin bundle and cortical actin defects. Scores were summed and the total binned into one of three categories: normal, mildly defective, and severely defective. For a detailed description of the quantification see the Materials and Methods and Supplemental Figure 1. *****p<0.0001,* Pearson's chi-squared test. Error bars, SD. Both actin bundles and cortical actin are largely normal in *PLIN2-/+* (A, G, I), *PLIN2-/+; pxt-/+* (C, G), or *PLIN2-/+; Jabba-/+* (F, I) Stage 10B follicles. In contrast, in *Jabba-/+; pxt-/+* follicles (E), actin bundles are absent, sparse, and stunted and there are instances of cortical actin breakdown. The double heterozygotes thus exhibit significantly more mild and severe actin defects than either *pxt-/+* (B, H) or *Jabba-/+* (D, H) follicles (H).

**S2 Fig. *PLIN2-/+* heterozygotes have reduced PLIN2 protein. (A)** Immunoblot comparing PLIN2 protein levels in wild type (WT, Oregon R), *PLIN2-/+* ((*Lsd-2$^{KG00149}$/+*), and *PLIN2-/-* (*Lsd-2$^{KG00149}$/ Lsd-2$^{KG00149}$*) Stage 10B follicles. **(B)** Quantification of (A), in which PLIN2 band intensity was normalized to the nonspecific bands (asterisk). *p=<0.0001*, unpaired t-test, two-tailed. PLIN2 protein levels are reduced by approximately half in *PLIN2-/+* Stage 10B follicles.

We next examined the relationship between Jabba and Pxt. Like before, the single heterozygotes have only minor actin defects, with the vast majority of all follicles exhibiting normal actin remodeling (Fig 5B, 5D, 5H). In contrast, only 11% of follicles from double

239 heterozygotes (*Jabba/+; pxt/+*) were normal, and the frequency of the severe class increased
240 almost tenfold (Fig 5E, 5H). This synergistic increase in actin defects suggests Pxt and Jabba
241 act in the same pathway to regulate actin remodeling.

242 For the relationship between Jabba and PLIN2, we considered two scenarios. In the first,
243 Jabba acts in two pathways, one with PLIN2 and one with Pxt, to regulate actin remodeling. In
244 the second, PLIN2 regulates actin remodeling independently of both Pxt and Jabba. The actin
245 phenotypes of PLIN2/+; *Jabba/+* double heterozygotes are mild, with the frequency of each
246 category similar to those seen in the single heterozygotes (Fig 5F, 5I). We conclude that actin
247 remodeling is regulated by two separate pathways involving LD proteins, with Jabba and Pxt
248 acting in the same pathway (see Fig 10).

249

250 *Pxt is not enriched on LDs*

251 The observed genetic interaction between Jabba and Pxt could be explained if the two proteins
252 directly or indirectly regulate each other's expression. However, Western analysis on extracts
253 from Stage 10B follicles revealed that Jabba protein levels in wild-type and *pxt* mutant follicles
254 were indistinguishable, as were Pxt levels in wild-type and *Jabba* mutant follicles (S3A-S3D
255 Fig). Thus, we find no evidence that Jabba and Pxt interact by regulating each other's
256 expression. We also find no effect of PLIN2 on the levels of Jabba and Pxt, and vice versa
257 (S3A, S3E-S3F Fig).

**S3 Fig. Pxt and LD proteins do not affect each other's expression. (A, C, E)** Immunoblots for Pxt and alpha-Tubulin (A), Jabba (C), and PLIN2 (E) of the indicated genotypes: WT, wild-type (Oregon R), *Jabba-/-* (*Jabba$^{z101}$/Jabba$^{z101}$*), *PLIN2-/-* (*Lsd-2$^{KG00149}$/Lsd-2$^{KG00149}$*), *ATGL-/-* (*bmm$^{1}$/bmm$^{1}$*) and *pxt-/-* (*pxt$^{f01000}$/pxt$^{f01000}$*). Asterisk indicates non-specific band in C and E. **(B, D, F)** Quantification of A, C, and E, respectively, in which band intensity was normalized as indicated. ns=p>0.05, unpaired t-test, two-tailed. Loss of Jabba, PLIN2, or ATGL have no effect on Pxt levels (A-B), and loss of Pxt has no effect on Jabba (C-D) or PLIN2 (E-F) levels.

258

Jabba and Pxt might also regulate each other's activity by being physically present in the same cellular compartment. Jabba localizes to LDs in embryos [33] and in nurse cells [23], and in other systems, components of the PG synthesis machinery are sometimes enriched on LDs [40]. Using immunostaining, LD purification, and *in vivo* centrifugation, we assessed Pxt's relationship to LDs in wild-type nurse cells. All three methods show that Pxt is not enriched on LDs. By immunostaining, Pxt localizes to the Golgi compartments prior to Stage 9 and to the Endoplasmic reticulum (ER) by Stage 10B, but not obviously to LDs (Fig 6A-6C'''). We also prepared an LD enriched biochemical fraction from ovary lysates, as previously described for embryos [33], and analyzed it by Western blotting for Pxt, PLIN2 (as a marker for LDs), and Calnexin (as marker for the ER). Pxt behaves like an ER protein, not like an LD protein (Fig 6D-6E). Finally, we separated LDs from other cellular components by *in vivo* centrifugation: when living *Drosophila* follicles are centrifuged, their contents separate by density within each nurse cell/oocyte, with LDs accumulating on the side that faced up [32, 33]. Staining of fixed centrifuged follicles reveals no enrichment of Pxt (magenta) in the LD layer (green, marked by yellow arrowhead) (Fig 6F). We conclude that the majority of Pxt is not present on LDs.

**Fig 6. Pxt is not enriched on LDs. (A-C''')** Single confocal slices of nurse cells of the indicated stages, stained for Pxt (A-C), organelle marker (A'-C'), and DNA (D''-G'', Hoechst). Merged image (A'''-C'''): Pxt, magenta; organelle marker, green; and DNA, cyan. Organelle marker: LDs (A', A'''; Nile red); Golgi-eYFP (B', B'''); and ER-eYFP (C', C'''). Scale bars=10μm. **(D)** Western blots of purified LDs and a dilution serious of ovary lysate (OL) for Calnexin (magenta) and Pxt (green) in the top half of the blot and α-Tubulin (magenta) and PLIN2 (green) in the bottom half of the blot; dashed line indicates where the membrane was cut. **(E)** Quantification the abundance of proteins in the LD fraction relative to undiluted ovary lysate (OL). The ratio of signal for the LD and OL lane in Western blots like in (F) were computed for the indicated proteins and normalized to the average value for PLIN2. Error bars, SD. ***p=<0.0028*, Tukey's multiple comparisons test. **(F-F''')** Single confocal slices of centrifuged wild-type Stage 10B follicle stained for Pxt (F), LDs (F', Nile red), and DNA (F'', Hoechst). Merged image (A'''-C'''): Pxt, magenta; LDs, green; and DNA, cyan. Scale bars=50μm. Pxt does not colocalize with LDs (A-A'''), is not enriched on purified LDs (D-E), and does not co-accumulate with LDs in centrifuged follicles (F-F'''). Instead, Pxt localizes to the Golgi during Stage 8 (B-B'') and the ER during Stage 10B (C-C''').

Alternatively, Pxt and Jabba might genetically interact because they influence each other's localization. We find that this is not the case, as in Stage 10B follicles, Pxt still robustly colocalizes with the ER in *Jabba* mutants (S4B-S4B''' compared to S4A-S4A''' Fig), and Jabba still localizes to LDs in *pxt* mutants (S4F-S4F''' compared to S4E-S4E'''). There are some changes in the overall spatial distribution of LDs and ER in these mutants: LDs are clustered in *pxt* mutant (consistent with Fig 4B-4B') and, in *Jabba* mutants, the ER has a more diffuse appearance and is excluded from areas occupied by LD clusters (S4B-S4B''' compared to S4A-S4A''' Fig). However, in either mutant condition, Jabba and Pxt remain enriched on LDs and ER, respectively, as in the wild type. Similarly, loss of PLIN2 has no effect on Pxt localization (S4C-S4C''' Fig).

**S4 Fig. LD proteins do not affect Pxt's localization to the ER. (A-D'''')** Single confocal slices of Stage 10B nurse cells, stained for Pxt (A-D), Calnexin (A'-D', ER marker), and DNA (A''-D'', Hoechst). Merged image (A''', A''''-D''', D''''): Pxt, magenta; Calnexin (ER marker), green; and DNA (Hoechst), cyan. **(E-F'''')** Single confocal slices of Stage 10B nurse cells, stained for Jabba (E-F), LDs (E'-F', Nile red) and DNA (E''-F'', Hoechst). Merged image (E''', E'''', F''', F''''): Jabba, magenta; LDs (Nile red), green; and DNA (Hoechst), cyan. Genotypes: WT, wild-type (Oregon R); *Jabba -/-* (*Jabba*$^{zl01}$/*Jabba*$^{zl01}$); *PLIN2 -/-* (*LSD-2*$^{KG00149}$/*LSD-2*$^{KG00149}$); *ATGL -/-* (*bmm*$^{1}$/*bmm*$^{1}$), and *pxt -/-* (*pxt*$^{f01000}$/*pxt*$^{f01000}$). Scale bars=10μm. Note that black boxes were added under some panel and/or channel labels to aid in visualization (A, A', A''', D, E, F' and F'''). In Stage 10B follicles, Pxt's localization to the ER is similar to wild-type in *Jabba* (B-B''''), *PLIN2* (C-C''''), and *ATGL* mutants (D-D''''). As in the wild type (E-E''''), Jabba localizes to LDs in *pxt* mutants (F-F''''), even though the spatial distribution of LDs is altered.

*The triglyceride lipase ATGL/Brummer and Pxt act in the same pathway to regulate actin*

If there is no clear physical relationship between LDs and Pxt, how else might LDs modulate PG production? In some mammalian cells, the substrate for COX enzymes, arachidonic acid (AA), can be released from triglycerides stored in LDs by the triglyceride lipase ATGL [28]. These FAs can either be directly used as COX substrate or be first incorporated into membrane phospholipids and subsequently released by phospholipases [41]. In the latter case, diffusing phospholipids may deliver AA to ER regions spatially distant from LDs. Thus, AA availability for PG production may ultimately depend on the breakdown of LD triglycerides.

The *Drosophila* homolog of ATGL is called Brummer (Bmm; referred thereafter as ATGL for clarity); it catalyzes the conversion of triacylglycerol to diacylglycerol and free FA [42]. Based on RNA-seq analyses, ATGL is highly expressed in ovaries [43], and in-situ analysis reveals that ATGL mRNA is expressed in the nurse cells and oocytes in early and mid-oogenesis [44]. Intriguingly, we find that loss of ATGL causes actin remodeling defects in Stage 10B follicles that resemble those seen in *pxt* and *Jabba* mutants, *i.e.*, defects in both cortical actin and actin bundles (Fig 3C, 3E, 3F compared to 3A); conversely, loss of ATGL does not alter LD dispersal (Fig. 4E-4F). Additionally, ATGL does not regulate the level or localization of Pxt (S3A and S4D-S4D''' Fig), similar to our findings related to Jabba and PLIN2.

To test if ATGL acts in the same pathway as Pxt to regulate actin remodeling, we used our quantitative dominant genetic interaction assay to assess actin remodeling during Stage 10B. As expected, actin remodeling is largely normal in single heterozygotes of *pxt* (87%) and *ATGL* (84%) (Fig 7A, 7D). In contrast, only 46% of the double heterozygotes of *pxt* and *ATGL* (*pxt/ATGL*) exhibit normal actin remodeling, and the frequency of severe cases is increased almost tenfold (Fig 7B, 7D). This synergistic increase in actin defects indicates that ATGL and Pxt regulate actin remodeling via a shared pathway.

**Fig 7. ATGL acts in a linear pathway with Pxt but not with Jabba to regulate actin remodeling. (A-C)** Maximum projections of three confocal slices of Stage 10B follicles stained for F-Actin (phalloidin) in white, and DNA (DAPI) in cyan. Arrowheads indicate examples of defective actin bundling (green) and disrupted cortical actin (magenta). Images were brightened by 30% to increase clarity. Scale bars=50μm. (A) *ATGL-/+* (*$bmm^{1}$/+*). (B) *ATGL/pxt* (*$bmm^{1}/pxt^{f01000}$*). (C) *Jabba-/+; ATGL-/+* (*$Jabba^{z101}$/+; $bmm^{1}$/+*). **(D-E)** Graphs of quantification of actin phenotypes of the indicated genotypes. Data were from the following genotypes: *pxt-/+* = *$pxt^{f01000}$-/+* and *$pxt^{EY03052}$-/+*, *ATGL-/+* = *$bmm^{1}$/+*, *ATGL/pxt* = *$bmm^{1}/pxt^{f01000}$* and *$bmm^{1}/pxt^{EY03052}$*; *Jabba-/+* = *$Jabba^{z101}$/+*; and *Jabba-/+; ATGL-/+* = *$Jabba^{z101}$/+;$bmm^{1}$/+*. Actin defects were quantified by scoring the penetrance of actin bundle and cortical actin defects. Scores were summed and the total binned into one of three categories: normal, mildly defective, and severely defective. For a detailed description of the quantification see the Materials and Methods and Supplemental Figure 1. *****p<0.0001,* Pearson's chi-squared test. Error bars, SD. Actin bundles and cortical actin are largely normal in the *ATGL-/+* and *pxt-/+* Stage 10B follicles (A-B, D-E). In contrast, *ATGL/pxt* Stage 10B follicles have stunted and incomplete bundles (green arrowheads) and breakdown of cortical actin (magenta arrowheads, B, D). Actin remodeling is normal in *Jabba-/+; ATGL-/+* Stage 10B follicles (C, E).

We also assessed dominant genetic interactions between ATGL and Jabba, and ATGL and PLIN2. We find that frequency of actin remodeling defects observed in the double heterozygotes (*Jabba/+; ATGL/+*) is similar to that seen in the single heterozygotes (Fig 7C, 7E), indicating that Jabba and ATGL act in different pathways to regulate actin remodeling. Similarly, we find that PLIN2 and ATGL do not interact genetically (S5 Fig).

**S5 Fig. ATGL and PLIN2 regulate actin remodeling via separate pathways. (A-C)** Maximum projections of three confocal slices of S10B follicles stained for F-Actin (phalloidin) in white, and DNA (DAPI) in cyan. Images were brightened by 30% to increase clarity. Scale bars=50μm. (A) *PLIN2-/+* (*Lsd-2$^{KG00149}$-/+*). (B) *ATGL-/+* (*bmm$^{1}$-/+*). (C) *PLIN2-/+;; ATGL-/+* (*Lsd-2$^{KG00149}$-/+;;bmm$^{1}$-/+*). **(D)** Graph of quantification of actin phenotypes of the indicated genotypes. Actin defects were quantified by scoring the penetrance of actin bundle and cortical actin defects. Scores were summed and the total binned into one of three categories: normal, mildly defective, and severely defective. For a detailed description of the quantification see the Materials and Methods and Supplemental Figure 1. ns=p>0.05, Pearson's chi-squared test. Error bars, SD. The level of actin defects in *PLIN2-/+; ATGL-/+* (C-D) is not significantly different from that in *PLIN2-/+* (A, D) or ATGL-/+ (B, D).

Taken together, these data reveal an intricate relationship between Pxt and LD proteins in which activity of both is necessary for proper actin remodeling. Specifically, our data supports that three pathways control actin remodeling. PLIN2 regulates actin dynamics independently of Jabba, ATGL, and Pxt. Conversely, Pxt acts in two separate pathways with Jabba and ATGL to regulate actin remodeling (see Fig 10). While there are no obvious mechanisms for how Pxt and Jabba work together to regulate actin remodeling, ATGL may regulate the availability of the substrate, AA, necessary for PG production.

*AA is present in ovary triglycerides*

If ATGL is indeed responsible for generating the substrate for Pxt, our model implies that AA-containing triglycerides are present in *Drosophila* follicles. We therefore extracted lipids from wild-type and *ATGL* mutant ovaries and analyzed them by LC-MS/MS mass spectrometry.

Among the 98 different triglyceride species identified (STable 1), two contain a twenty-carbon FA with four double bonds (20:4), presumably AA. AA was relatively rare, making up on the order of 0.06-0.07% of all FAs detected in triglycerides (Fig 8A), with four FA species accounting for the bulk (~85%) of FAs: the mono-unsaturated palmitoleic (16:1) and oleic (18:1) acids, and the saturated myristic (14:0) and palmitic (16:0) acids. We did not detect AA in the phospholipids recovered in our analysis (data not shown).

**STable 1. Quantitation of triglyceride species in ovaries**
Column A lists the fatty acid content of various triglyceride species detected in ovaries by lipidomics.
Columns B through H show the relative amount of those species in three wild-type and four ATGL-/- samples. Reads are background corrected. A fourth wild-type sample was discarded as an outlier because the detected lipid amounts were an order of magnitude lower than in the other samples.

**Fig 8. Ovary triglycerides contain arachidonic acid. (A-F)** Lipids were extracted from wild-type and *ATGL-/-* (*bmm*$^{1}$*/bmm*$^{1}$) ovaries and analyzed by mass spectrometry. Error bars, SD. **(A)** Abundance of individual fatty acids in triglycerides expressed as fraction of all such fatty acids; significance evaluated using Sidak's multiple comparisons test. **(B)** Total amount of saturated (SF), monounsaturated (MUFA) or polyunsaturated (PUFA) fatty acids relative to all fatty acids in triglycerides; significance evaluated using Tukey's multiple comparisons test. **(C)** Levels of the three phospholipid classes phosphatidylcholine (PC), phosphatidylethanolamine (PE), and phosphatidylinositol (PI); significance evaluated using Sidak's multiple comparisons test. **(D)** Overall triglyceride levels. ns = *p = 0.1239*, unpaired t-test, two-tailed. **(E)** Thin layer chromatograph of whole-lipid extracts from Stage 14 follicles of the indicated genotypes. **(F)** Quantitation of the triacylglycerol (TAG) to cholesterol ratio in (D). **p=0.0477*, Dunnett's multiple comparisons test. **(G, H)** Quantification of two triglyceride species containing arachidonic acid (AA). **p=0.0419, **p=0.0019*, unpaired t-tests, two-tailed. Wild-type and *ATGL* mutant ovaries exhibit a similar abundance of fatty acids in triglycerides (A, B), phospholipids (C), and total triglycerides (D) by lipidomic analysis. Similarly, thin layer chromatographic analysis of Stage 14 follicles reveals no significant differences in triglycerides (E-F). However, two AA-containing triglyceride species are present in wild-type ovaries, and their levels are elevated in the absence of ATGL (G, H).

Our lipidomic analysis did not uncover a significant difference in the content of phospholipids (Fig 8C) or of total triglycerides (Fig 8D) between wild-type and *ATGL* mutant ovaries. The overall FA profile in triglycerides was also similar between the two genotypes (Fig 8A-B). In addition, there was no significant difference in total triglycerides in Stage 14 oocytes,

as detected by thin layer chromatography (Fig 8E-8F), even though we could confirm the previously described reduced triglyceride loading in PLIN2 mutants [18]. Thus, ATGL mediated lipolysis during oogenesis does not appear to lead to bulk turnover of LDs and may be restricted to supporting lipid signaling.

However, wild-type and *ATGL* mutant ovaries exhibited differences in the AA-containing triglycerides, both of which were elevated in the absence of ATGL (Fig 8G-8H). This trend persisted even when measurements were normalized to total triglycerides (not shown) or all lipids in the sample (S6A-S6B Fig). These observations are consistent with the possibility that in the *ATGL* mutants less AA is released from triglycerides, resulting in a reduced pool of free AA available for signaling or phospholipid production.

**S6 Fig. AA-containing TAG and total TAG normalized to total lipids in sample.** Lipids were extracted from wild-type and *ATGL-/-* (*bmm$^{1}$/bmm$^{1}$*) ovaries and analyzed by mass spectrometry. Data from main Figure 8 has been re-plotted as relative abundance normalized to total lipids in the sample. Error bars, SD. **(A, B)** Two triglyceride species containing arachidonic acid (AA). Error bars, SD, **p=0.0279, **p=0.0019*, unpaired t-tests, two-tailed. **(C)** Overall triglyceride levels are slightly increased in *ATGL-/-* ovary lipids. Error bars, SD, ***p=0.002*, unpaired t-test, two-tailed. **(D)** Relative amounts of phosphatidylcholine (PC), phosphatidylethanolamine (PE), and phosphatidylinositol (PI) in wild-type versus *ATGL-/-* ovary lipids. Error bars, SD, **p=0.0329, *p=0.0416, ***p=0.0001*, Sidak's multiple comparisons test. While overall triglyceride levels are similar between the two genotypes (C), the AA-containing triglycerides are increased (A, B), and three classes of phospholipids are decreased (D) in the absence of ATGL. The reason for the decrease in phospholipids is not clear. One possibility is that ATGL breaks down triglycerides to generate precursors for phospholipid production; alternatively, in the absence of ATGL, ovaries may contain a different mix of follicle stages (and thus different levels of triglyceride accumulation) due to altered developmental progression.

*ATGL limits arachidonic acid levels to control PG-dependent actin remodeling*

We hypothesize that ATGL acts on LD triglycerides to release AA, which then serves as the substrate for Pxt-dependent PG production; PG, in turn, controls actin remodeling necessary for follicle development. Thus, the actin defects due to reduction or loss of ATGL, or co-reduction in ATGL and Pxt should be suppressed by exogenous free AA.

We utilized our *in vitro* egg maturation (IVEM) assay, in which isolated Stage 10B follicles mature *in vitro* in a simple culture medium [45]. One of its key components is fetal bovine serum (FBS), which supplies numerous nutrients and growth factors. Using this assay, we find that the majority of Stage 10B follicles from single heterozygotes of *pxt* and *ATGL* develop *in vitro*, while 55% of the follicles from double heterozygotes fail to develop (S7 Fig). These data recapitulate what we observed when we quantitatively assessed the actin defects in the double heterozygotes (Fig 7B, 7D). To test if ATGL supplies AA for PG production, we hoped to use the IVEM assay to determine if exogenous AA rescues follicle development in the double heterozygotes (*pxt/ATGL*). Unfortunately, this experiment yielded highly variable results (data not shown), likely because FBS contains unknown amounts of FAs, including AA.

**S7 Fig. ATGL and Pxt genetically interact in the *in vitro* egg maturation assay.** Graph of the percentage of Stage 10B follicles developing *in vitro*, normalized to wild-type (*yw*) development, for the following genotypes: *ATGL-/+* (*bmm$^{1}$-/+*), *pxt-/+* (*pxt$^{f01000}$-/+*), and *ATGL/pxt* (*bmm$^{1}$/pxt$^{f01000}$*). *ATGL/pxt* follicle development is reduced by ~50% compared to the *ATGL-/+* and *pxt-/+* controls.

As an alternative approach, we reduced the amount of FBS in the medium and assessed follicle response to exogenous free AA (Fig 9A). At ~60μM, a slightly higher percentage of follicles developed than in control medium, but that fraction dropped steadily as AA concentrations were raised further. This finding indicates that high levels of AA are toxic to follicle development; AA is known to be cytotoxic for cultured cells, at least in part due to pleotropic effects unrelated to PG production [46].

373

**Fig 9. ATGL controls free arachidonic acid. (A)** Graph of the percentage of wild-type (*yw*) Stage 10B follicles that develop *in vitro* in control (EtOH, ethanol) or arachidonic acid (AA) media. Error bars, SD. **(B-C')** Maximum projection of three confocal slices of wild-type (*yw*) S10B follicles treated with either IVEM medium containing EtOH or 500μM AA for 1 hour and stained for LDs (Nile red) in white; B' and C' are zoomed in images of the boxed regions in B and C. All images were brightened by 70% to improve visibility. B and C, scale bars=50μm. B' and C', scale bars=10μm. **(D)** Graph of quantification of LD clustering in nurse cells of wild-type (*yw*) S10B follicles exposed to either EtOH or 500μM AA for one hour. Pearson's chi-square test, *p>0.05.* **(E)** Schematic depicting the rationale of the experimental approach used in F (created with Biorender.com). **(F)** Graph of relative percentage of follicles from the indicated genotypes developing in 500μM AA media versus control media (EtOH). Genotypes tested are *wild-type* (*yw*), *pxt*-/+ ($pxt^{f01000}$/+), *ATGL-/+* ($bmm^{1}$/+), and *ATGL/pxt* ($bmm^{1}/pxt^{f01000}$). Error bars=SD. **p<0.05, **p<.001* by paired t-test. Wild-type follicle development, *in vitro*, is inhibited with increasing AA concentration (A). Exposure to high doses of AA causes LD clustering (C-D), suggesting AA is accumulating in the LDs. If the release of AA from LDs is mediated by ATGL, and this free AA contributed to impairing *in vitro* follicle development when exogenous AA is provided, then reducing ATGL will improve the percentage of follicles developing (E). While reducing Pxt does not alter the relative percentage of follicles developing in 500μM AA media compared to wild-type follicles, reducing ATGL alone or in combination with reduced Pxt results in increased follicle development compared to wild-type follicles (F).

374

375 In other systems, exogenous AA is initially stored in LDs [40, 47, 48]. Similarly, we find
376 that high-doses of AA (500μM AA) result in LD clustering in 60% of the follicles, and perhaps an
377 increase in LD size (Fig 9B-9D). These observations are consistent with the notion that some
378 exogenous free AA can be sequestered by LDs, but at higher levels AA inhibits follicle
379 development.

380 The dose-dependent AA inhibition of follicle development provided a new approach to
381 determine the contribution of ATGL in this system. We reasoned that if ATGL is required to
382 release AA from internal stores and thus generate free AA, then reducing ATGL levels will
383 partially suppress the inhibition of follicle development by high levels of exogenous AA (Fig 9E)
384 as total free AA levels will be lower. We find that development of *pxt* heterozygous follicles is
385 impaired to the same level as wild-type follicles in the presence of 500μM AA (Fig 9F). In
386 contrast, two-fold more Stage10B follicles from *ATGL* heterozygotes or double heterozygotes of

387 *ATGL* and *pxt* develop in the presence of 500μM AA than wild-type follicles (Fig 9F). These data
388 are consistent with the model that ATGL releases AA, which is required for PG production (Fig
389 10). These PGs then regulate actin remodeling necessary for follicle development.
390

**Fig 10. LD proteins regulate actin remodeling via three pathways.** Schematic (created with Biorender.com) summarizing the findings presented. Synthesis of TAG (triglyceride) by DGAT1 (magenta) leads to accumulation of TAG between the inner and outer leaflets of the ER membrane (dashed inset=zoomed in schematic) and eventually LD budding from the ER. Arachidonic acid (AA, red lines) is stored either in the form of TAG or is incorporated into the phospholipid membrane. We identified three pathways by which LD proteins regulate actin remodeling. In the first, PLIN2 (blue) regulates actin remodeling by a PG-independent pathway. In the second, Jabba (green) and Pxt act together to regulate actin remodeling, but the precise nature of this relationship is unknown (dashed arrow). In the third pathway, ATGL (red) can liberate AA from TAG stored in LDs, providing the substrate, either directly or indirectly, for Pxt and PG production (orange) to regulate actin remodeling. The AA freed from TAG by ATGL (red) could be supplied directly to Pxt or be first incorporated into phospholipids (surrounding the neutral lipid core of LDs or present in the ER or other cellular membranes). In a second step, cPLA2 can then release AA from these phospholipids to provide the substrate for PG production.

## Discussion

Our data reveal that multiple LD proteins have critical roles in regulating actin cytoskeletal dynamics during *Drosophila* follicle development. Loss of either ATGL, PLIN2, or Jabba results in cortical actin breakdown, cortical contraction failure, and defective actin bundle formation during Stage 10B of oogenesis (Fig 3). This phenotype is uncommon, but is observed in flies lacking Pxt, the *Drosophila* COX-like enzyme [26]. Dominant genetic interactions reveal that LDs participate in three distinct pathways to regulate actin remodeling (Fig 10): PLIN2 acts independent of PGs, and Jabba and ATGL act in two separate PG-dependent pathways (Figs 5 and 7). For the ATGL-dependent pathway, we provide evidence that ATGL controls actin remodeling by regulating the availability of AA for PG synthesis (Fig 9). While PG signaling is known to have a conserved role in regulating actin remodeling across organisms and cell-types [49-54], this study provides the first evidence linking LDs to PG-dependent actin remodeling.

### *LDs provide the substrate for PG production*

The rate limiting step for PG production is the enzymatic release of AA from cellular lipids [8, 27]. To explain the genetic interaction between Pxt and the triglyceride lipase ATGL, we propose that ATGL regulates the release of AA from triglyceride stores, and that this AA serves – directly or indirectly – as substrate for Pxt-dependent PG production. Consistent with our model, we detect triglycerides containing AA in the ovary (Fig 8) and find that the toxic effect of exogenous AA on development is modulated by ATGL levels (Fig 9). While 500μM AA severely impairs *in vitro* wild-type follicle development, reducing ATGL dosage significantly increases the number of developing follicles (Fig 9F). These finding suggest that release of endogenous AA is impaired in ATGL-/+ follicles and therefore total free AA levels do not as readily reach toxic levels (Fig 9E); free AA is likely toxic due to its many diverse roles in cellular signaling [55, 56].

Our studies also provide the first evidence that AA has a functional role during *Drosophila* oogenesis: AA is present in ovary triglycerides; exogenous AA has both beneficial

and detrimental effects on follicle development, depending on concentration; and ATGL heterozygosity shifts the sensitivity of follicles to exogenous AA (Figs. 8 and 9). These findings are particularly important as it has been debated whether AA is present in flies. Some studies report that AA is not detectable in various life stages and body parts [57-59], while others find it [60-62]. These differences may be due to varying detection sensitivities and the fact that lipid profiles vary dramatically between tissues and/or on different diets [63].

The free AA that serves as Pxt substrate might originate from two different sources: phospholipids and triglycerides. In mammalian systems, both sources make contributions to PG synthesis [47]. Cytoplasmic phospholipase A2 (cPLA2) releases AA from phospholipids, and in many cell types, inhibiting cPLA2 severely impairs PG production [64-66]. Conversely, knockdown/inhibition of ATGL decreases PG production in mast cells [28] and leukocytes [29]. The AA released by ATGL might either directly serve as substrate for PG synthesis, or it might first be incorporated into phospholipids, to be released by cPLA2 in a subsequent step (Fig 10).

The site of PG synthesis in *Drosophila* Stage 10B nurse cells remains to be determined. In a variety of mammalian cell types, the PG synthesis machinery localizes to LDs [40]. For example, cPLA2, and its activators, localize to LDs and provide AA for PG production [67, 68], and COX2 and $PGE_2$ synthases localize to and produce $PGE_2$ on LDs in cultured colon adenocarcinoma cells [69]. Similarly, $PGE_2$ production is observed on LDs in normal rat intestinal epithelial cells [67] and in macrophages during parasitic infection [70]. In fly ovaries, PG may also be produced directly on LDs, or LDs may regulate the concentration of AA-containing phospholipids and free AA and thus indirectly control PG synthesis on the ER. As the cytoplasm of Stage 10B follicles is full of both ER and LDs (S4A-S4A''' and S4E-S4E''' Fig), the two organelles are in very close proximity; in addition, in many cells, LDs remain physically connected to the ER via lipidic bridges, which could convey AA or AA-containing phospholipids to the ER [71]. Further, although we do not observe enrichment of Pxt on LDs by immunofluorescence or biochemical purification (Fig 6), these observations do not rule out that

a fraction of Pxt is intimately associated with LDs. To resolve exactly where in nurse cells PG synthesis occurs, it will be important to determine if cPLA2 and PG-type specific synthases are enriched on LDs or elsewhere and to directly visualize the site of PG production.

*Why LDs?*

As Pxt resides in the ER and AA can be released from ER phospholipids, why would the organism use LDs to control AA availability? LDs are increasingly recognized as a critical way station during FA trafficking in cells [11] and often transiently sequester excess FAs from external and internal sources to prevent cellular damage, such as ER stress and mitochondrial dysfunction [72, 73]. Once safely stored in LDs, FAs can then be released in a regulated manner and directed to specific intracellular fates, like energy production or signaling [74, 75]. Thus, LDs serve as FA trafficking hubs to both channel FAs to the correct intracellular destinations and buffer the FA supply.

Proper channeling is particularly important for AA because it is cytotoxic, even at concentrations that overlap physiological ones [46]. For example, in cultured hippocampal neurons, low concentrations of AA support survival, but higher concentrations are quite toxic, much more so than other FAs [76]. This pattern also holds true for oogenesis: a recent study on bovine granulosa cells found that while low doses increase survival, high levels (200μM) induce apoptosis [77]. We observe the same trend when we incubate *Drosophila* follicles, *in vitro*, in AA. Low doses support a small increase in follicle development, while higher doses largely inhibit development (Fig 9A). This sensitivity to AA suggests that cells need to carefully buffer AA availability. Indeed, microscopic audioradiographic experiments reveal that in both immune and epithelial cells exogenous AA is initially almost exclusively incorporated into LDs, in both the phospholipid and neutral lipid pools [40, 47, 48].

We hypothesize that *Drosophila* follicles face a similar challenge. During Stages 9 and 10, nurse cells generate tens of thousands of LDs (Fig 1A-C) from lipids taken up from the

hemolymph [22]. This massive influx of FAs presumably includes AA, and AA, like other FAs, is likely initially sequestered into LDs upon arrival. Exposing follicles to AA promoted LD clustering and possibly LD enlargement (Fig 9B-D), consistent with the idea that AA is taken up by the follicles and incorporated into LDs. Currently, we cannot tell if all the AA present in Stage 10B follicles passed through LDs at some point or whether some is incorporated into phospholipids directly. The penetrance and severity of actin defects in Stage 10B follicles of *ATGL* mutants is somewhat variable, but can approach those of *pxt* mutants (Fig 3). These data are consistent with the model that ATGL-dependent release of AA from LDs is a substantial, and possibly the primary, source of AA for PG production during late-stage *Drosophila* oogenesis.

*ATGL function in Drosophila*

Given this critical role of ATGL in controlling PG synthesis during specific periods of *Drosophila* follicle development, it will be interesting to determine whether it contributes to PG signaling in other tissues. ATGL is best known for its role in fat storage [42] and is highly expressed in the larval and adult fat body, the adipose tissue of the fly. Loss of ATGL causes triglyceride overaccumulation in this tissue [42]. Notably, PG may be involved in regulating fat body development: normally, cells of the larval fat body persist through pupal stages and are cleared in early adulthood [78]; however, loss of Pxt results in their accumulation in adult abdomens (TLT, unpublished observation). In males, ATGL function in neurons and testes regulates whole-body energy storage by an as-yet uncharacterized mechanism thought to involve systemic signaling. And ectopic ATGL expression has beneficial roles in two *Drosophila* disease models, neurodegeneration due to mitochondrial dysfunction [79] and impairment of nephrocytes, components of the renal system, due to high fat diet [80]. Here, tissue-specific overexpression of ATGL in glia or nephrocytes, respectively, reverts disease-induced LD accumulation as well as disease phenotypes. Intriguingly, glia cells in other organisms activate PG signaling during brain inflammation/neurodegeneration [81, 82]. In the nephrocyte example,

ectopic ATGL affects transcription via lipid signaling, but exact mechanisms remain unknown. Our work identifies a specific signaling pathway, PG signaling, that is regulated by ATGL during oogenesis and provides evidence that AA is the relevant lipid released by ATGL. It will be important to determine how widely used this new signaling pathway is, given the strong potential for PGs to be playing roles in tissues with known ATGL functions.

*LDs regulate actin remodeling via multiple mechanisms*

ATGL is not the only LD protein promoting actin remodeling in nurse cells. The actin cytoskeleton is similarly disturbed in mutants that lack two other LD proteins, Jabba and PLIN2 (Fig 3). Our genetic interaction tests suggest that PLIN2 affects actin remodeling via a mechanism that does not involve PGs (Fig 5) and that Jabba and ATGL act in distinct PG-dependent pathways (Fig 7). Thus, neither PLIN2 nor Jabba are likely to regulate ATGL activity, suggesting the existence of additional mechanisms by which LDs control actin remodeling in nurse cells.

One such mechanism might be an alternate means of generating AA. This possibility seems unlikely for PLIN2 since there is no genetic interaction with Pxt. Jabba, however, might regulate a distinct lipase pathway that acts in parallel to ATGL to release AA. Indeed, Jabba has been proposed to regulate lipid metabolism in the ovary [38]. Jabba recruits numerous proteins to LDs [32, 33], which might include lipases or their regulators, such as the ATGL paralog Dob [42] or a cPLA2 ortholog. Another intriguing candidate is Hsl, an enzyme involved in the breakdown of sterol esters in *Drosophila* [83]. Hsl is among the most abundant proteins on maternally inherited LDs of early embryos [32], and its substrates, sterol esters, are present in ovary LDs (Fig 1K and 8E-8F).

Jabba might alternatively regulate the localization of PG synthesis machinery. The direct product of COX-like Pxt is the intermediate $PGH_2$ which is then converted by various synthases into PGs with distinct functions. Previous work suggests that Stage 9 follicles produce an

unknown PG that inhibits actin remodeling, while during Stage 10B $PGF_{2\alpha}$ promotes remodeling [84]. Because Pxt relocalizes from the Golgi to the ER during this time (Fig 6), we hypothesize that these two compartments recruit different PG synthases, leading to the production of distinct PGs. If this hypothesis is correct, a role of Jabba might be to directly or indirectly control the targeting of PG synthases between these compartments, e.g., Jabba might recruit certain synthases to ER regions adjacent to LDs. Intriguingly, work in mammalian systems has suggested that spatial segregation of PG synthesis enzymes between Golgi and ER is functionally important [85].

A final possibility is that PLIN2 or Jabba regulate actin dynamics by recruiting actin and actin binding proteins to LDs. Actin and actin-regulators have been found in purified LD preparations in numerous biochemical and proteomic studies [e.g., 86, 87-89]. LDs might therefore regulate the concentration of these molecules free in the cytosol and thus their availability for actin assembly. If Jabba's ability to recruit these proteins is regulated by PG signaling, it would explain how Pxt and Jabba act in the same pathway. Further, since LDs are highly motile [88], including in nurse cells [1], they may deliver actin and its binding partners to sites of actin remodeling within the cell. Intriguingly, PLIN2 regulates LD transport during early *Drosophila* embryogenesis [90], and the extensive LD clustering in *Jabba* mutants may interfere with their motility (Fig 4C-4C", 4F).

While many questions remain, our findings have uncovered a critical role of LD proteins in regulating actin cytoskeletal remodeling. Given the conservation of ATGL and PLIN2 protein and metabolic functions, it is likely this new actin regulatory function is also conserved across organisms.

*LD dispersal*

The intracellular distribution of LDs is highly regulated and can change with the cell cycle, developmental stage, and nutritional state [88, 91]. We find that PG signaling promotes LD

547 dispersal as loss of Pxt causes severe LD clustering in Stage 10B (Fig 4B-4B', 4F). Because LD
548 clustering also occurs after just ~1hr treatment with the COX inhibitor aspirin (Fig 4G, 4H-H"),
549 this phenotype is indeed due to loss of PG synthesis and signaling within the follicle, and is not
550 an artifact of poor health of the follicles. These findings are exciting as there is little evidence yet
551 in the literature that PGs regulate LDs. One study implicated $PGE_2$ signaling in inhibiting
552 triglyceride storage in LDs in white adipose tissue [92]. Conversely, in granulosa cells of
553 periovulatory follicles, $PGE_2$ upregulates PLIN2 [93]. And in human trophoblastic cells, COX2
554 inhibition reduces LD production induced by the intracellular parasite *Toxoplasma gondii* [94].
555 These limited studies suggest that PGs may have cell-type specific roles in regulating LD
556 dynamics and lipid storage. Our results now reveal a dramatic effect of PGs on the spatial
557 distribution of LDs in a genetically tractable model, setting the stage for a mechanistic dissection
558 in the future.

559 PGs may regulate LD distribution by controlling actin dynamics. Indeed, actomyosin is
560 known to regulate LD transport, distribution, and shape from plants to mammals [95-97]. In
561 osteosarcoma cells, non-muscle myosin-dependent actin remodeling is required to drive
562 clustered LDs apart [87]. Whether actin cytoskeletal dynamics regulate LDs during *Drosophila*
563 oogenesis is unknown, but it is tempting to speculate that the LD clustering observed in *pxt*
564 mutants is due to defective actin remodeling. Indeed, evidence suggests that PGs promote
565 myosin activity during Stage 10B [98]. Alternatively, PGs may control ER integrity and/or LD
566 biogenesis or lipolysis and thereby regulate LD distribution.

567 We also find that LD proteins regulate LD distribution. Specifically, loss of PLIN2 or
568 Jabba causes dramatically clustered LDs (Fig 4). In embryos, LDs are normally dispersed in
569 *PLIN2* mutants [90] and less dramatically clustered in *Jabba* mutants [33], suggesting that these
570 proteins promote oogenesis-specific dispersal. A key question is whether the LD clustering is
571 related to the disrupted actin remodeling observed in the LD protein mutants. We deem this
572 unlikely, as the severity of LD clustering does not correlate with the level of actin defects when

the LD proteins are lost. For example, *Jabba* mutants have mild actin defects, but severe LD clustering, whereas *ATGL* mutants have limited LD clustering and severe actin defects (Figs 3, 4, 5, and 7). Thus, we favor the model that the LD proteins regulate LD clustering at least in part independently of PG signaling controlled actin remodeling.

Live imaging of *ex vivo* follicles and inhibition of various cytoskeletal components will likely be critical to determine how LD clustering arises. For example, clustering may arise during LD biogenesis, if LDs originate from a limited region of the ER and do not disperse. *PLIN2* mutants have been proposed to exhibit LD biogenesis defects in nurse cells [18]. If like in oocytes and embryos, nurse cell LDs move along microtubules, defects in the arrangement of microtubules or in kinesin-1 and cytoplasmic dynein activity could also induce clustering [99-101]. PLIN2 regulates the relative activity of these motors on embryonic LDs [90]. Alternatively, if like in osteosarcoma cells, LDs nucleate actin filaments to segregate from each other [87], Jabba and PLIN2 may recruit actin and actin-regulators, and PG signaling may regulate their actin remodeling activity.

*LDs as regulators of development and female fertility*

Animal development requires careful regulation of metabolism, specific to tissue type and developmental stage [102]. Yet despite the fact that LDs have a central role in lipid metabolism and energy homeostasis in normal physiology and diseases [10, 11, 103], they have so far been implicated as regulators of development in only a handful of cases [23, 33, 37, 104]. Our analysis now reveals that LDs not only play a critical role at a specific transition during follicle development, but identifies PG signaling as one of the mechanisms by which they exert their regulatory role.

We speculate that this pathway is conserved across organisms. Indeed, LD accumulation, composition, and localization are dynamic during oocyte maturation [4, 12], LDs are hubs for FA trafficking, and FA levels (including that of AA) are critical for oocyte

development in many species [7, 13, 105]. Further, in both mouse models and human patients, metabolic syndrome causes LD clustering in oocytes, failures in oocyte maturation, and decreased fertility [13-15, 106, 107]. But does this relate to PG signaling? It is already well-established that PG signaling plays critical roles in oocyte development across organisms [108-114]. Recent evident implicates LDs as a foci of PG production during reproduction. For example, COX enzymes localize to LDs in the rat corpus luteum [115], and in fetal membranes during advanced gestation and at induction of labor, times when PG synthesis and signaling are upregulated [116, 117]. In mammals, it is not yet known whether the PG effects on oogenesis and reproduction are due to changes in the actin cytoskeleton. However, cytoplasmic actin density and cortical actin thickness increase during oocyte maturation, contribute to meiotic resumption, and play roles in fertilization and early embryonic divisions [118, 119]. Given these data, and our findings connecting LDs, PG signaling, and actin remodeling during *Drosophila* oogenesis, we speculate the same pathways that regulate oocyte development in the fly are conserved across organisms to regulate oocyte development, and contribute to infertility issues due to limited or excess nutrition.

## Materials and Methods

### *Fly stocks*

Flies used in actin quantification and *in vitro* egg maturation experiments were maintained on cornmeal/agar/yeast food at room temperature except as noted below. Flies used in all other experiments were maintained on molasses/agar/yeast/malt extract/corn flour/soy flour food at room temperature except as noted below. Stocks used were $y^1w^1$ (BDSC1495), Oregon R (BDSC 5), $pxt^{f01000}$ (Harvard Exelixis Collection, [120]), $pxt^{EY03052}$ (BDSC 15620), $Jabba^{DL}$ [33], $Jabba^{z101}$ [33], $bmm^1$ [34], $Lsd\text{-}2^{KG00149}$ (BDSC13382), *osk3-GAL4* (BDSC 44242), *DGAT1 RNAi* (TRiP.HMC06242, BDSC 65963), $mdy^{QX25}$ (BDSC5095), $mdy^{RF48}$ [16], *mat-alpha4 GAL4-VP16*

(BDSC 7063), *Lsd-2* RNAi (TRiP.HMS00629, BDSC 32846), *Lsd-2 RNAi* (TRiP.HMS01292, BDSC 34617), *sqh-EYFP-ER* (BDSC7195, [121]), and *sqh-EYFP-Golgi* (BDSC7193, [121]). For the *DGAT1* RNAi germline knockdown, either mat-alpha4 GAL4-VP16>*DGAT1* RNAi or *osk3-GAL4>DGAT1* RNAi crosses were performed at room temperature. For mat-alpha4-GAL4 knockdown, adult progeny were shifted to 29°C for 5 days and were fed on wet yeast paste (paste replaced once on day 2 or 3). For *osk3-GAL4* knockdown, progeny were fed wet yeast paste at room temp for 48 hours, then shifted to 29ºC for 24 hours. Ovaries were subsequently dissected and treated as described.

*Immunofluorescence and fluorescent reagent staining*

For Figures 1, 2, 4, 6, and Supplemental Figure 4 the following method, referred to as Staining Method 1, was used. Adult female and male flies (to allow for mating) younger than two weeks old were fed dry yeast for 48 hours at room temperature before ovary dissection in PBS-T (phosphate buffered saline, 0.1% Triton X-100), except for RNAi knockdown as noted above. Ovaries were fixed with 3.6% formaldehyde in PBS for 12 minutes at room temperature. Ovaries were washed with PBS-T, and follicles of desired stages were isolated using forceps and pin vises. Follicles were blocked in ovary block (10% BSA, PBS, 0.1% Triton X-100, 0.02% sodium azide) overnight at 4°C. Primary antibodies were diluted in ovary block and incubated overnight at 4°C. The following primary antibodies were obtained from the Developmental Studies Hybridoma Bank (DSHB) developed under the auspices of the National Institute of Child Health and Human Development and maintained by the Department of Biology, University of Iowa (Iowa City, Iowa): mouse anti-Calnexin99A at 1:1000 (Cnx99A 6-2-1, Munro, S.) and mouse anti-Golgin84 at 1:1000 (Golgin84 12-1, Munro, S.) [122]. Additionally, the following primary antibodies were used: rabbit anti-Jabba preabsorbed at 1:10 against *Jabba -/-* embryos in ovary block and used at 1:1000 [37] and rabbit anti-Pxt preabsorbed at 1:10 on *pxt-/-* ovaries in ovary block and used at 1:1000 [84]. Samples were washed 3x with PBS-T, and then protected from

light for the remainder of the experiment. Samples were incubated in the following secondary antibodies diluted to 1:1000 in ovary block overnight at 4°C: goat anti-rabbit IgG Alexa Fluor 633 (Invitrogen), goat anti-mouse IgG Alexa Fluor 488 (Invitrogen), and goat anti-rabbit IgG Alexa Fluor 488 (Invitrogen). Samples were washed 3x with PBS-T and then stained with the following reagents diluted in ovary block: Phalloidin Alexa Fluor 633 (Invitrogen) 1:150, 1 hour at room temperature; Nile Red (1 mg/ml, Sigma-Aldrich) 1:50, 1 hour at room temperature; and Hoechst 33342 (1 mg/ml, Thermo Fisher Scientific) 1:1000, 20 minutes room temperature. Samples were washed 3x with PBS-T, and then mounted on coverslips in Aqua Polymount (PolySciences).

For Figures 3, 5, 7, 9, and Supplemental Figures 1 and 5 the following protocol, referred to as Staining Method 2, was used: Adult female and male flies (to allow for mating) within 24hrs of eclosion were fed wet yeast paste for 72 hours at room temperature before dissection in room-temperature Grace's medium (Lonza). Ovaries were fixed in 4% paraformaldehyde in Grace's medium for 10 minutes at room temperature. Ovaries were washed 6x 10 minutes in antibody wash (1X PBS-T + 0.1% Bovine Serum Albumin (BSA)). Samples were stained overnight at 4°C with Alexa Fluor-488, -568, or -647 Phalloidin (Invitrogen) at 1:250. Samples were then washed 5-6 times in 1X PBS for 10 minutes each and stained with 4'6'-diamidino-2-phenylindole (DAPI, 5 mg/mL) at 1:5000 in 1X PBS for 10 minutes. Samples were rinsed in 1X PBS and mounted in 1 mg/mL phenylenediamine in 50% glycerol, pH 9 [123].

*Image acquisition and processing*

Microscope images of fixed and stained *Drosophila* follicles were obtained using the following microscopes: Leica SPE confocal microscope with an ACS APO x20/0.60 IMM CORR-/D or ACS APO x40/1.5 oil CS objective (Leica Microsystems), Zeiss 700 confocal microscope or Zeiss 880 confocal microscope (Carl Zeiss Microscopy) using a Plan-Apochromat x20/0.8 working distance (WD)=0.55 M27 objective, or Leica SP5 confocal microscope (Leica Microsystems) using an HCX PL APO CS 63.0x1.40 oil UV objective and Leica HyD detectors.

Maximum projections of images, image cropping, and image rotation were performed in Fiji/ImageJ software [124], scale bars were added in either Adobe Illustrator or Adobe Photoshop (Adobe, San Jose, CA) and figures were assembled using Adobe Illustrator. Images in Figures 3, 5, 7, and Supplemental Figures 1 and 5 were brightened by 30% and images in Figure 9 were brightened 70% in Adobe Photoshop to improve visualization.

*Quantification of actin defects*

Confocal images of phalloidin stained Stage 10B follicles were collected as described. Actin bundle and cortical actin defects were scored by scanning through confocal z-stacks of Stage 10B follicles in ImageJ in a genotypically blinded manner. Representative images of follicles and scoring criteria are provided in Supplemental Figure 1. Briefly, actin bundles were scored as normal (score = 0) if they were straight, forming from the nurse cell plasma membrane and oriented inwards toward the nurse cell nuclei. Mild defects in bundling (score = 1) were defined as sparse bundle formation or slight delay in bundle growth relative to follicle development. Moderate defects (score = 2) were defined as collapsed, thick, and/or missing bundles from regions of the nurse cell plasma membrane. Severe defects (score=3) included those previously described, as well as a complete failure of bundles to form. Cortical actin was scored based on whether the cortical actin was intact or disrupted. Defects in cortical actin are evident by an absence or incomplete phalloidin staining between nurse cells and/or by nurse cell nuclei in close proximity or contacting each other. Normal cortical actin (score = 0) is defined as being completely intact and fully surrounding each nurse cell. Degree of severity of cortical actin defect was determined by the relative number of disruptions in cortical actin observed with mild defects (score=1) having a single instance, moderate defects (score=2) having two instances, and severe defects (score = 3) having three or more instances of disrupted cortical actin. The actin defect index (ADI) was then calculated by adding the bundle and cortical actin defect scores and binning them into normal (total score = 0-1), mildly defective (total score = 2-3), or

703 severely defective (score = 4-6). Pearson's chi-squared analysis was performed using R
704 (www.r-project.org).
705
706 *In vitro egg maturation (IVEM) assay*
707 Adult female and male flies (to allow for mating) within 24hrs of eclosion were fed wet yeast
708 paste daily for 3 days prior to dissection. Ovaries were dissected in room temperature Grace's
709 medium (Lonza) containing 1x penicillin/streptomycin (100x, Gibco) and either 10% (S7 Fig) or
710 2.5% (Fig 9) fetal bovine serum (FBS, Atlanta Biologicals); this is termed IVEM medium. Stage
711 10B follicles were isolated and distributed between wells of a 24-well plastic tissue culture plate
712 (Falcon) and 1ml of fresh media was added with no additions (S7 Fig), arachidonic acid (AA,
713 Cayman Chemicals) diluted in 100% ethanol (EtOH) at the final concentrations listed, or an
714 equivalent amount of EtOH. Follicles were incubated overnight at room temperature in the dark.
715 The next day the number of follicles at each developmental stage were counted, and the
716 percentage developing was calculated; follicles that reached Stage 12 and older were
717 considered developed. For Supplemental Figure 7, the percent developing was normalized for
718 each experiment to the percent of wild-type follicles developing. Statistical analysis was
719 performed using the paired t-test function in Prism 8 (GraphPad Software).
720
721 *Aspirin or arachidonic treatment, staining, and phenotypic quantification of follicles*
722 Adult female and male flies (to allow for mating) within 24hrs of eclosion were fed wet yeast
723 paste daily for 3 days prior to dissection. Ovaries were dissected in room temperature Grace's
724 medium containing 1x penicillin/streptomycin and either 10% (Fig 4) or 2.5% (Fig 9) FBS. Stage
725 10B follicles were isolated and transferred to wells of a 24 well plastic cell culture plate. Fresh
726 medium was added to each well, to which 3mM aspirin (Cayman Chemicals) dissolved in EtOH
727 or DMSO, 500μM AA (dissolved in EtOH), or the same volume of solvent was added. Follicles
728 were incubated at room temperature in the dark for 1-1.5 hours. For Figure 4, samples were

729 stained with Phalloidin and Nile Red as described above in Staining Method 1. For Figure 9, the
730 medium was removed and follicles were fixed in 4% paraformaldehyde in 1X PBS for 10
731 minutes. Follicles were washed 3 times in PBS-T and stained for 2 hours at room temperature
732 with Nile Red 1:5000 (1 mg/mL) and Alexa 647 Phalloidin 1:250 (Invitrogen). Follicles were then
733 stained with DAPI (5 mg/mL) at 1:5000 in 1X PBS for 10 minutes and then washed 2 times in
734 1X PBS. Samples were mounted in Aqua-Polymount (PolySciences, Inc.).
735 Confocal images of Stage 10B follicles were scored in a genotypically blinded manner
736 for LD clustering and actin defects. LD clustering was scored based on the penetrance of the
737 phenotype with normal defined as ≤2 nurse cells exhibiting clustering, mild being defined as 3 to
738 4 nurse cells with clustering, and severe defined as >4 nurse cells with clustering. Follicles were
739 scored as having actin defects if actin bundle defects and/or disrupted cortical actin were
740 observed. Pearson's chi squares analysis was performed using R.
741
742 *Western blots*
743 Follicles from well-fed females of the indicated genotypes and stage were dissected and fixed
744 as described in Staining Method 1. Note that proteins from such samples run at the same
745 molecular weight as those from lysates prepared from live ovary tissue (S8 Fig). 25-50 follicles
746 were collected per sample and boiled in sample buffer (Laemmli Sample Buffer, Bio-Rad + 2-
747 mercaptoethanol, Bio-Rad). Samples were run on 4-15% gradient gels (Bio-Rad) at 80-120V
748 and transferred onto PVDF membrane (Immobilon-FL, EMD Millipore) in either Towbin (10%
749 Tris-Glycine + 20% MeOH; 80V for 30 minutes; for anti-PLIN2, anti-Pxt, anti-Calnexin) or CAPS
750 (Sigma-Aldrich; 10mM CAPS + 20% MeOH; 50V for 40 minutes; for anti-Jabba) transfer buffer.
751 Membranes were blocked for 1 hour at room temperature in Li-COR Odyssey Block (LI-COR
752 Biosciences). Primary antibodies diluted in Odyssey Block were performed overnight at 4
753 degrees. The following primary antibodies were used rabbit anti-Jabba (1:5000) [37], rabbit anti-
754 Pxt (1:5000) [84], rabbit anti-PLIN2 (1:5000) [90], mouse anti-Calnexin99A (1:5000, DSHB),

Mouse anti-α-Tubulin (1:5000, Cell Signaling Technologies). Before use, anti-Jabba had been preabsorbed against PVDF membranes with samples from *Jabba -/-* ovaries. Membranes were washed 3 times in 1X PBS-0.1% Tween 20 (PBS-Tween). The following secondary antibody incubations were performed for 1 hour at room temperature: IRDye 800CW Goat anti-Rabbit IgG (1:5000, Li-COR), and IRDy3 680RD Goat anti-Mouse IgG (1:5000, Li-COR). After secondary antibody incubation, membranes were washed two times in PBS-Tween and once in 1X PBS. Membranes were imaged on a Li-COR Odyssey CLx imager and blots were processed and quantified in Image Studio Lite 5.2 (Li-COR). To quantify, fluorescence intensity of each band was measured and normalized to respective experimental controls. Data were analyzed and plotted using Prism (GraphPad).

**S8 Fig. Immunoblots comparing live vs. fixed samples.** (**A-C)** Three simultaneously scanned immunoblots comparing the blotting patterns of live versus formaldehyde fixed wild-type whole-ovary samples, 5 ovaries per lane. **(A)** anti-Jabba immunoblot. **(B)** anti-Pxt immunoblot. **(C)** anti-PLIN2 immunoblot. The live vs. fixed banding pattern is comparable for all three antibodies tested. Fixed samples were used in S1 and S2 Fig immunoblots.

*Ovary centrifugation*

Mated adult females of mixed ages fed dry yeast were anesthetized and beheaded before being mounted in Eppendorf tubes filled with 2.5% apple juice agar as described in [125]. Tubes were spun for 10 minutes at 10,000 rpm at room temperature using an Eppendorf Microcentrifuge (Model 5415D). Flies were removed from agar with forceps and ovaries were isolated and treated as described in Staining Method 1 above.

*Lipid droplet purification*

250-300 ovaries per sample were rapidly dissected from mated and dry yeast fed females and kept on ice in TSS (68 mM Na $Cl_2$, 0.03% Triton X-100) in 2mL Eppendorf tubes. Ovaries were then washed 3x with TKM (50 mM Tris, pH 7.4, 25 mM KCl, 5 mM $MgCl_2$) to remove detergent.

778 TKM was removed and the volume of ovaries was estimated visually. Ovaries were kept on ice,
779 to which were added: 2 times the estimated ovary volume of TKM + 1M sucrose, protease
780 inhibitor cocktail to final concentration of 1X protease inhibitor cocktail (Sigma-Aldrich), and
781 calyculin A serine/threonine phosphatase inhibitor (10µL per mL of volume; Cell Signaling).
782 Ovaries were homogenized on ice by grinding with an automated tissue grinder (KONTES pellet
783 pestle) for 1-2 minutes, and then 20µL ovary lysate samples were transferred from the total
784 lysate to 0.65mL Eppendorf tubes and stored at -80°C. The remaining ovary lysates were spun
785 at 13200rpm for 10 minutes in an Eppendorf Microcentrifuge (Model 5145D) at 4°C. The
786 following was then added to samples slowly to avoid disturbing the LD layer: 300µL TKM + 0.5M
787 sucrose, 300µL TKM + 0.25M sucrose, 400µL TKM (no sucrose). Tubes were spun for 20
788 minutes at 4°C, with the speed adjusted as follows: 1000rpm for 5 minutes, 5000rpm for 5
789 minutes, 13200rpm for 10 minutes. Purified LDs were then scooped off the top of the sucrose
790 gradient using a drawn Pasteur pipette loop (Fisher Scientific, loop drawn by holding over a
791 flame). LDs were washed off the pipette loop with 20µL TKM (no sucrose) and stored at -80°C
792 until analyzed.
793 In past Western analyses, we loaded equal amounts of protein from LD preparations and
794 original tissue lysate for easy comparison [33]. This approach was not feasible here because of
795 the relatively low amounts of LDs recovered from the large volume of ovaries used. Instead, we
796 compared the LD sample to dilutions of ovary lysate. Purified LDs and ovary lysates were
797 diluted as indicated in 2X Laemmli Sample Buffer before being boiled for 30 minutes and
798 subsequently run on 4-15% SDS-PAGE gradient gels (Western blot protocol as described
799 above). Before the blocking step, the membrane was cut with a razor blade between 50 and
800 75kDa and each half was treated separately. Quantification was performed as described above
801 in Western blots.
802
803 *Lipid extractions*

804 25 ovaries per sample were dissected from mated, mixed-age, and dry yeast fed females and
805 homogenized in a 2mL Eppendorf tube with a motorized pestle (KONTES pellet pestle) in 1X
806 PBS and kept on ice. Lysates were then incubated 1:1 in a 2:1 chloroform/methanol mixture
807 overnight at 4°C. Samples were spun in an Eppendorf Microcentrifuge (model 5415D) at max
808 speed at room temperature for 1 minute, and the bottom organic layer was transferred to an
809 0.65mL Eppendorf tube. Samples were then vacuum dried and either analyzed immediately or
810 stored at -80°C for thin layer chromatography (TLC) analysis, or stored at -80°C before being
811 shipped on dry ice for mass spectrometry analysis.
812
813 *Thin layer chromatography*
814 Evaporated lipids were resuspended in 10µL 2:1 chloroform/methanol and spotted on
815 dehydrated silica plates (EMD Millipore; dehydrated by baking for 30 minutes at 100°C). Plates
816 were placed in a chamber (Millipore Sigma/Sigma-Aldrich Z266000) pre-saturated for 30
817 minutes with Petroleum Ether/Diethyl Ether/acetic acid (32:8:0.8)) and allowed to develop until
818 the solvent almost reached the top of the plates, and the solvent line was quickly marked with a
819 pencil after removing plates from the chamber. The plates were then air-dried and briefly
820 submerged in charring solution (50% ethanol, 3.2% $H_2SO_4$, 0.5% $MgCl_2$). Plates were air-dried
821 briefly and were charred for 30 minutes at 120°C. Plates were imaged using a Bio-Rad Gel Doc
822 and bands were quantified using Fiji. Lipids were identified according to Knittelfelder & Kohlwein
823 [126] and by comparing whole lipid extracts to lipid standards (Millipore Sigma, data not shown).
824 Colorimetric band intensities were quantified in Fiji and triglyceride or sterol ester bands were
825 normalized to cholesterol band intensity. Statistical tests were run in GraphPad Prism as
826 follows: Figure 2D, Sidak's multiple comparisons test and Figure 8F, Dunnett's multiple
827 comparisons test.
828
829 *LC-MS/MS Mass Spectrometry Analysis*

Extracted lipids were dissolved in corresponding volumes of 2:1 methanol:chloroform (v/v) and 5 µl of each sample was injected for positive and negative acquisition modes, respectively. Mobile phase A consisted of 3:2 (v/v) water/acetonitrile, including 10 mM ammonium formate and 0.1% formic acid, and mobile phase B consisted of 9:1 (v/v) 2- propanol/acetonitrile, also including 10 mM ammonium formate and 0.1% formic acid. Lipids were separated using an UltiMate 3000 UHPLC (Thermo Fisher Scientific) under a 90 min gradient; during 0–7 minutes, elution starts with 40% B and increases to 55%; from 7 to 8 min, increases to 65% B; from 8 to 12 min, elution is maintained with 65% B; from 12 to 30 min, increase to 70% B; from 30 to 31 min, increase to 88% B; from 31 to 51 min, increase to 95% B; from 51 to 53 min, increase to 100% B; during 53 to 73 min, 100% B is maintained; from 73 to 73.1 min, solvent B was decreased to 40% and then maintained for another 16.9 min for column re-equilibration. The flow-rate was set to 0.2 mL/min. The column oven temperature was set to 55° C, and the temperature of the autosampler tray was set to 4° C. Eluted lipids were analyzed using Orbitrap Q Exactive (Thermo Fisher Scientific) Orbitrap mass analyzer. The spray voltage was set to 4.2 kV, and the heated capillary and the HESI were held at 320° C and 300° C, respectively. The S-lens RF level was set to 50, and the sheath and auxiliary gas were set to 35 and 3 units, respectively. These conditions were held constant for both positive and negative ionization mode acquisitions. External mass calibration was performed using the standard calibration mixture every 7 days. MS spectra of lipids were acquired in full-scan/data-dependent MS2 mode. For the full-scan acquisition, the resolution was set to 70,000, the AGC target was 1e6, the maximum integration time was 50 msec, and the scan range was m/z = 133.4–2000. For data-dependent MS2, the top 10 ions in each full scan were isolated with a 1.0 Da window, fragmented at a stepped normalized collision energy of 15, 25, and 35 units, and analyzed at a resolution of 17,500 with an AGC target of 2e5 and a maximum integration time of 100 msec. The underfill ratio was set to 0. The selection of the top 10 ions was subject to isotopic exclusion with a dynamic exclusion window of 5.0 sec. Mass spectrometry data was analyzed using

LipidSearch version 4.1 SP (Thermo Fisher Scientific). Identified lipid species with grade A and B were manually curated. A total of 98 different triglyceride species were identified (STable 1).

For the quantitative analysis in Figures 8A-AD, 8G-H and Supplemental Figure 6, four ovaries each from wild-type and *ATGL* mutant females were analyzed and the quantity of the 98 triglyceride species determined, relative to background. One wild-type sample contained an order of magnitude less lipid and was discarded as an outlier (STable 1). In total, 25 different types of FAs were identified in the ovary triglycerides. The abundance of each FA was estimated by summing the amount of each triglyceride species containing that FA, weighted by how many times that FA is represented in that triglyceride. For Figures 8A-8B, this abundance is expressed as fraction of the total amount of fatty acids such identified. For Figure 8C, the signal for all species of phosphatidylcholine, phosphatidylethanolamine, and phosphatidylinositol, respectively, was summed and normalized to the average of the wild type. For Figure 8D, the signal for all triglyceride species was summed and normalized to the average of the wild type. To express the abundance of various lipid species relative to total lipids recovered (S6 Fig), values for various lipid species were divided by the sum of all lipids in the sample. For Figure 8G and 8H, the signal for two AA-containing triglyceride species was computed, and normalized to the average of the wild-type signal. Amounts and fractions were calculated using Microsoft Excel and graphed using Prism 8 (GraphPad Software). Statistical tests for Figure 8 were as follows: 8A and 8C was Sidak's multiple comparisons test, 8B was Tukey's multiple comparisons test, 8D was an unpaired t-test, two-tailed, and 8G-H were unpaired t-tests, two-tailed.

**Acknowledgements:** We thank the Dunnwald lab for helpful discussions, and Dr. Martine Dunnwald, the Tootle lab and the Welte lab for helpful discussions and careful review of the manuscript. We are grateful to Marcus Kilwein for help with thin layer chromatography. We thank the Harvard T.H. Chan Advanced Multi-omics Platform at the Harvard T.H. Chan School

882 of Public Health for performing the lipidomics analysis. Stocks obtained from the Bloomington
883 Drosophila Stock Center (NIH P40OD018537) were used in this study. At the University of Iowa,
884 Information Technology Services – Research Services provided data storage support**.** This
885 project is supported by National Institutes of Health (NIH) R01 GM116885 (T.L.T.) and R01
886 GM12155 (M.A.W), as well as a PumpPrimerII grant from the University of Rochester (M.A.W).
887 M.S.G. was partially supported by NIH T32 CA078586 Free Radical and Radiation Biology,
888 University of Iowa.
889

## References


1. Lu W, Lakonishok M, Gelfand VI. Gatekeeper function for Short stop at the ring canals of the Drosophila ovary. Curr Biol. 2021. Epub 2021/06/06. doi: 10.1016/j.cub.2021.05.010. PubMed PMID: 34089646.
2. National Public Health Action Plan for the Detection, Prevention, and Management of Infertility. . Atlanta, Georgia: Centers for Disease Control and Prevention; 2014.
3. Brusentsev EY, Mokrousova VI, Igonina TN, Rozhkova IN, Amstislavsky SY. Role of Lipid Droplets in the Development of Oocytes and Preimplantation Embryos in Mammals. Russian Journal of Developmental Biology. 2019;50(5):230-7. doi: 10.1134/S1062360419050102.
4. Dunning KR, Russell DL, Robker RL. Lipids and oocyte developmental competence: the role of fatty acids and beta-oxidation. Reproduction. 2014;148(1):R15-27. Epub 2014/04/25. doi: 10.1530/REP-13-0251. PubMed PMID: 24760880.
5. Dunning KR, Akison LK, Russell DL, Norman RJ, Robker RL. Increased beta-oxidation and improved oocyte developmental competence in response to l-carnitine during ovarian in vitro follicle development in mice. Biol Reprod. 2011;85(3):548-55. Epub 2011/05/27. doi: 10.1095/biolreprod.110.090415. PubMed PMID: 21613630.
6. Dunning KR, Cashman K, Russell DL, Thompson JG, Norman RJ, Robker RL. Beta-oxidation is essential for mouse oocyte developmental competence and early embryo development. Biol Reprod. 2010;83(6):909-18. Epub 2010/08/06. doi: 10.1095/biolreprod.110.084145. PubMed PMID: 20686180.
7. Prates EG, Nunes JT, Pereira RM. A role of lipid metabolism during cumulus-oocyte complex maturation: impact of lipid modulators to improve embryo production. Mediators Inflamm. 2014;2014:692067. Epub 2014/04/16. doi: 10.1155/2014/692067. PubMed PMID: 24733963; PubMed Central PMCID: PMCPMC3964899.
8. Tootle TL. Genetic insights into the in vivo functions of prostaglandin signaling. The international journal of biochemistry & cell biology. 2013;45(8):1629-32. Epub 2013/05/21. doi: 10.1016/j.biocel.2013.05.008. PubMed PMID: 23685076.
9. Sugimoto Y, Inazumi T, Tsuchiya S. Roles of prostaglandin receptors in female reproduction. J Biochem. 2015;157(2):73-80. Epub 2014/12/07. doi: 10.1093/jb/mvu081. PubMed PMID: 25480981.
10. Walther TC, Farese RV, Jr. Lipid droplets and cellular lipid metabolism. Annu Rev Biochem. 2012;81:687-714. doi: 10.1146/annurev-biochem-061009-102430. PubMed PMID: 22524315; PubMed Central PMCID: PMCPMC3767414.
11. Welte MA. Expanding roles for lipid droplets. Curr Biol. 2015;25(11):R470-81. Epub 2015/06/03. doi: 10.1016/j.cub.2015.04.004. PubMed PMID: 26035793; PubMed Central PMCID: PMCPMC4452895.
12. Ami D, Mereghetti P, Natalello A, Doglia SM, Zanoni M, Redi CA, et al. FTIR spectral signatures of mouse antral oocytes: molecular markers of oocyte maturation and developmental competence. Biochim Biophys Acta. 2011;1813(6):1220-9. Epub 2011/03/26. doi: 10.1016/j.bbamcr.2011.03.009. PubMed PMID: 21435359.
13. Cardozo E, Pavone ME, Hirshfeld-Cytron JE. Metabolic syndrome and oocyte quality. Trends Endocrinol Metab. 2011;22(3):103-9. Epub 2011/02/01. doi: 10.1016/j.tem.2010.12.002. PubMed PMID: 21277789.
14. Jungheim ES, Schoeller EL, Marquard KL, Louden ED, Schaffer JE, Moley KH. Diet-induced obesity model: abnormal oocytes and persistent growth abnormalities in the offspring. Endocrinology. 2010;151(8):4039-46. Epub 2010/06/25. doi: 10.1210/en.2010-0098. PubMed PMID: 20573727; PubMed Central PMCID: PMCPMC2940512.
15. Marei WFA, Smits A, Mohey-Elsaeed O, Pintelon I, Ginneberge D, Bols PEJ, et al. Differential effects of high fat diet-induced obesity on oocyte mitochondrial functions in

inbred and outbred mice. Sci Rep. 2020;10(1):9806. Epub 2020/06/20. doi: 10.1038/s41598-020-66702-6. PubMed PMID: 32555236; PubMed Central PMCID: PMCPMC7299992.

16. Buszczak M, Lu X, Segraves WA, Chang TY, Cooley L. Mutations in the midway gene disrupt a Drosophila acyl coenzyme A: diacylglycerol acyltransferase. Genetics. 2002;160(4):1511-8. Epub 2002/04/26. PubMed PMID: 11973306; PubMed Central PMCID: PMCPMC1462074.
17. Buszczak M, Cooley L. Eggs to die for: cell death during Drosophila oogenesis. Cell Death Differ. 2000;7(11):1071-4. Epub 2001/01/04. doi: 10.1038/sj.cdd.4400755. PubMed PMID: 11139280.
18. Teixeira L, Rabouille C, Rorth P, Ephrussi A, Vanzo NF. Drosophila Perilipin/ADRP homologue Lsd2 regulates lipid metabolism. Mech Dev. 2003;120(9):1071-81. Epub 2003/10/11. doi: 10.1016/s0925-4773(03)00158-8. PubMed PMID: 14550535.
19. Guild GM, Connelly PS, Shaw MK, Tilney LG. Actin filament cables in Drosophila nurse cells are composed of modules that slide passively past one another during dumping. J Cell Biol. 1997;138(4):783-97. Epub 1997/08/25. doi: 10.1083/jcb.138.4.783. PubMed PMID: 9265646; PubMed Central PMCID: PMCPMC2138051.
20. Huelsmann S, Ylanne J, Brown NH. Filopodia-like actin cables position nuclei in association with perinuclear actin in Drosophila nurse cells. Developmental cell. 2013;26(6):604-15. Epub 2013/10/05. doi: 10.1016/j.devcel.2013.08.014. PubMed PMID: 24091012; PubMed Central PMCID: PMCPMC3791400.
21. Wheatley S, Kulkarni S, Karess R. Drosophila nonmuscle myosin II is required for rapid cytoplasmic transport during oogenesis and for axial nuclear migration in early embryos. Development. 1995;121(6):1937-46. Epub 1995/06/01. PubMed PMID: 7601006.
22. Parra-Peralbo E, Culi J. Drosophila lipophorin receptors mediate the uptake of neutral lipids in oocytes and imaginal disc cells by an endocytosis-independent mechanism. PLoS Genet. 2011;7(2):e1001297. Epub 2011/02/25. doi: 10.1371/journal.pgen.1001297. PubMed PMID: 21347279; PubMed Central PMCID: PMCPMC3037410.
23. Stephenson RA, Thomalla JM, Chen L, Kolkhof P, White RP, Beller M, et al. Sequestration to lipid droplets promotes histone availability by preventing turnover of excess histones. Development. 2020.
24. McCall K. Eggs over easy: cell death in the Drosophila ovary. Dev Biol. 2004;274(1):3-14. Epub 2004/09/10. doi: 10.1016/j.ydbio.2004.07.017. PubMed PMID: 15355784.
25. Spracklen AJ, Tootle TL. Drosophila – a model for studying prostaglandin signaling. In: Yokomizo T, Murakami M, editors. Bioactive Lipid Mediators: Current Reviews and Protocols: Springer Protocols; 2015. p. 181-97.
26. Tootle TL, Spradling AC. Drosophila Pxt: a cyclooxygenase-like facilitator of follicle maturation. Development. 2008;135(5):839-47. Epub 2008/01/25. doi: 10.1242/dev.017590. PubMed PMID: 18216169; PubMed Central PMCID: PMCPMC2818214.
27. Funk CD. Prostaglandins and leukotrienes: advances in eicosanoid biology. Science. 2001;294(5548):1871-5. Epub 2001/12/01. doi: 10.1126/science.294.5548.1871. PubMed PMID: 11729303.
28. Dichlberger A, Schlager S, Maaninka K, Schneider WJ, Kovanen PT. Adipose triglyceride lipase regulates eicosanoid production in activated human mast cells. J Lipid Res. 2014;55(12):2471-8. Epub 2014/08/13. doi: 10.1194/jlr.M048553. PubMed PMID: 25114172; PubMed Central PMCID: PMCPMC4242440.
29. Schlager S, Goeritzer M, Jandl K, Frei R, Vujic N, Kolb D, et al. Adipose triglyceride lipase acts on neutrophil lipid droplets to regulate substrate availability for lipid mediator

synthesis. J Leukoc Biol. 2015;98(5):837-50. Epub 2015/06/26. doi: 10.1189/jlb.3A0515-206R. PubMed PMID: 26109679; PubMed Central PMCID: PMCPMC4594763.

30. Yen CL, Stone SJ, Koliwad S, Harris C, Farese RV, Jr. Thematic review series: glycerolipids. DGAT enzymes and triacylglycerol biosynthesis. J Lipid Res. 2008;49(11):2283-301. Epub 2008/09/02. doi: 10.1194/jlr.R800018-JLR200. PubMed PMID: 18757836; PubMed Central PMCID: PMCPMC3837458.

31. Chintapalli VR, Wang J, Dow JA. Using FlyAtlas to identify better Drosophila melanogaster models of human disease. Nat Genet. 2007;39(6):715-20. Epub 2007/05/31. doi: 10.1038/ng2049. PubMed PMID: 17534367.

32. Cermelli S, Guo Y, Gross SP, Welte MA. The lipid-droplet proteome reveals that droplets are a protein-storage depot. Curr Biol. 2006;16(18):1783-95. Epub 2006/09/19. doi: 10.1016/j.cub.2006.07.062. PubMed PMID: 16979555.

33. Li Z, Thiel K, Thul PJ, Beller M, Kuhnlein RP, Welte MA. Lipid droplets control the maternal histone supply of Drosophila embryos. Curr Biol. 2012;22(22):2104-13. Epub 2012/10/23. doi: 10.1016/j.cub.2012.09.018. PubMed PMID: 23084995; PubMed Central PMCID: PMCPMC3513403.

34. Gronke S, Beller M, Fellert S, Ramakrishnan H, Jackle H, Kuhnlein RP. Control of fat storage by a Drosophila PAT domain protein. Curr Biol. 2003;13(7):603-6. Epub 2003/04/05. doi: 10.1016/s0960-9822(03)00175-1. PubMed PMID: 12676093.

35. Beller M, Bulankina AV, Hsiao HH, Urlaub H, Jackle H, Kuhnlein RP. PERILIPIN-dependent control of lipid droplet structure and fat storage in Drosophila. Cell Metab. 2010;12(5):521-32. Epub 2010/11/03. doi: 10.1016/j.cmet.2010.10.001. PubMed PMID: 21035762.

36. Bi J, Xiang Y, Chen H, Liu Z, Gronke S, Kuhnlein RP, et al. Opposite and redundant roles of the two Drosophila perilipins in lipid mobilization. J Cell Sci. 2012;125(Pt 15):3568-77. Epub 2012/04/17. doi: 10.1242/jcs.101329. PubMed PMID: 22505614.

37. Johnson MR, Stephenson RA, Ghaemmaghami S, Welte MA. Developmentally regulated H2Av buffering via dynamic sequestration to lipid droplets in Drosophila embryos. Elife. 2018;7. Epub 2018/07/26. doi: 10.7554/eLife.36021. PubMed PMID: 30044219; PubMed Central PMCID: PMCPMC6089599.

38. McMillan EA, Longo SM, Smith MD, Broskin S, Lin B, Singh NK, et al. The protein kinase CK2 substrate Jabba modulates lipid metabolism during Drosophila oogenesis. J Biol Chem. 2018;293(8):2990-3002. Epub 2018/01/13. doi: 10.1074/jbc.M117.814657. PubMed PMID: 29326167; PubMed Central PMCID: PMCPMC5827434.

39. Groen CM, Spracklen AJ, Fagan TN, Tootle TL. Drosophila Fascin is a novel downstream target of prostaglandin signaling during actin remodeling. Mol Biol Cell. 2012;23(23):4567-78. Epub 2012/10/12. doi: 10.1091/mbc.E12-05-0417. PubMed PMID: 23051736; PubMed Central PMCID: PMCPMC3510018.

40. Bozza PT, Bakker-Abreu I, Navarro-Xavier RA, Bandeira-Melo C. Lipid body function in eicosanoid synthesis: an update. Prostaglandins Leukot Essent Fatty Acids. 2011;85(5):205-13. Epub 2011/05/14. doi: 10.1016/j.plefa.2011.04.020. PubMed PMID: 21565480.

41. Jarc E, Petan T. A twist of FATe: Lipid droplets and inflammatory lipid mediators. Biochimie. 2020;169:69-87. Epub 2019/12/02. doi: 10.1016/j.biochi.2019.11.016. PubMed PMID: 31786231.

42. Gronke S, Mildner A, Fellert S, Tennagels N, Petry S, Muller G, et al. Brummer lipase is an evolutionary conserved fat storage regulator in Drosophila. Cell Metab. 2005;1(5):323-30. Epub 2005/08/02. doi: 10.1016/j.cmet.2005.04.003. PubMed PMID: 16054079.

43. Brown JB, Boley N, Eisman R, May GE, Stoiber MH, Duff MO, et al. Diversity and dynamics of the Drosophila transcriptome. Nature. 2014;512(7515):393-9. Epub

2014/03/29. doi: 10.1038/nature12962. PubMed PMID: 24670639; PubMed Central PMCID: PMCPMC4152413.

44. Jambor H, Surendranath V, Kalinka AT, Mejstrik P, Saalfeld S, Tomancak P. Systematic imaging reveals features and changing localization of mRNAs in Drosophila development. Elife. 2015;4. Epub 2015/04/04. doi: 10.7554/eLife.05003. PubMed PMID: 25838129; PubMed Central PMCID: PMCPMC4384636.

45. Spracklen AJ, Tootle TL. The utility of stage-specific mid-to-late Drosophila follicle isolation. J Vis Exp. 2013;(82):50493. Epub 2013/12/12. doi: 10.3791/50493. PubMed PMID: 24326735; PubMed Central PMCID: PMCPMC4011191.

46. Pompeia C, Lima T, Curi R. Arachidonic acid cytotoxicity: can arachidonic acid be a physiological mediator of cell death? Cell Biochem Funct. 2003;21(2):97-104. Epub 2003/05/09. doi: 10.1002/cbf.1012. PubMed PMID: 12736897.

47. Weller PF, Dvorak AM. Lipid bodies: intracellular sites for eicosanoid formation. J Allergy Clin Immunol. 1994;94(6 Pt 2):1151-6. Epub 1994/12/01. doi: 10.1016/0091-6749(94)90325-5. PubMed PMID: 7798553.

48. Bozza PT, Magalhaes KG, Weller PF. Leukocyte lipid bodies - Biogenesis and functions in inflammation. Biochim Biophys Acta. 2009;1791(6):540-51. Epub 2009/05/07. doi: 10.1016/j.bbalip.2009.01.005. PubMed PMID: 19416659; PubMed Central PMCID: PMCPMC2693476.

49. Peppelenbosch MP, Tertoolen LG, Hage WJ, de Laat SW. Epidermal growth factor-induced actin remodeling is regulated by 5-lipoxygenase and cyclooxygenase products. Cell. 1993;74(3):565-75. Epub 1993/08/13. doi: 10.1016/0092-8674(93)80057-l. PubMed PMID: 8348619.

50. Tamma G, Wiesner B, Furkert J, Hahm D, Oksche A, Schaefer M, et al. The prostaglandin E2 analogue sulprostone antagonizes vasopressin-induced antidiuresis through activation of Rho. J Cell Sci. 2003;116(Pt 16):3285-94. Epub 2003/06/28. doi: 10.1242/jcs.00640. PubMed PMID: 12829746.

51. Bulin C, Albrecht U, Bode JG, Weber AA, Schror K, Levkau B, et al. Differential effects of vasodilatory prostaglandins on focal adhesions, cytoskeletal architecture, and migration in human aortic smooth muscle cells. Arterioscler Thromb Vasc Biol. 2005;25(1):84-9. Epub 2004/10/02. doi: 10.1161/01.ATV.0000146814.81581.68. PubMed PMID: 15458982.

52. Pierce KL, Fujino H, Srinivasan D, Regan JW. Activation of FP prostanoid receptor isoforms leads to Rho-mediated changes in cell morphology and in the cell cytoskeleton. J Biol Chem. 1999;274(50):35944-9. Epub 1999/12/10. doi: 10.1074/jbc.274.50.35944. PubMed PMID: 10585482.

53. Dormond O, Bezzi M, Mariotti A, Ruegg C. Prostaglandin E2 promotes integrin alpha Vbeta 3-dependent endothelial cell adhesion, rac-activation, and spreading through cAMP/PKA-dependent signaling. J Biol Chem. 2002;277(48):45838-46. Epub 2002/09/19. doi: 10.1074/jbc.M209213200. PubMed PMID: 12237321.

54. Birukova AA, Zagranichnaya T, Fu P, Alekseeva E, Chen W, Jacobson JR, et al. Prostaglandins PGE(2) and PGI(2) promote endothelial barrier enhancement via PKA- and Epac1/Rap1-dependent Rac activation. Exp Cell Res. 2007;313(11):2504-20. Epub 2007/05/12. doi: 10.1016/j.yexcr.2007.03.036. PubMed PMID: 17493609; PubMed Central PMCID: PMCPMC1974901.

55. Tallima H, El Ridi R. Arachidonic acid: Physiological roles and potential health benefits - A review. J Adv Res. 2018;11:33-41. Epub 2018/07/24. doi: 10.1016/j.jare.2017.11.004. PubMed PMID: 30034874; PubMed Central PMCID: PMCPMC6052655.

56. Brash AR. Arachidonic acid as a bioactive molecule. J Clin Invest. 2001;107(11):1339-45. Epub 2001/06/08. doi: 10.1172/JCI13210. PubMed PMID: 11390413; PubMed Central PMCID: PMCPMC209328.

57. Yoshioka T, Inoue H, Kasama T, Seyama Y, Nakashima S, Nozawa Y, et al. Evidence that arachidonic acid is deficient in phosphatidylinositol of Drosophila heads. J Biochem. 1985;98(3):657-62. Epub 1985/09/01. doi: 10.1093/oxfordjournals.jbchem.a135322. PubMed PMID: 3936840.
58. Shen LR, Lai CQ, Feng X, Parnell LD, Wan JB, Wang JD, et al. Drosophila lacks C20 and C22 PUFAs. J Lipid Res. 2010;51(10):2985-92. Epub 2010/07/27. doi: 10.1194/jlr.M008524. PubMed PMID: 20656917; PubMed Central PMCID: PMCPMC2936753.
59. Tan L, Xin X, Zhai L, Shen L. Drosophila Fed ARA and EPA Yields Eicosanoids, 15S-Hydroxy-5Z,8Z, 11Z, 13E-Eicosatetraenoic Acid, and 15S-Hydroxy-5Z,8Z,11Z,13E,17Z-Eicosapentaenoic Acid. Lipids. 2016;51(4):435-49. Epub 2016/03/05. doi: 10.1007/s11745-016-4131-3. PubMed PMID: 26931457.
60. Steinhauer J, Gijon MA, Riekhof WR, Voelker DR, Murphy RC, Treisman JE. Drosophila lysophospholipid acyltransferases are specifically required for germ cell development. Mol Biol Cell. 2009;20(24):5224-35. Epub 2009/10/30. doi: 10.1091/mbc.E09-05-0382. PubMed PMID: 19864461; PubMed Central PMCID: PMCPMC2793297.
61. Parisi M, Li R, Oliver B. Lipid profiles of female and male Drosophila. BMC Res Notes. 2011;4:198. Epub 2011/06/17. doi: 10.1186/1756-0500-4-198. PubMed PMID: 21676256; PubMed Central PMCID: PMCPMC3146437.
62. Sieber MH, Spradling AC. Steroid Signaling Establishes a Female Metabolic State and Regulates SREBP to Control Oocyte Lipid Accumulation. Curr Biol. 2015;25(8):993-1004. Epub 2015/03/25. doi: 10.1016/j.cub.2015.02.019. PubMed PMID: 25802149; PubMed Central PMCID: PMCPMC6894397.
63. Carvalho M, Sampaio JL, Palm W, Brankatschk M, Eaton S, Shevchenko A. Effects of diet and development on the Drosophila lipidome. Mol Syst Biol. 2012;8:600. Epub 2012/08/07. doi: 10.1038/msb.2012.29. PubMed PMID: 22864382; PubMed Central PMCID: PMCPMC3421444.
64. Miyaura C, Inada M, Matsumoto C, Ohshiba T, Uozumi N, Shimizu T, et al. An essential role of cytosolic phospholipase A2alpha in prostaglandin E2-mediated bone resorption associated with inflammation. J Exp Med. 2003;197(10):1303-10. Epub 2003/05/14. doi: 10.1084/jem.20030015. PubMed PMID: 12743173; PubMed Central PMCID: PMCPMC2193787.
65. Barbour SE, Dennis EA. Antisense inhibition of group II phospholipase A2 expression blocks the production of prostaglandin E2 by P388D1 cells. J Biol Chem. 1993;268(29):21875-82. Epub 1993/10/15. PubMed PMID: 8408042.
66. Ghosh M, Stewart A, Tucker DE, Bonventre JV, Murphy RC, Leslie CC. Role of cytosolic phospholipase A(2) in prostaglandin E(2) production by lung fibroblasts. Am J Respir Cell Mol Biol. 2004;30(1):91-100. Epub 2003/07/05. doi: 10.1165/rcmb.2003-0005OC. PubMed PMID: 12842849.
67. Moreira LS, Piva B, Gentile LB, Mesquita-Santos FP, D'Avila H, Maya-Monteiro CM, et al. Cytosolic phospholipase A2-driven PGE2 synthesis within unsaturated fatty acids-induced lipid bodies of epithelial cells. Biochim Biophys Acta. 2009;1791(3):156-65. Epub 2009/04/16. doi: 10.1016/j.bbalip.2009.01.003. PubMed PMID: 19367763.
68. Yu W, Bozza PT, Tzizik DM, Gray JP, Cassara J, Dvorak AM, et al. Co-compartmentalization of MAP kinases and cytosolic phospholipase A2 at cytoplasmic arachidonate-rich lipid bodies. Am J Pathol. 1998;152(3):759-69. Epub 1998/03/21. PubMed PMID: 9502418; PubMed Central PMCID: PMCPMC1858398.
69. Accioly MT, Pacheco P, Maya-Monteiro CM, Carrossini N, Robbs BK, Oliveira SS, et al. Lipid bodies are reservoirs of cyclooxygenase-2 and sites of prostaglandin-E2 synthesis in colon cancer cells. Cancer Res. 2008;68(6):1732-40. Epub 2008/03/15. doi: 10.1158/0008-5472.CAN-07-1999. PubMed PMID: 18339853.

70. D'Avila H, Freire-de-Lima CG, Roque NR, Teixeira L, Barja-Fidalgo C, Silva AR, et al. Host cell lipid bodies triggered by Trypanosoma cruzi infection and enhanced by the uptake of apoptotic cells are associated with prostaglandin E(2) generation and increased parasite growth. J Infect Dis. 2011;204(6):951-61. Epub 2011/08/19. doi: 10.1093/infdis/jir432. PubMed PMID: 21849292.
71. Hugenroth M, Bohnert M. Come a little bit closer! Lipid droplet-ER contact sites are getting crowded. Biochim Biophys Acta Mol Cell Res. 2020;1867(2):118603. Epub 2019/11/17. doi: 10.1016/j.bbamcr.2019.118603. PubMed PMID: 31733263.
72. Nguyen TB, Louie SM, Daniele JR, Tran Q, Dillin A, Zoncu R, et al. DGAT1-Dependent Lipid Droplet Biogenesis Protects Mitochondrial Function during Starvation-Induced Autophagy. Dev Cell. 2017;42(1):9-21 e5. Epub 2017/07/12. doi: 10.1016/j.devcel.2017.06.003. PubMed PMID: 28697336; PubMed Central PMCID: PMCPMC5553613.
73. Chitraju C, Mejhert N, Haas JT, Diaz-Ramirez LG, Grueter CA, Imbriglio JE, et al. Triglyceride Synthesis by DGAT1 Protects Adipocytes from Lipid-Induced ER Stress during Lipolysis. Cell Metab. 2017;26(2):407-18 e3. Epub 2017/08/03. doi: 10.1016/j.cmet.2017.07.012. PubMed PMID: 28768178; PubMed Central PMCID: PMCPMC6195226.
74. Rambold AS, Cohen S, Lippincott-Schwartz J. Fatty acid trafficking in starved cells: regulation by lipid droplet lipolysis, autophagy, and mitochondrial fusion dynamics. Dev Cell. 2015;32(6):678-92. Epub 2015/03/11. doi: 10.1016/j.devcel.2015.01.029. PubMed PMID: 25752962; PubMed Central PMCID: PMCPMC4375018.
75. Haemmerle G, Moustafa T, Woelkart G, Buttner S, Schmidt A, van de Weijer T, et al. ATGL-mediated fat catabolism regulates cardiac mitochondrial function via PPAR-alpha and PGC-1. Nat Med. 2011;17(9):1076-85. Epub 2011/08/23. doi: 10.1038/nm.2439. PubMed PMID: 21857651; PubMed Central PMCID: PMCPMC3244833.
76. Okuda S, Saito H, Katsuki H. Arachidonic acid: toxic and trophic effects on cultured hippocampal neurons. Neuroscience. 1994;63(3):691-9. Epub 1994/12/01. doi: 10.1016/0306-4522(94)90515-0. PubMed PMID: 7898670.
77. Zhang N, Wang L, Luo G, Tang X, Ma L, Zheng Y, et al. Arachidonic Acid Regulation of Intracellular Signaling Pathways and Target Gene Expression in Bovine Ovarian Granulosa Cells. Animals (Basel). 2019;9(6). Epub 2019/06/30. doi: 10.3390/ani9060374. PubMed PMID: 31248190; PubMed Central PMCID: PMCPMC6617051.
78. Aguila JR, Suszko J, Gibbs AG, Hoshizaki DK. The role of larval fat cells in adult Drosophila melanogaster. J Exp Biol. 2007;210(Pt 6):956-63. Epub 2007/03/06. doi: 10.1242/jeb.001586. PubMed PMID: 17337708.
79. Liu L, Zhang K, Sandoval H, Yamamoto S, Jaiswal M, Sanz E, et al. Glial lipid droplets and ROS induced by mitochondrial defects promote neurodegeneration. Cell. 2015;160(1-2):177-90. Epub 2015/01/17. doi: 10.1016/j.cell.2014.12.019. PubMed PMID: 25594180; PubMed Central PMCID: PMCPMC4377295.
80. Lubojemska A, Stefana MI, Sorge S, Bailey AP, Lampe L, Yoshimura A, et al. Adipose triglyceride lipase protects renal cell endocytosis in a Drosophila dietary model of chronic kidney disease. PLoS Biol. 2021;19(5):e3001230. Epub 2021/05/05. doi: 10.1371/journal.pbio.3001230. PubMed PMID: 33945525; PubMed Central PMCID: PMCPMC8121332.
81. Lima IV, Bastos LF, Limborco-Filho M, Fiebich BL, de Oliveira AC. Role of prostaglandins in neuroinflammatory and neurodegenerative diseases. Mediators Inflamm. 2012;2012:946813. Epub 2012/07/11. doi: 10.1155/2012/946813. PubMed PMID: 22778499; PubMed Central PMCID: PMCPMC3385693.

82. Tzeng SF, Hsiao HY, Mak OT. Prostaglandins and cyclooxygenases in glial cells during brain inflammation. Curr Drug Targets Inflamm Allergy. 2005;4(3):335-40. Epub 2005/08/17. doi: 10.2174/1568010054022051. PubMed PMID: 16101543.
83. Heier C, Knittelfelder O, Hofbauer HF, Mende W, Pornbacher I, Schiller L, et al. Hormone-sensitive lipase couples intergenerational sterol metabolism to reproductive success. Elife. 2021;10. Epub 2021/02/05. doi: 10.7554/eLife.63252. PubMed PMID: 33538247; PubMed Central PMCID: PMCPMC7880688.
84. Spracklen AJ, Kelpsch DJ, Chen X, Spracklen CN, Tootle TL. Prostaglandins temporally regulate cytoplasmic actin bundle formation during Drosophila oogenesis. Mol Biol Cell. 2014;25(3):397-411. Epub 2013/11/29. doi: 10.1091/mbc.E13-07-0366. PubMed PMID: 24284900; PubMed Central PMCID: PMCPMC3907279.
85. Yuan C, Smith WL. A cyclooxygenase-2-dependent prostaglandin E2 biosynthetic system in the Golgi apparatus. J Biol Chem. 2015;290(9):5606-20. Epub 2014/12/31. doi: 10.1074/jbc.M114.632463. PubMed PMID: 25548276; PubMed Central PMCID: PMCPMC4342474.
86. Fong TH, Wu CH, Liao EW, Chang CY, Pai MH, Chiou RJ, et al. Association of globular beta-actin with intracellular lipid droplets in rat adrenocortical cells and adipocytes. Biochem Biophys Res Commun. 2001;289(5):1168-74. Epub 2001/12/14. doi: 10.1006/bbrc.2001.6080. PubMed PMID: 11741315.
87. Pfisterer SG, Gateva G, Horvath P, Pirhonen J, Salo VT, Karhinen L, et al. Role for formin-like 1-dependent acto-myosin assembly in lipid droplet dynamics and lipid storage. Nat Commun. 2017;8:14858. Epub 2017/04/01. doi: 10.1038/ncomms14858. PubMed PMID: 28361956; PubMed Central PMCID: PMCPMC5380971.
88. Kilwein MD, Welte MA. Lipid droplet motility and organelle contacts. Contact (Thousand Oaks). 2019;2. Epub 2020/01/08. doi: 10.1177/2515256419895688. PubMed PMID: 31909374; PubMed Central PMCID: PMCPMC6943980.
89. Bersuker K, Peterson CWH, To M, Sahl SJ, Savikhin V, Grossman EA, et al. A Proximity Labeling Strategy Provides Insights into the Composition and Dynamics of Lipid Droplet Proteomes. Dev Cell. 2018;44(1):97-112 e7. Epub 2017/12/26. doi: 10.1016/j.devcel.2017.11.020. PubMed PMID: 29275994; PubMed Central PMCID: PMCPMC5764092.
90. Welte MA, Cermelli S, Griner J, Viera A, Guo Y, Kim DH, et al. Regulation of lipid-droplet transport by the perilipin homolog LSD2. Curr Biol. 2005;15(14):1266-75. Epub 2005/07/30. doi: 10.1016/j.cub.2005.06.062. PubMed PMID: 16051169.
91. Herms A, Bosch M, Reddy BJ, Schieber NL, Fajardo A, Ruperez C, et al. AMPK activation promotes lipid droplet dispersion on detyrosinated microtubules to increase mitochondrial fatty acid oxidation. Nat Commun. 2015;6:7176. Epub 2015/05/28. doi: 10.1038/ncomms8176. PubMed PMID: 26013497; PubMed Central PMCID: PMCPMC4446796.
92. Ying F, Cai Y, Cai Y, Wang Y, Tang EHC. Prostaglandin E receptor subtype 4 regulates lipid droplet size and mitochondrial activity in murine subcutaneous white adipose tissue. FASEB J. 2017;31(9):4023-36. Epub 2017/05/24. doi: 10.1096/fj.201700191R. PubMed PMID: 28533326.
93. Seachord CL, VandeVoort CA, Duffy DM. Adipose differentiation-related protein: a gonadotropin- and prostaglandin-regulated protein in primate periovulatory follicles. Biol Reprod. 2005;72(6):1305-14. Epub 2005/02/04. doi: 10.1095/biolreprod.104.037523. PubMed PMID: 15689536.
94. de Souza G, Silva RJ, Milian ICB, Rosini AM, de Araujo TE, Teixeira SC, et al. Cyclooxygenase (COX)-2 modulates Toxoplasma gondii infection, immune response and lipid droplets formation in human trophoblast cells and villous explants. Sci Rep.

2021;11(1):12709. Epub 2021/06/18. doi: 10.1038/s41598-021-92120-3. PubMed PMID: 34135407; PubMed Central PMCID: PMCPMC8209052.

95. Dutta A, Kumar Sinha D. Turnover of the actomyosin complex in zebrafish embryos directs geometric remodelling and the recruitment of lipid droplets. Sci Rep. 2015;5:13915. Epub 2015/09/12. doi: 10.1038/srep13915. PubMed PMID: 26355567; PubMed Central PMCID: PMCPMC4650301.

96. Gupta P, Martin R, Knolker HJ, Nihalani D, Kumar Sinha D. Myosin-1 inhibition by PCIP affects membrane shape, cortical actin distribution and lipid droplet dynamics in early Zebrafish embryos. PLoS One. 2017;12(7):e0180301. Epub 2017/07/06. doi: 10.1371/journal.pone.0180301. PubMed PMID: 28678859; PubMed Central PMCID: PMCPMC5498032.

97. Veerabagu M, L KP, Rinne PL, van der Schoot C. Plant Lipid Bodies Traffic on Actin to Plasmodesmata Motorized by Myosin XIs. Int J Mol Sci. 2020;21(4). Epub 2020/02/26. doi: 10.3390/ijms21041422. PubMed PMID: 32093159; PubMed Central PMCID: PMCPMC7073070.

98. Spracklen AJ, Lamb MC, Groen CM, Tootle TL. Pharmaco-Genetic Screen To Uncover Actin Regulators Targeted by Prostaglandins During Drosophila Oogenesis. G3 (Bethesda). 2019;9(11):3555-65. Epub 2019/09/12. doi: 10.1534/g3.119.400704. PubMed PMID: 31506320; PubMed Central PMCID: PMCPMC6829128.

99. Gaspar I, Szabad J. In vivo analysis of MT-based vesicle transport by confocal reflection microscopy. Cell Motil Cytoskeleton. 2009;66(2):68-79. Epub 2009/01/09. doi: 10.1002/cm.20334. PubMed PMID: 19130480.

100. Shubeita GT, Tran SL, Xu J, Vershinin M, Cermelli S, Cotton SL, et al. Consequences of motor copy number on the intracellular transport of kinesin-1-driven lipid droplets. Cell. 2008;135(6):1098-107. Epub 2008/12/17. doi: 10.1016/j.cell.2008.10.021. PubMed PMID: 19070579; PubMed Central PMCID: PMCPMC2768369.

101. Gross SP, Welte MA, Block SM, Wieschaus EF. Dynein-mediated cargo transport in vivo. A switch controls travel distance. J Cell Biol. 2000;148(5):945-56. Epub 2000/03/08. doi: 10.1083/jcb.148.5.945. PubMed PMID: 10704445; PubMed Central PMCID: PMCPMC2174539.

102. Sieber MH, Spradling AC. The role of metabolic states in development and disease. Curr Opin Genet Dev. 2017;45:58-68. Epub 2017/03/30. doi: 10.1016/j.gde.2017.03.002. PubMed PMID: 28347941; PubMed Central PMCID: PMCPMC6894399.

103. Hashemi HF, Goodman JM. The life cycle of lipid droplets. Curr Opin Cell Biol. 2015;33:119-24. doi: 10.1016/j.ceb.2015.02.002. PubMed PMID: 25703629; PubMed Central PMCID: PMCPMC4380764.

104. Chan AP, Kloc M, Larabell CA, LeGros M, Etkin LD. The maternally localized RNA fatvg is required for cortical rotation and germ cell formation. Mech Dev. 2007;124(5):350-63. Epub 2007/03/23. doi: 10.1016/j.mod.2007.02.001. PubMed PMID: 17376659; PubMed Central PMCID: PMCPMC2435194.

105. Robker RL. Evidence that obesity alters the quality of oocytes and embryos. Pathophysiology. 2008;15(2):115-21. Epub 2008/07/05. doi: 10.1016/j.pathophys.2008.04.004. PubMed PMID: 18599275.

106. Wattanakumtornkul S, Damario MA, Stevens Hall SA, Thornhill AR, Tummon IS. Body mass index and uterine receptivity in the oocyte donation model. Fertil Steril. 2003;80(2):336-40. Epub 2003/08/12. doi: 10.1016/s0015-0282(03)00595-8. PubMed PMID: 12909496.

107. Styne-Gross A, Elkind-Hirsch K, Scott RT, Jr. Obesity does not impact implantation rates or pregnancy outcome in women attempting conception through oocyte donation. Fertil Steril. 2005;83(6):1629-34. Epub 2005/06/14. doi: 10.1016/j.fertnstert.2005.01.099. PubMed PMID: 15950629.

108. Lim H, Paria BC, Das SK, Dinchuk JE, Langenbach R, Trzaskos JM, et al. Multiple female reproductive failures in cyclooxygenase 2-deficient mice. Cell. 1997;91(2):197-208. Epub 1997/11/05. doi: 10.1016/s0092-8674(00)80402-x. PubMed PMID: 9346237.
109. Wang H, Ma WG, Tejada L, Zhang H, Morrow JD, Das SK, et al. Rescue of female infertility from the loss of cyclooxygenase-2 by compensatory up-regulation of cyclooxygenase-1 is a function of genetic makeup. J Biol Chem. 2004;279(11):10649-58. Epub 2004/01/01. doi: 10.1074/jbc.M312203200. PubMed PMID: 14701858.
110. Takahashi T, Morrow JD, Wang H, Dey SK. Cyclooxygenase-2-derived prostaglandin E(2) directs oocyte maturation by differentially influencing multiple signaling pathways. J Biol Chem. 2006;281(48):37117-29. Epub 2006/10/07. doi: 10.1074/jbc.M608202200. PubMed PMID: 17023426.
111. Takahashi T, Igarashi H, Amita M, Hara S, Kurachi H. Roles of Prostaglandins During Oocyte Maturation: Lessons from Knockout Mice. Journal of Mammalian Ova Research. 2010;27(1):11-20. doi: 10.1274/jmor.27.11.
112. Pall M, Friden BE, Brannstrom M. Induction of delayed follicular rupture in the human by the selective COX-2 inhibitor rofecoxib: a randomized double-blind study. Hum Reprod. 2001;16(7):1323-8. Epub 2001/06/27. doi: 10.1093/humrep/16.7.1323. PubMed PMID: 11425807.
113. Akil M, Amos RS, Stewart P. Infertility may sometimes be associated with NSAID consumption. Br J Rheumatol. 1996;35(1):76-8. Epub 1996/01/01. doi: 10.1093/rheumatology/35.1.76. PubMed PMID: 8624628.
114. Smith G, Roberts R, Hall C, Nuki G. Reversible ovulatory failure associated with the development of luteinized unruptured follicles in women with inflammatory arthritis taking non-steroidal anti-inflammatory drugs. Br J Rheumatol. 1996;35(5):458-62. Epub 1996/05/01. doi: 10.1093/rheumatology/35.5.458. PubMed PMID: 8646437.
115. Arend A, Masso R, Masso M, Selstam G. Electron microscope immunocytochemical localization of cyclooxygenase-1 and -2 in pseudopregnant rat corpus luteum during luteolysis. Prostaglandins Other Lipid Mediat. 2004;74(1-4):1-10. Epub 2004/11/25. doi: 10.1016/j.prostaglandins.2004.05.002. PubMed PMID: 15560112.
116. Meadows JW, Eis AL, Brockman DE, Myatt L. Expression and localization of prostaglandin E synthase isoforms in human fetal membranes in term and preterm labor. J Clin Endocrinol Metab. 2003;88(1):433-9. Epub 2003/01/10. doi: 10.1210/jc.2002-021061. PubMed PMID: 12519887.
117. Meadows JW, Pitzer B, Brockman DE, Myatt L. Expression and localization of adipophilin and perilipin in human fetal membranes: association with lipid bodies and enzymes involved in prostaglandin synthesis. J Clin Endocrinol Metab. 2005;90(4):2344-50. Epub 2005/01/20. doi: 10.1210/jc.2004-1199. PubMed PMID: 15657374.
118. Namgoong S, Kim NH. Roles of actin binding proteins in mammalian oocyte maturation and beyond. Cell Cycle. 2016;15(14):1830-43. Epub 2016/05/07. doi: 10.1080/15384101.2016.1181239. PubMed PMID: 27152960; PubMed Central PMCID: PMCPMC4968894.
119. Coticchio G, Dal Canto M, Mignini Renzini M, Guglielmo MC, Brambillasca F, Turchi D, et al. Oocyte maturation: gamete-somatic cells interactions, meiotic resumption, cytoskeletal dynamics and cytoplasmic reorganization. Hum Reprod Update. 2015;21(4):427-54. Epub 2015/03/07. doi: 10.1093/humupd/dmv011. PubMed PMID: 25744083.
120. Thibault ST, Singer MA, Miyazaki WY, Milash B, Dompe NA, Singh CM, et al. A complementary transposon tool kit for Drosophila melanogaster using P and piggyBac. Nat Genet. 2004;36(3):283-7. Epub 2004/02/26. doi: 10.1038/ng1314. PubMed PMID: 14981521.

121. LaJeunesse DR, Buckner SM, Lake J, Na C, Pirt A, Fromson K. Three new Drosophila markers of intracellular membranes. Biotechniques. 2004;36(5):784-8, 90. Epub 2004/05/22. doi: 10.2144/04365ST01. PubMed PMID: 15152597.
122. Riedel F, Gillingham AK, Rosa-Ferreira C, Galindo A, Munro S. An antibody toolkit for the study of membrane traffic in Drosophila melanogaster. Biol Open. 2016;5(7):987-92. Epub 2016/06/04. doi: 10.1242/bio.018937. PubMed PMID: 27256406; PubMed Central PMCID: PMCPMC4958275.
123. Platt JL, Michael AF. Retardation of fading and enhancement of intensity of immunofluorescence by p-phenylenediamine. The journal of histochemistry and cytochemistry : official journal of the Histochemistry Society. 1983;31(6):840-2. Epub 1983/06/01. doi: 10.1177/31.6.6341464. PubMed PMID: 6341464.
124. Abramoff M, Magalhaes P, Ram S. Image processing with ImageJ. Biophotonics Int. 2004;11(7):36-42.
125. Tran SL, Welte MA. In-vivo centrifugation of Drosophila embryos. J Vis Exp. 2010;(40). Epub 2010/07/09. doi: 10.3791/2005. PubMed PMID: 20613707; PubMed Central PMCID: PMCPMC3153895.
126. Knittelfelder OL, Kohlwein SD. Thin-Layer Chromatography to Separate Phospholipids and Neutral Lipids from Yeast. Cold Spring Harb Protoc. 2017;2017(5). Epub 2017/05/04. doi: 10.1101/pdb.prot085456. PubMed PMID: 28461652.

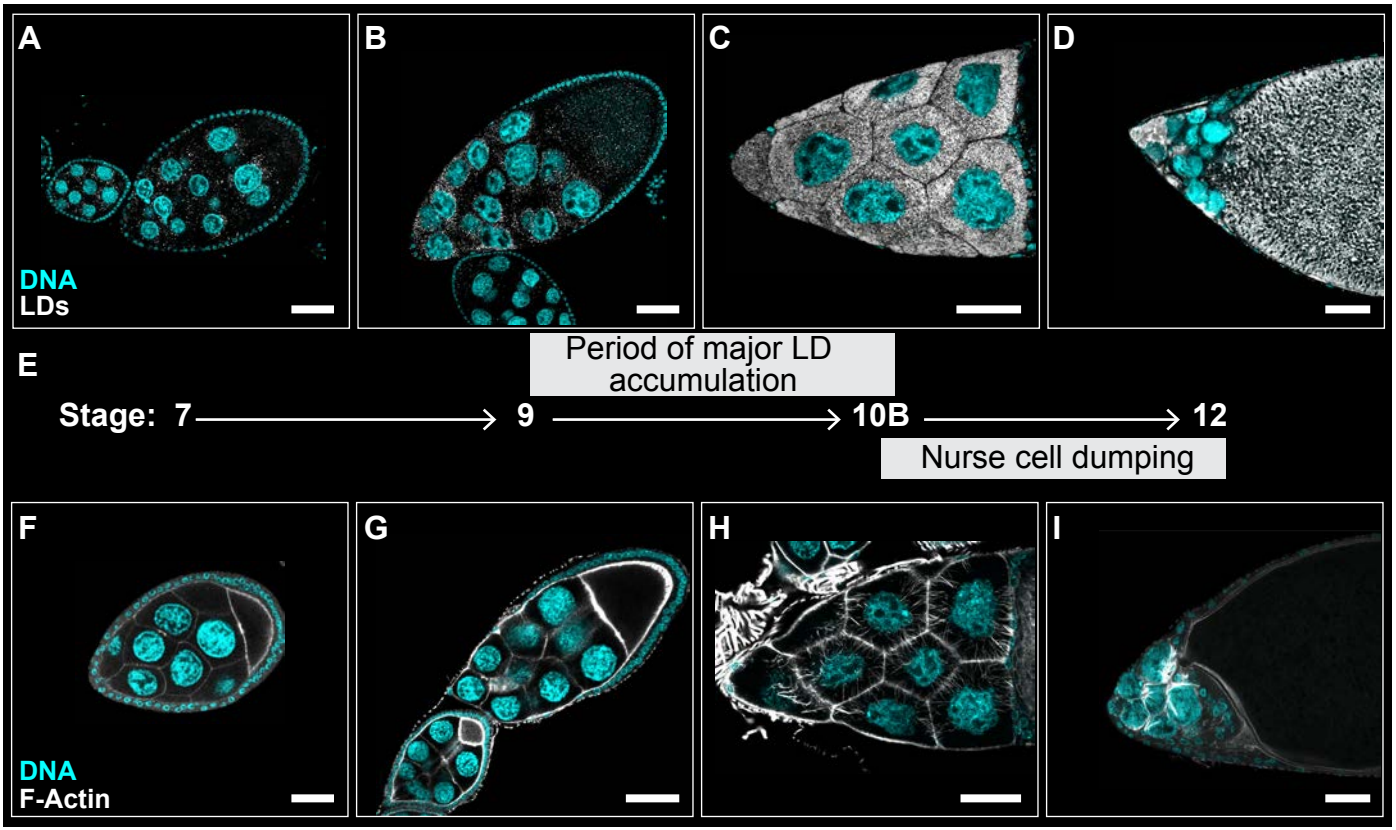
A
B
C
D
DNA
LDs
E
Period of major LD accumulation
Stage: 7
9
10B
12
Nurse cell dumping
F
G
H
I
DNA
F-Actin

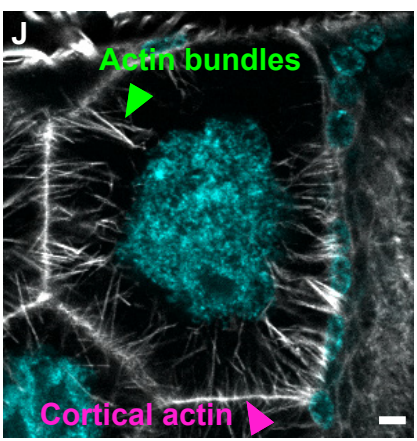
J
Actin bundles
Cortical actin

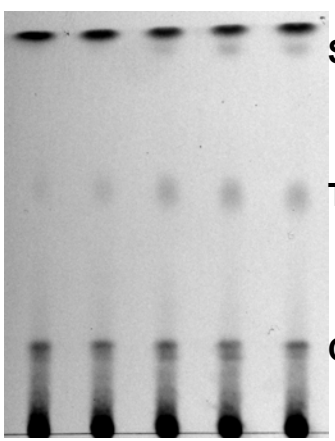
K
SE
TAG
Cholesterol
9
10A
10B
12
14
Stage

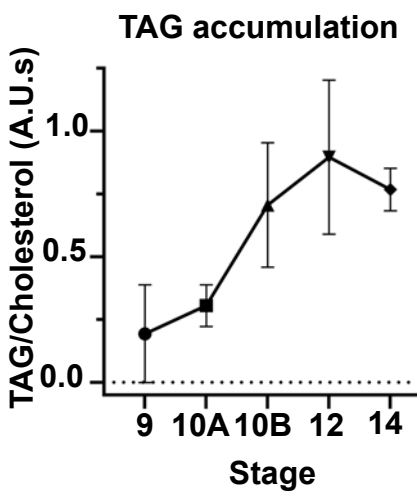
TAG accumulation
L
TAG/Cholesterol (A.U.s)
1.0
0.5
0.0
9
10A
10B
12
14
Stage

Fig 1

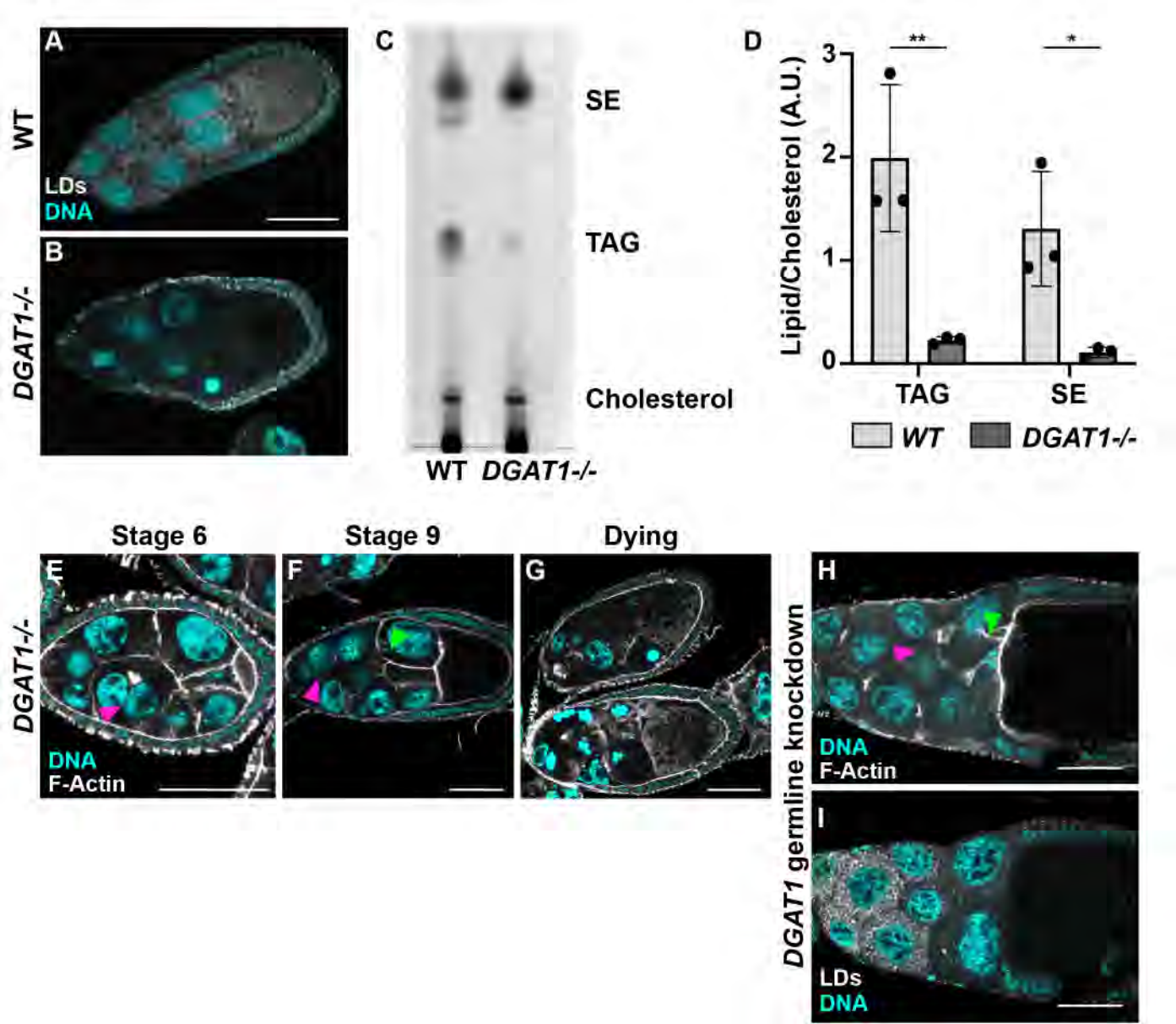
A
WT
LDs
DNA
B
DGAT1-/-
C
SE
TAG
Cholesterol
WT
DGAT1-/-
D
Lipid/Cholesterol (A.U.)
3
2
1
0
**
*
TAG
SE
WT
DGAT1-/-
Stage 6
Stage 9
Dying
E
F
G
DGAT1-/-
DNA
F-Actin
H
DNA
F-Actin
DGAT1 germline knockdown
I
LDs
DNA

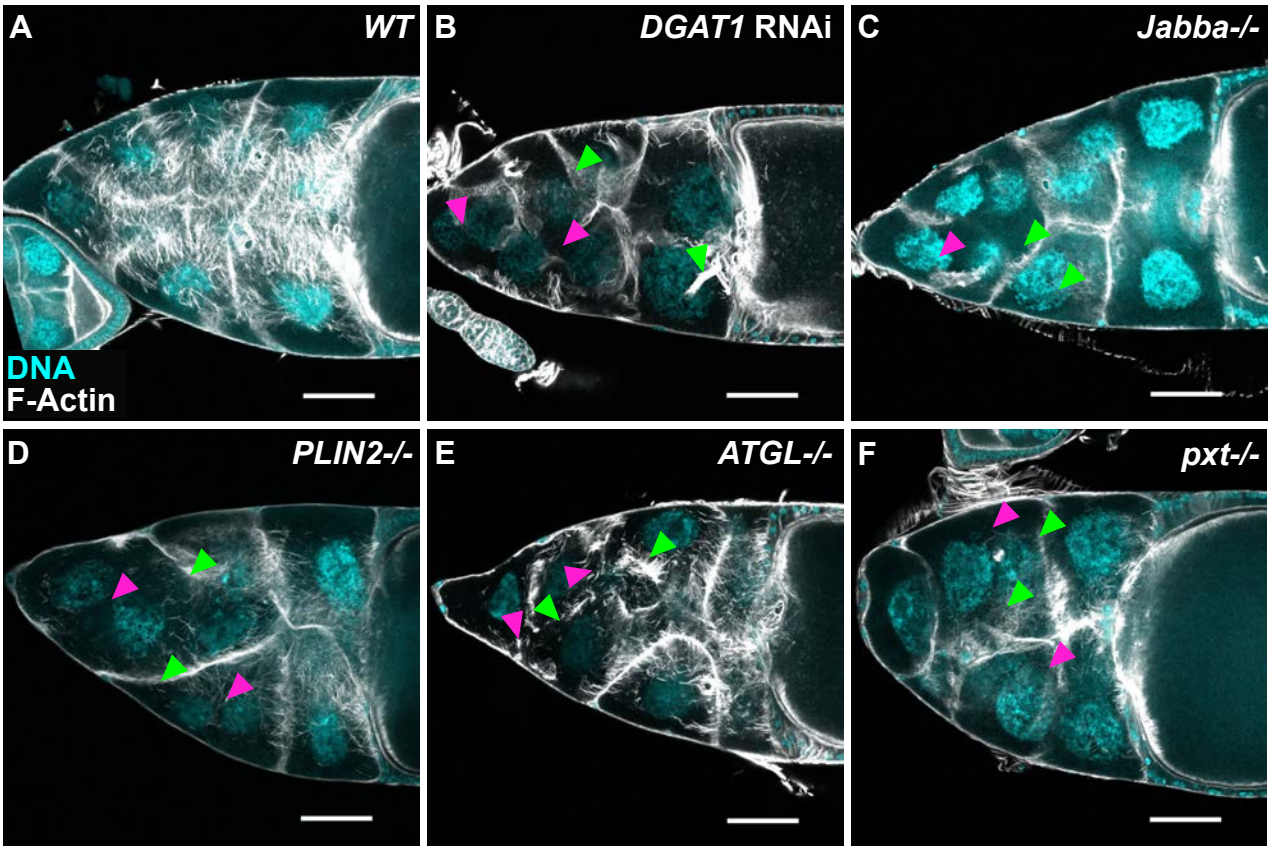


Fig 3

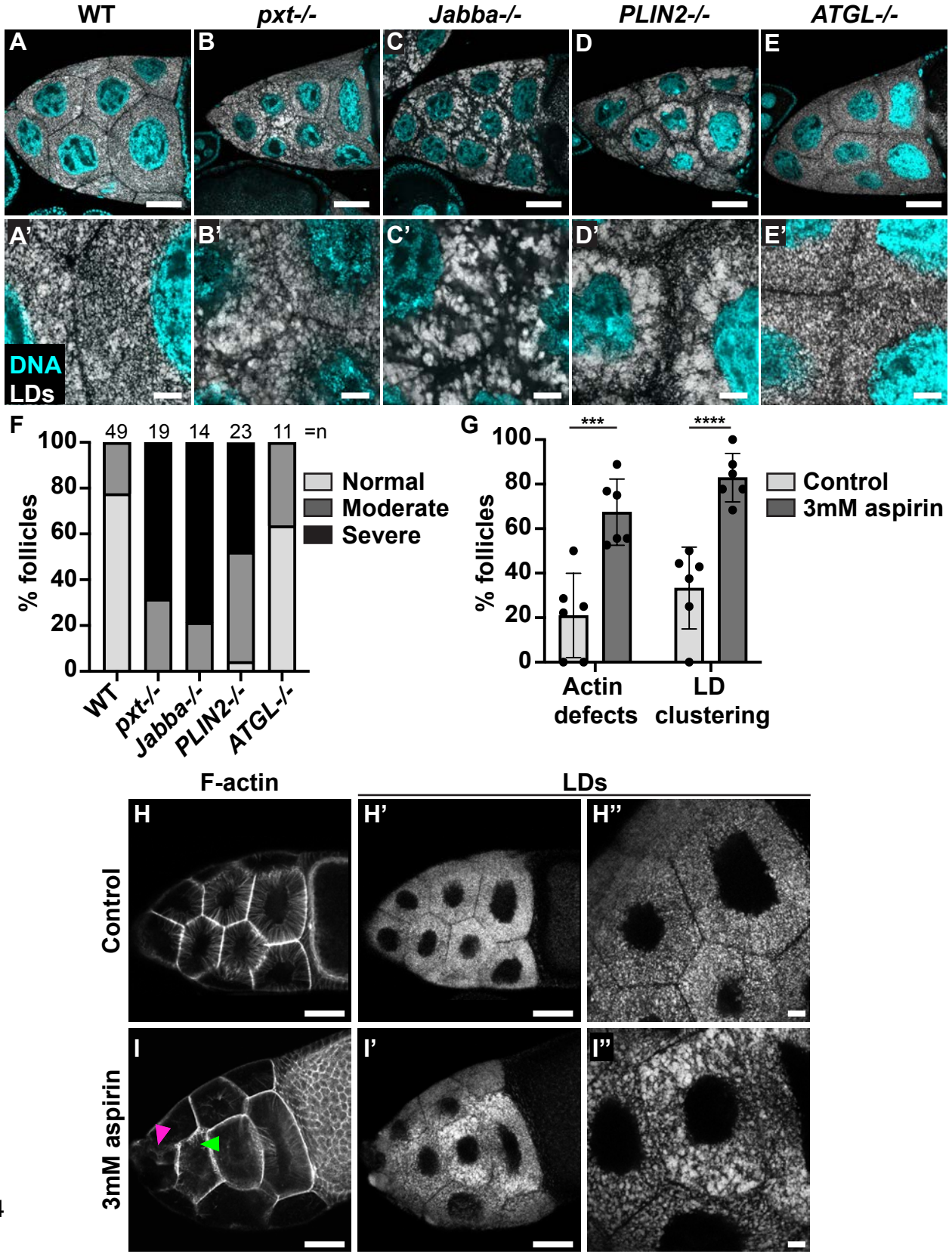
WT
pxt-/-
Jabba-/-
PLIN2-/-
ATGL-/-
A
B
C
D
E
A'
B'
C'
D'
E'
DNA
LDs
F
49
19
14
23
11
=n
100
80
60
40
20
0
% follicles
Normal
Moderate
Severe
WT
pxt-/-
Jabba-/-
PLIN2-/-
ATGL-/-
G
***
****
% follicles
Control
3mM aspirin
Actin defects
LD clustering
F-actin
LDs
H
H'
H''
Control
I
I'
I''
3mM aspirin

Fig 4

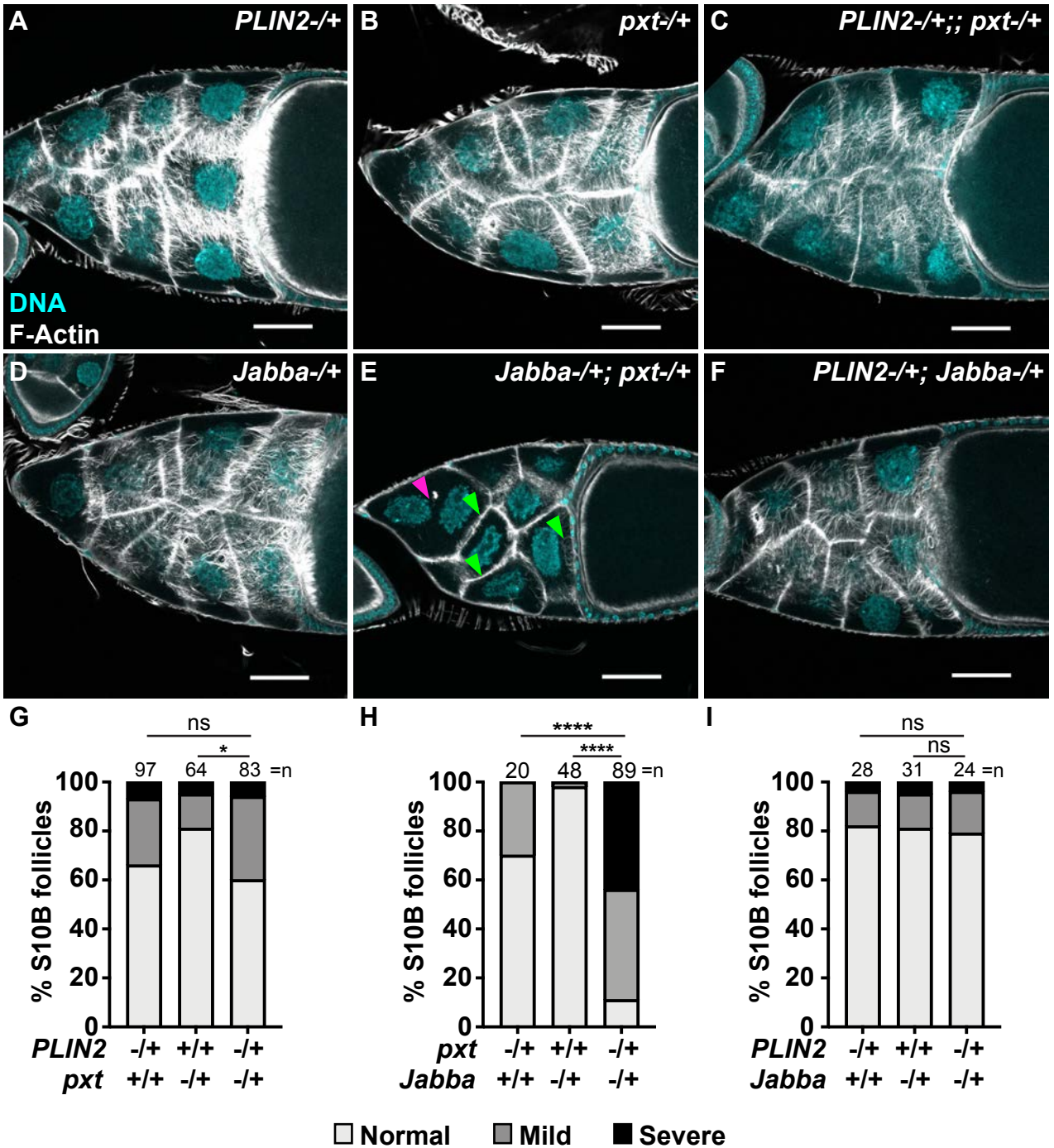
A
PLIN2-/+
B
pxt-/+
C
PLIN2-/+;; pxt-/+
DNA
F-Actin
D
Jabba-/+
E
Jabba-/+; pxt-/+
F
PLIN2-/+; Jabba-/+
G
ns
*
97
64
83
=n
% S10B follicles
100
80
60
40
20
0
PLIN2
pxt
-/+
+/+
-/+
+/+
-/+
-/+
H
****
****
20
48
89
=n
% S10B follicles
pxt
Jabba
I
ns
ns
28
31
24
=n
% S10B follicles
PLIN2
Jabba
Normal
Mild
Severe

Fig 5

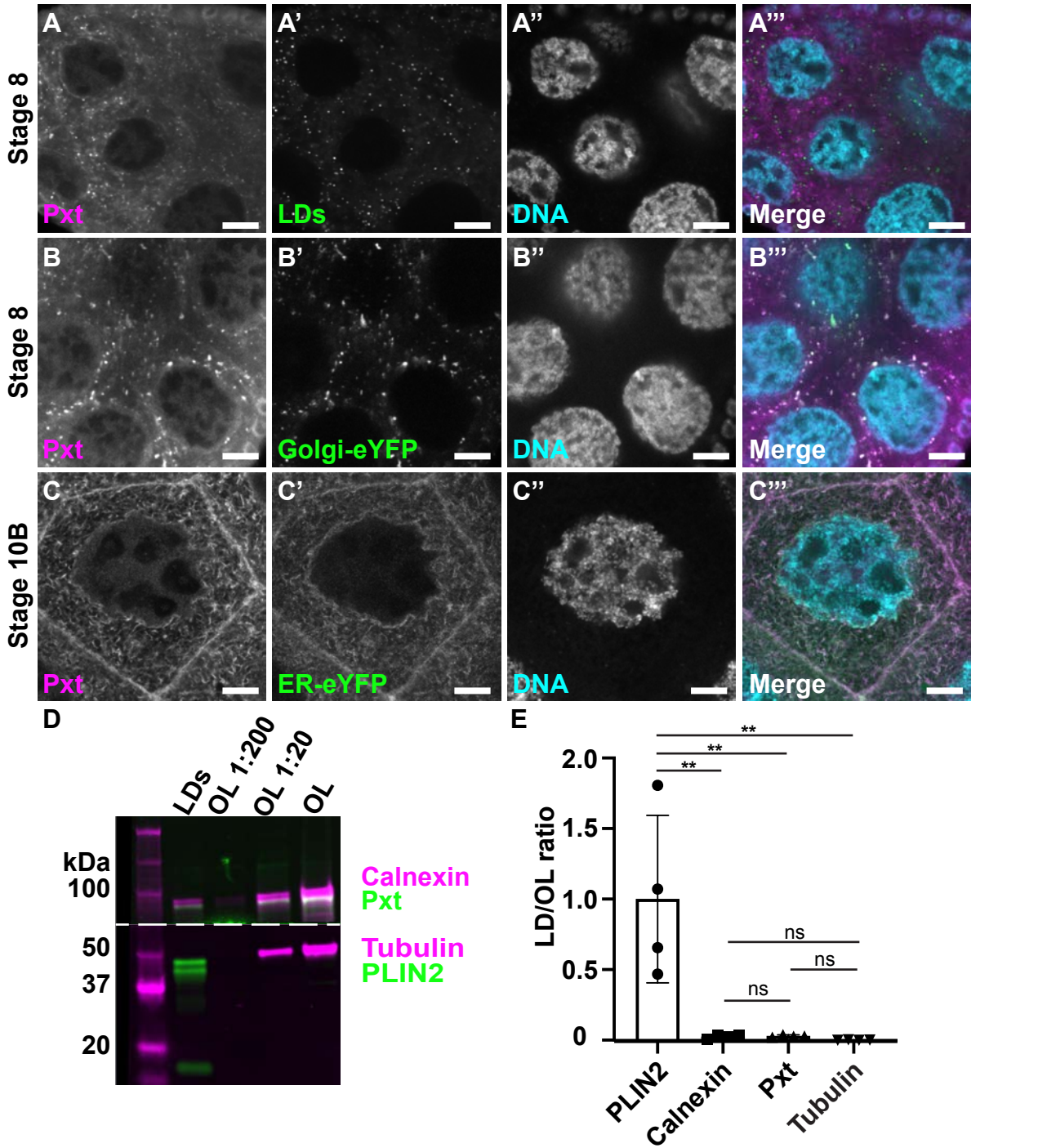
Stage 8
A
A'
A''
A'''
Pxt
LDs
DNA
Merge
Stage 8
B
B'
B''
B'''
Pxt
Golgi-eYFP
DNA
Merge
Stage 10B
C
C'
C''
C'''
Pxt
ER-eYFP
DNA
Merge
D
LDs
OL 1:200
OL 1:20
OL
kDa
100
50
37
20
Calnexin
Pxt
Tubulin
PLIN2
E
LD/OL ratio
2.0
1.5
1.0
0.5
0
**
**
**
ns
ns
ns
PLIN2
Calnexin
Pxt
Tubulin
Stage 10B
F
F'
F''
F'''
Pxt
LDs
DNA
Merge

Fig 6

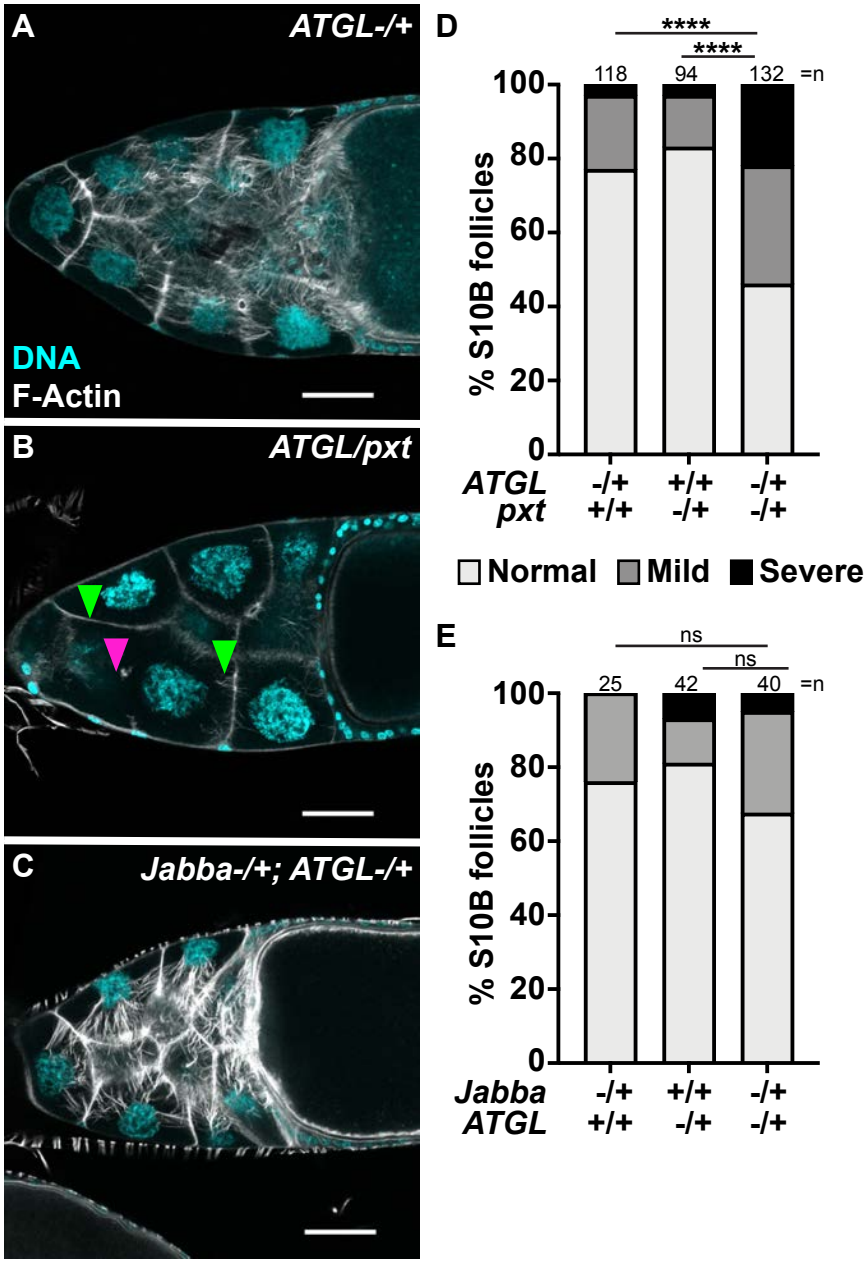
A
ATGL-/+
DNA
F-Actin
B
ATGL/pxt
C
Jabba-/+; ATGL-/+
D
****
****
118
94
132
=n
100
80
60
40
20
0
% S10B follicles
ATGL -/+ +/+ -/+
pxt +/+ -/+ -/+
Normal
Mild
Severe
E
ns
ns
25
42
40
=n
100
80
60
40
20
0
% S10B follicles
Jabba -/+ +/+ -/+
ATGL +/+ -/+ -/+

Fig 7

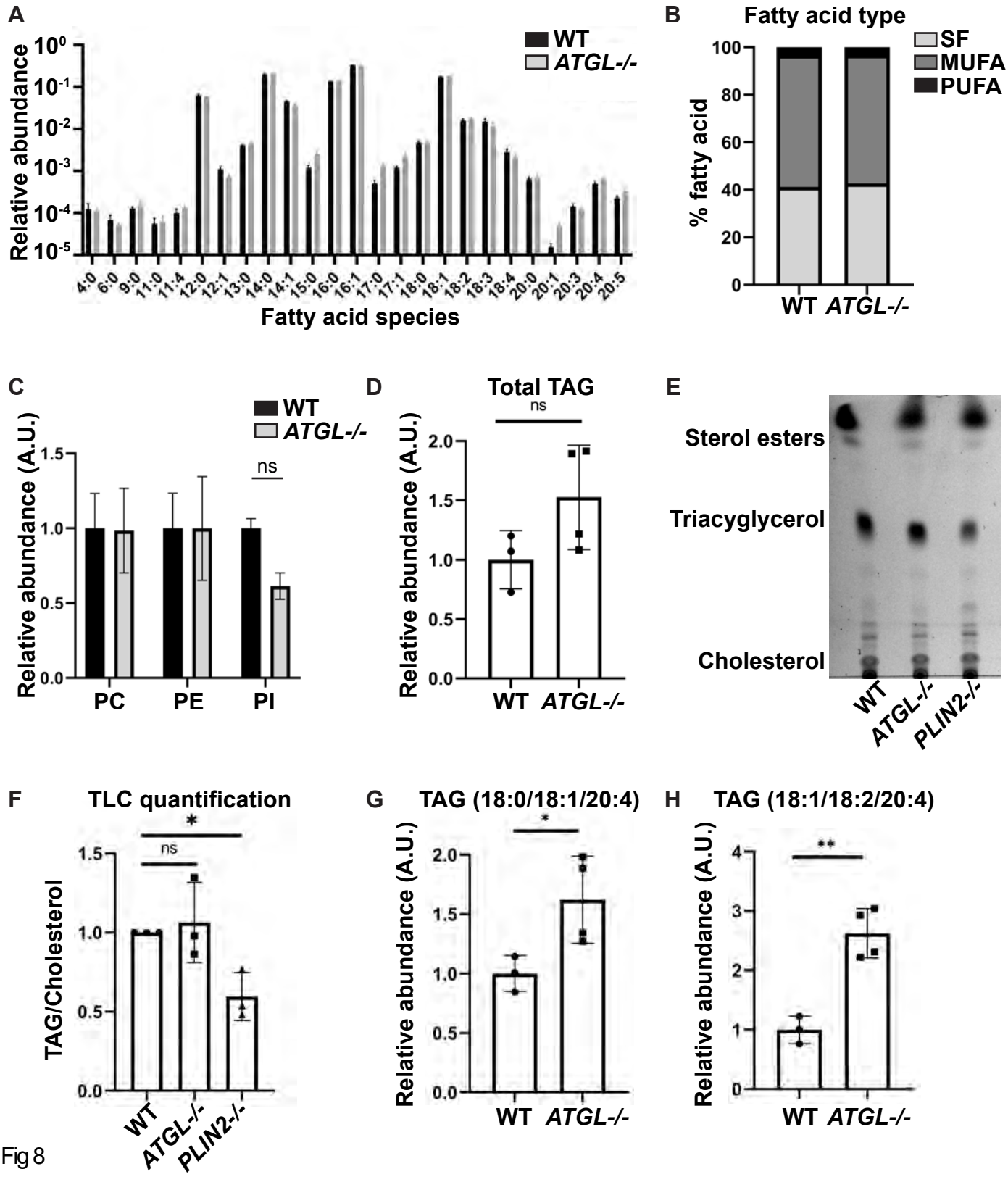
A
Relative abundance
WT
ATGL-/-
Fatty acid species
B
Fatty acid type
SF
MUFA
PUFA
% fatty acid
WT ATGL-/-
C
Relative abundance (A.U.)
WT
ATGL-/-
ns
PC
PE
PI
D
Total TAG
ns
Relative abundance (A.U.)
WT ATGL-/-
E
Sterol esters
Triacyglycerol
Cholesterol
WT
ATGL-/-
PLIN2-/-
F
TLC quantification
TAG/Cholesterol
ns
WT
ATGL-/-
PLIN2-/-
G
TAG (18:0/18:1/20:4)
Relative abundance (A.U.)
WT ATGL-/-
H
TAG (18:1/18:2/20:4)
Relative abundance (A.U.)
WT ATGL-/-

Fig 8

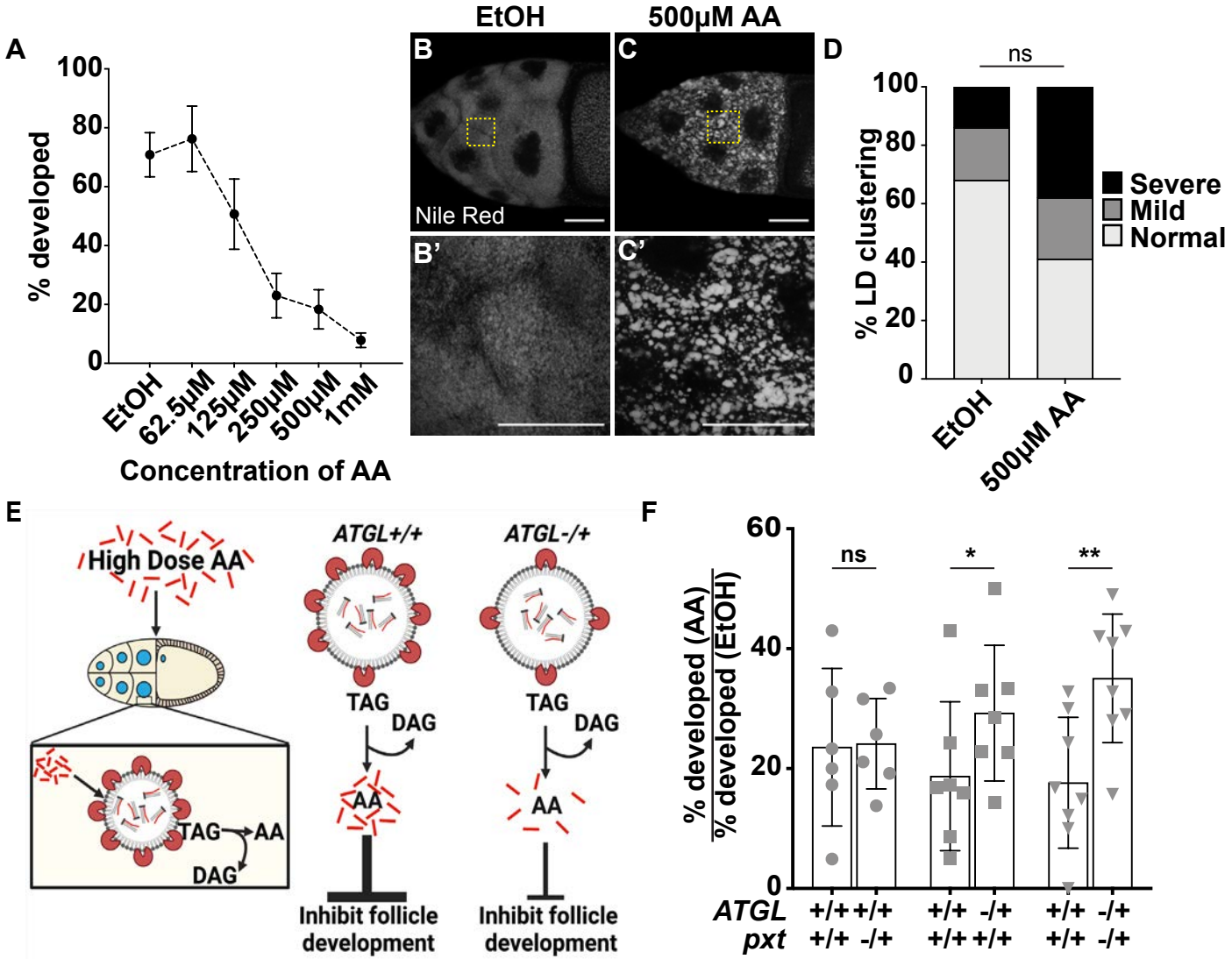
A
% developed
100
80
60
40
20
0
EtOH
62.5μM
125μM
250μM
500μM
1mM
Concentration of AA
EtOH
500μM AA
B
C
Nile Red
B'
C'
D
ns
% LD clustering
Severe
Mild
Normal
EtOH
500μM AA
E
High Dose AA
TAG
DAG
AA
ATGL+/+
ATGL-/+
Inhibit follicle development
Inhibit follicle development
F
% developed (AA) / % developed (EtOH)
ns
*
**
ATGL
pxt
+/+ +/+
+/+ -/+
+/+ +/+
+/+ -/+
+/+ +/+
+/+ -/+

Fig 9

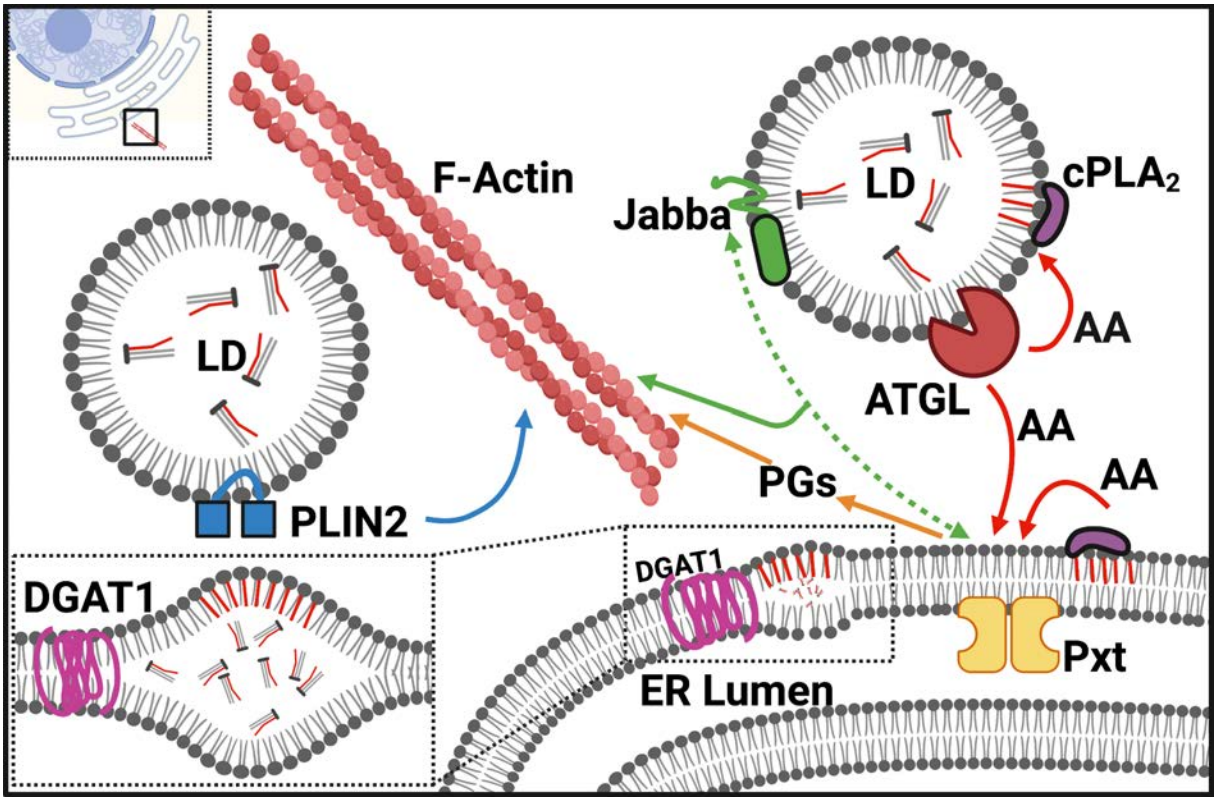
F-Actin
LD
PLIN2
Jabba
LD
cPLA2
AA
ATGL
AA
AA
PGs
DGAT1
DGAT1
Pxt
ER Lumen

Fig 10

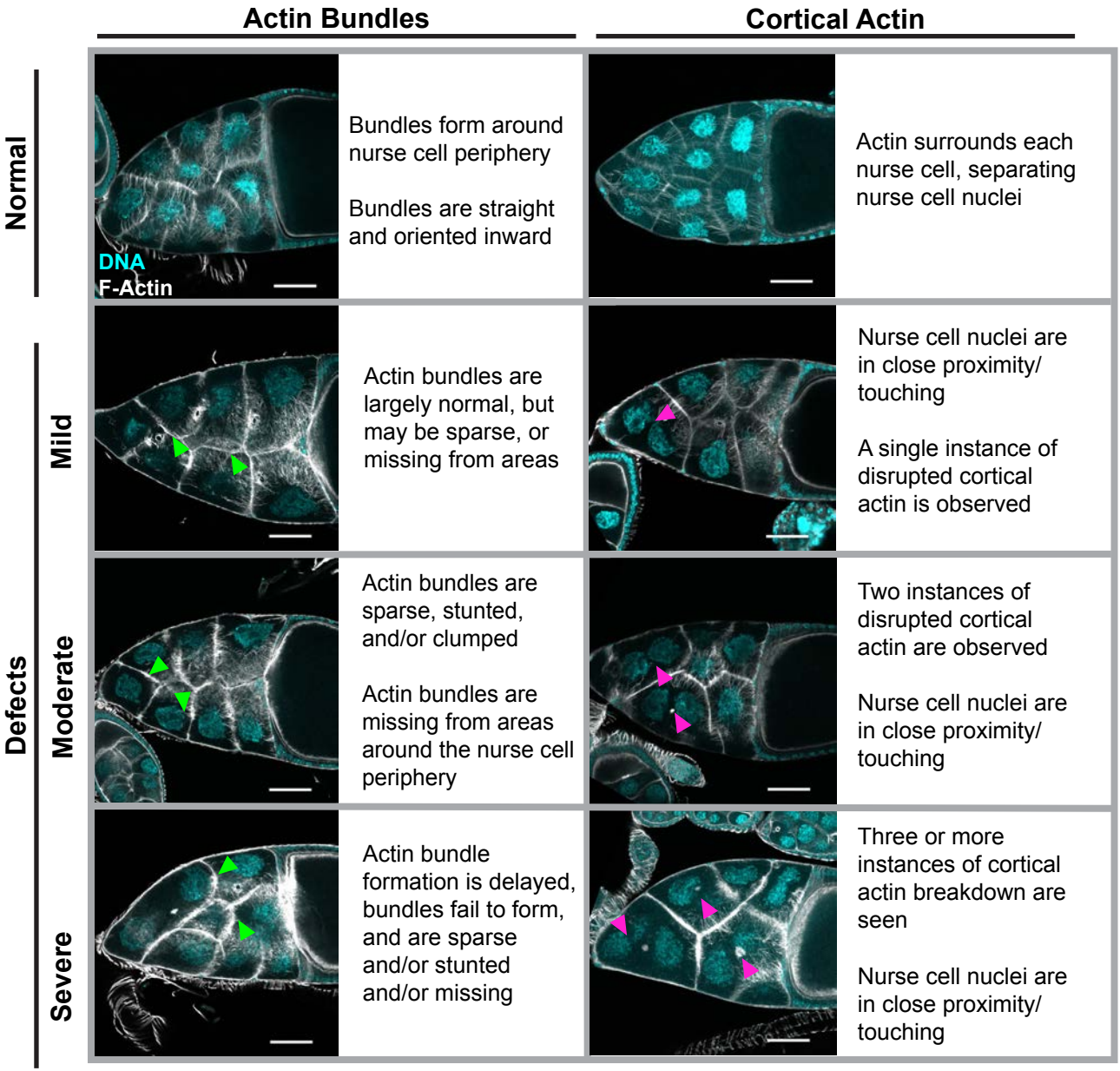
Actin Bundles
Cortical Actin
Normal
Defects
Mild
Moderate
Severe
DNA
F-Actin
Bundles form around nurse cell periphery
Bundles are straight and oriented inward
Actin surrounds each nurse cell, separating nurse cell nuclei
Actin bundles are largely normal, but may be sparse, or missing from areas
Nurse cell nuclei are in close proximity/ touching
A single instance of disrupted cortical actin is observed
Actin bundles are sparse, stunted, and/or clumped
Actin bundles are missing from areas around the nurse cell periphery
Two instances of disrupted cortical actin are observed
Nurse cell nuclei are in close proximity/ touching
Actin bundle formation is delayed, bundles fail to form, and are sparse and/or stunted and/or missing
Three or more instances of cortical actin breakdown are seen
Nurse cell nuclei are in close proximity/ touching

SFig 1

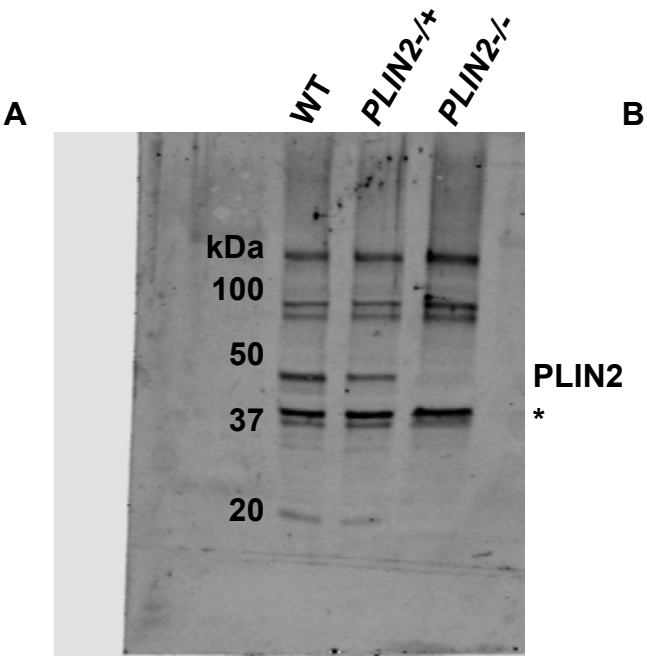
A
WT
PLIN2-/+
PLIN2-/-
kDa
100
50
37
20
PLIN2
*
B
PLIN2/Nonspecific bands
1.5
1.0
0.5
0
****
WT
PLIN2-/+

SFig 2

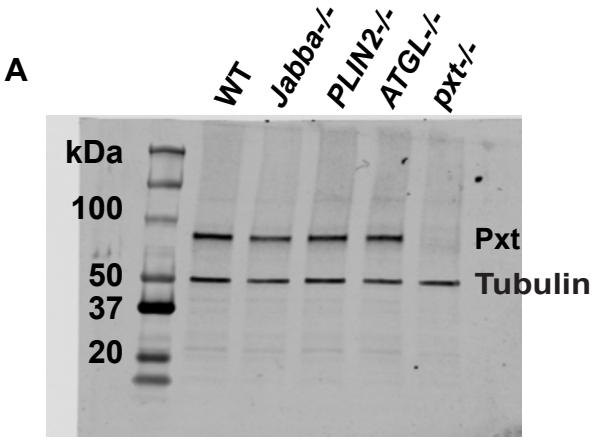
A
WT
Jabba-/-
PLIN2-/-
ATGL-/-
pxt-/-
kDa
100
50
37
20
Pxt
Tubulin

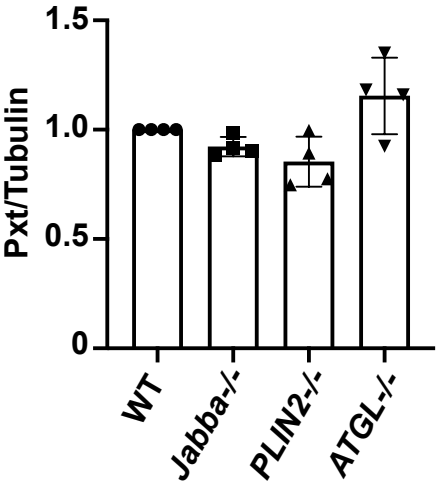
B
Pxt/Tubulin
1.5
1.0
0.5
0
WT
Jabba-/-
PLIN2-/-
ATGL-/-

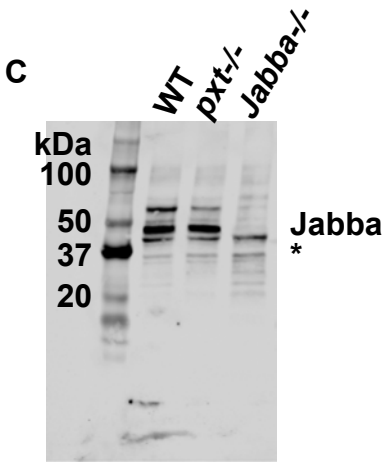
C
WT
pxt-/-
Jabba-/-
kDa
100
50
37
20
Jabba
*

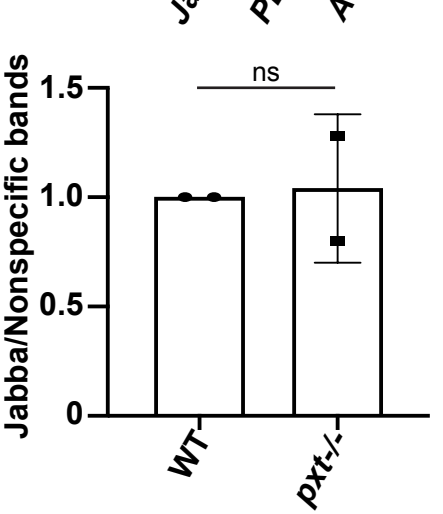
D
Jabba/Nonspecific bands
ns
1.5
1.0
0.5
0
WT
pxt-/-

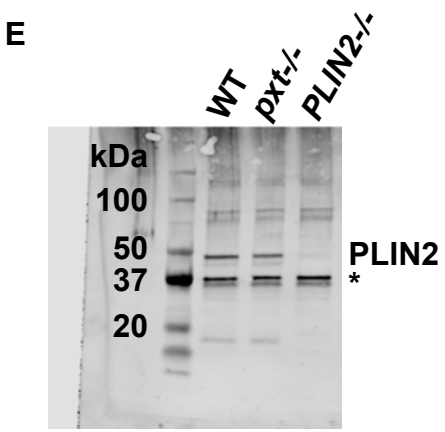
E
WT
pxt-/-
PLIN2-/-
kDa
100
50
37
20
PLIN2
*

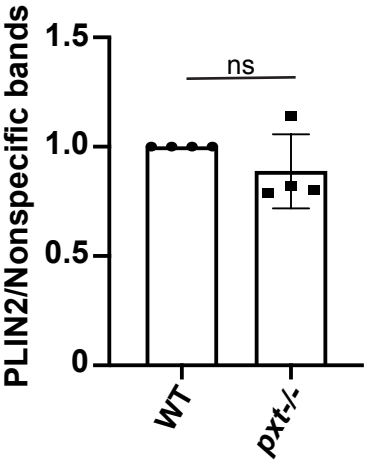
F
PLIN2/Nonspecific bands
ns
1.5
1.0
0.5
0
WT
pxt-/-

SFig 3

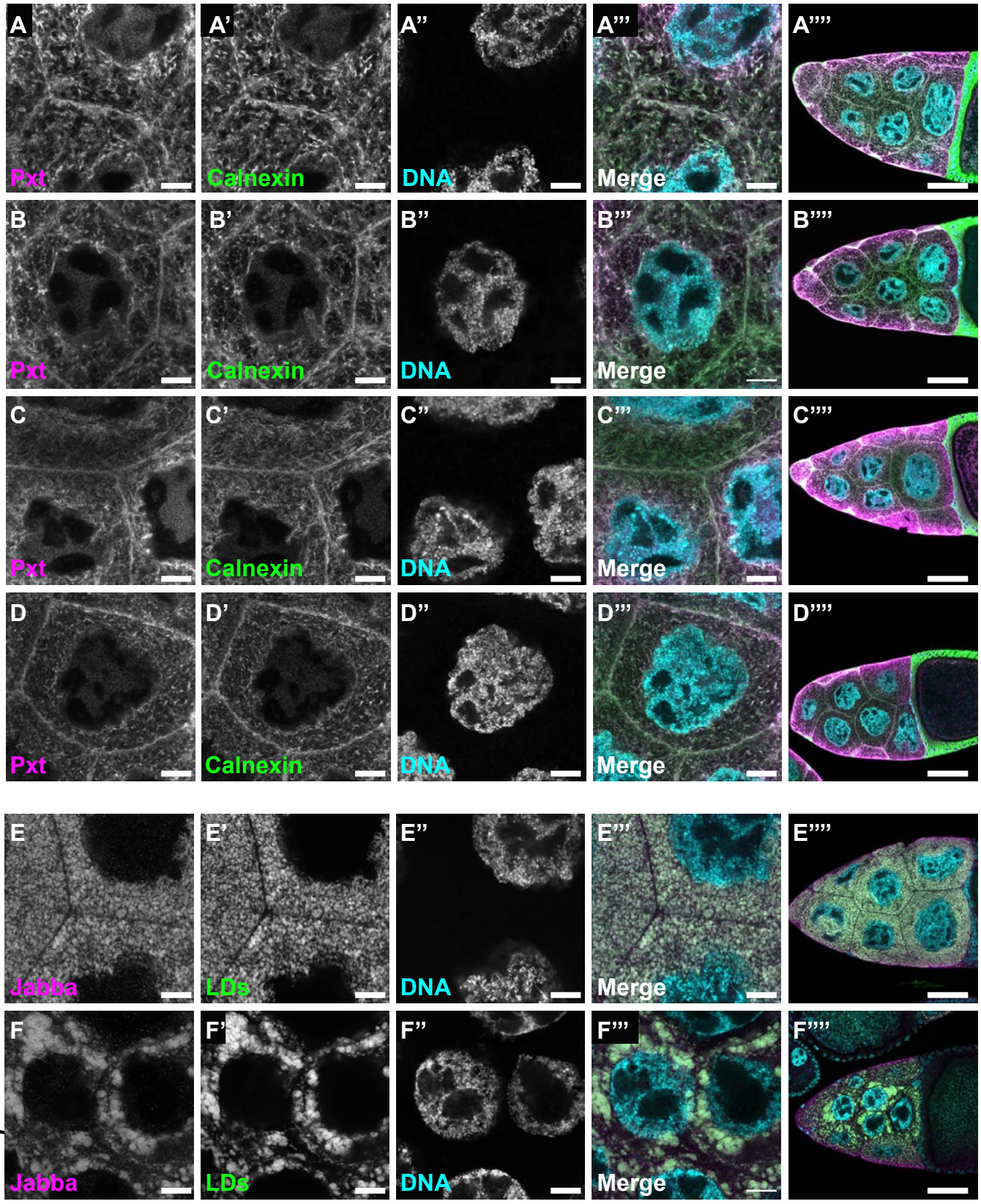
WT
Jabba-/-
PLIN2-/-
ATGL-/-
pxt-/-
A
A'
A''
A'''
A''''
B
B'
B''
B'''
B''''
C
C'
C''
C'''
C''''
D
D'
D''
D'''
D''''
E
E'
E''
E'''
E''''
F
F'
F''
F'''
F''''
Pxt
Calnexin
DNA
Merge
Jabba
LDs

SFig 4

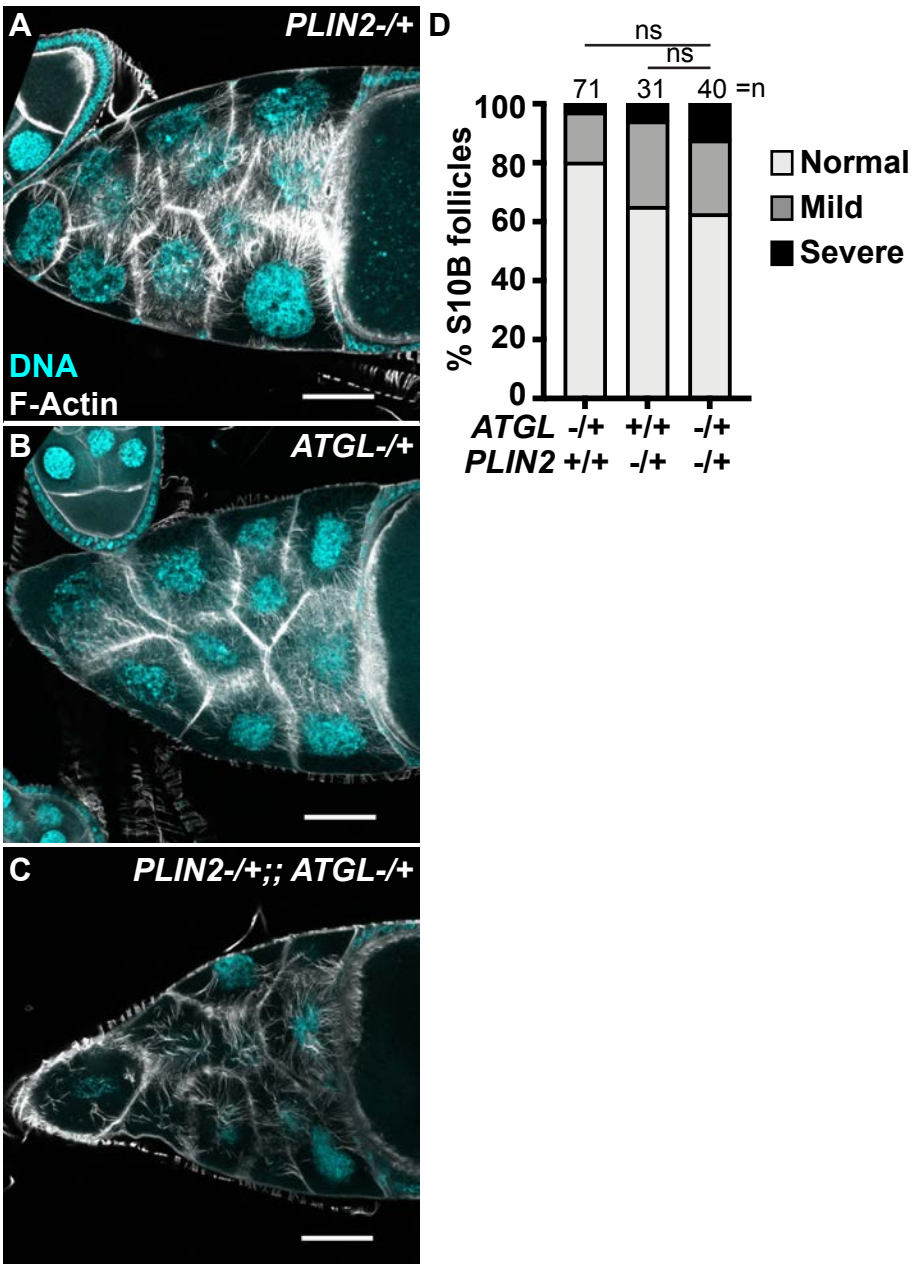
A
PLIN2-/+
DNA
F-Actin
B
ATGL-/+
C
PLIN2-/+;; ATGL-/+
D
ns
ns
71
31
40 =n
100
80
60
40
20
0
% S10B follicles
Normal
Mild
Severe
ATGL -/+ +/+ -/+
PLIN2 +/+ -/+ -/+

SFig 5

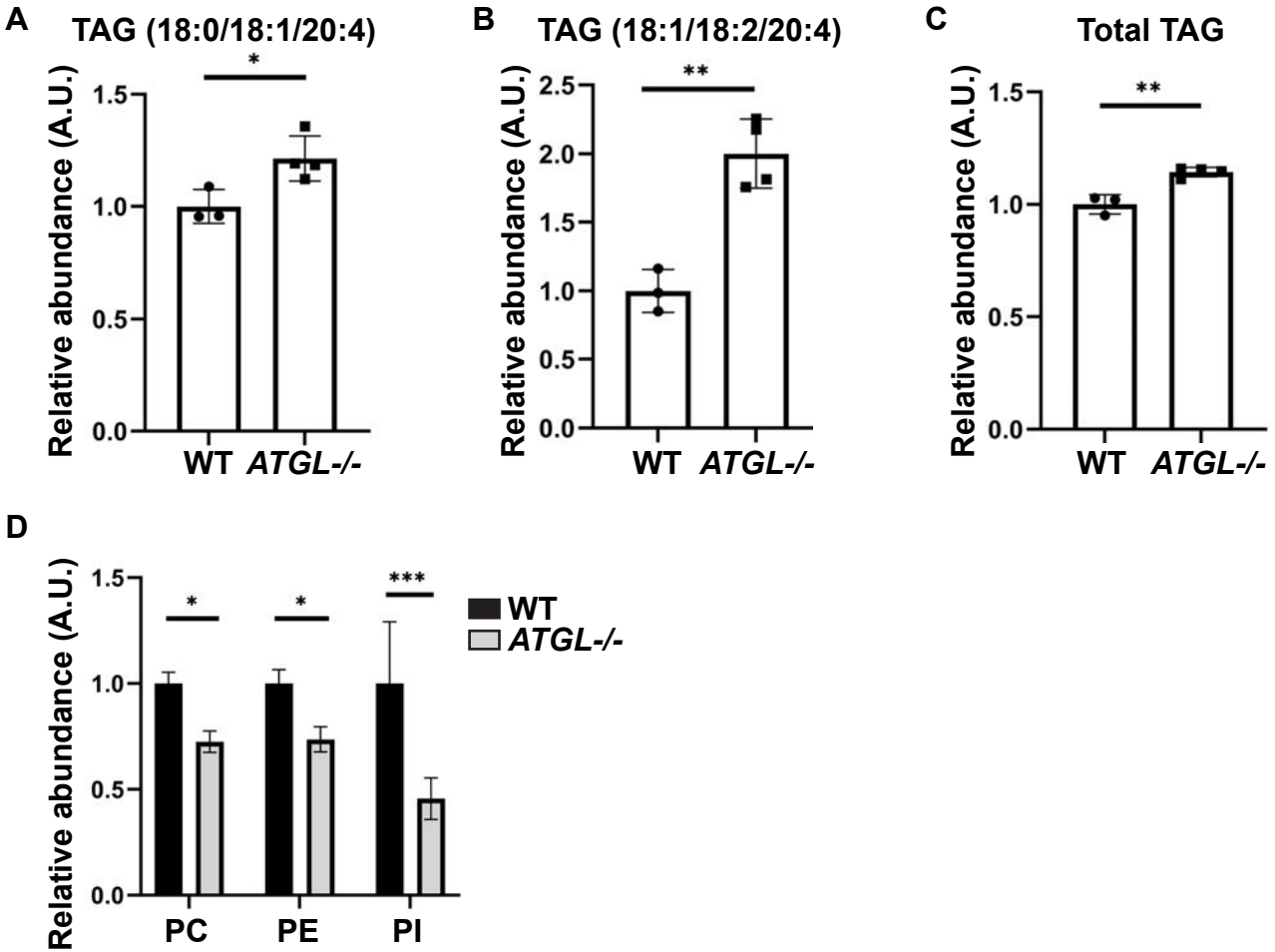
A
TAG (18:0/18:1/20:4)
Relative abundance (A.U.)
1.5
1.0
0.5
0.0
*
WT
ATGL-/-
B
TAG (18:1/18:2/20:4)
Relative abundance (A.U.)
2.5
2.0
1.5
1.0
0.5
0.0
**
WT
ATGL-/-
C
Total TAG
Relative abundance (A.U.)
1.5
1.0
0.5
0.0
**
WT
ATGL-/-
D
Relative abundance (A.U.)
1.5
1.0
0.5
0.0
*
*
***
PC
PE
PI
WT
ATGL-/-

SFig 6

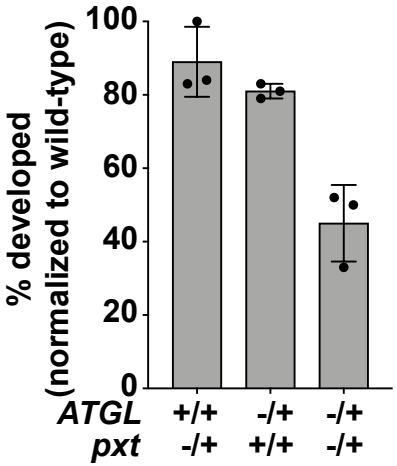


SFig 7

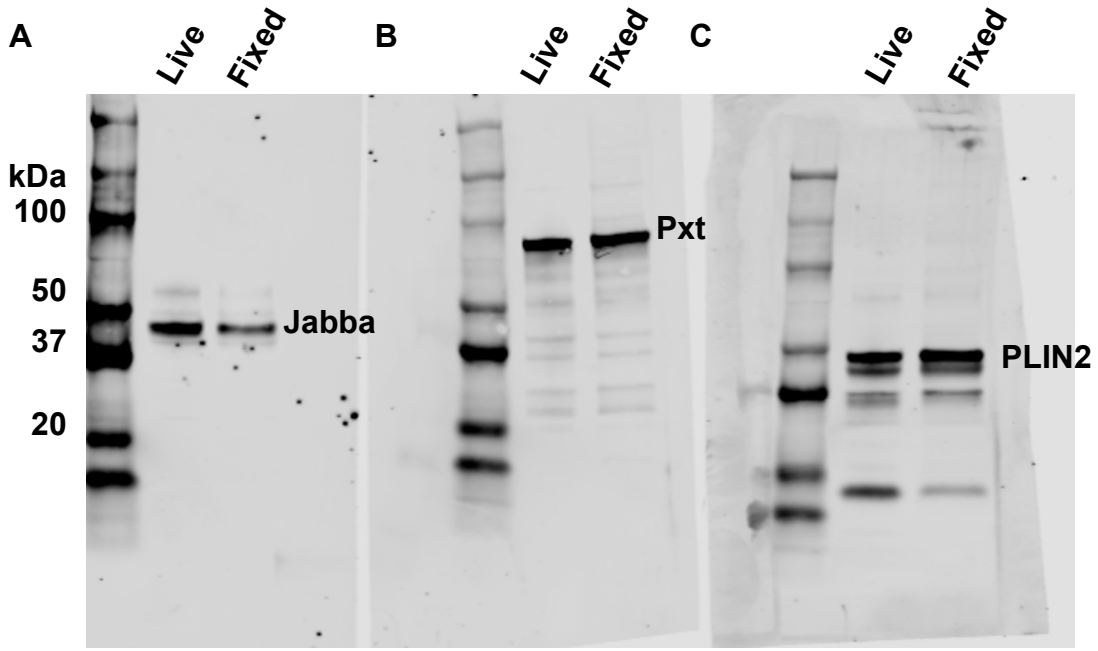
A
Live
Fixed
B
Live
Fixed
C
Live
Fixed
kDa
100
50
37
20
Jabba
Pxt
PLIN2

SFig 8

| Triglyceride species | wild type 2 | wild type 3 | wild type 4 | ATGL 1 | ATGL 2 | ATGL 3 | ATGL 4 |
|---|---|---|---|---|---|---|---|
| 16:1/17:1/18:2 | 4028800 | 5894800 | 5037800 | 9625800 | 8910800 | 17357800 | 11937800 |
| 16:1/17:1/18:1 | 12114670 | 30224670 | 23104670 | 33724670 | 52254670 | 81364670 | 76874670 |
| 16:0/17:0/18:1 | 9373400 | 16235400 | 9343400 | 51165400 | 28065400 | 65165400 | 90555400 |
| 16:0/17:1/18:1 | 4137000 | 16844000 | 13074000 | 100434000 | 36974000 | 93664000 | 209534000 |
| 16:1/18:2/18:3 | 6618000 | 7563000 | 8387000 | 8656000 | 7124000 | 11580000 | 12230000 |
| 16:1/18:2/18:2 | 60132600 | 76802600 | 84792600 | 96572600 | 84822600 | 154002600 | 144702600 |
| 16:0/18:3/18:3 | 239213200 | 265713200 | 280313200 | 289213200 | 293313200 | 336713200 | 351213200 |
| 16:0/18:1/18:1 | 651417000 | 889417000 | 1044717000 | 1131717000 | 1049717000 | 1967717000 | 1790717000 |
| 16:1/18:1/18:1 | 350998000 | 620098000 | 728198000 | 575298000 | 611898000 | 1101198000 | 1008198000 |
| 18:0/16:0/18:0 | -1351000 | 5946000 | -274000 | 766000 | 404000 | 293000 | 5596000 |
| 18:0/16:0/18:1 | 204881000 | 251781000 | 294481000 | 255881000 | 261981000 | 460181000 | 484981000 |
| 18:1/17:1/18:1 | 3689500 | 5196500 | 5905500 | 11836500 | 11186500 | 19696500 | 21746500 |
| 17:0/18:1/18:1 | 3882870 | 10355870 | 5462870 | 14605870 | 14895870 | 26285870 | 30315870 |
| 18:0/17:0/18:1 | 1815370 | 2666370 | 2927370 | 6245370 | 6207370 | 13873370 | 14393370 |
| 16:0/18:2/18:3 | 358861000 | 410861000 | 423761000 | 401361000 | 383261000 | 456261000 | 453961000 |
| 16:1/18:1/18:2 | 197861810 | 362561810 | 252361810 | 516761810 | 494661810 | 520561810 | 554361810 |
| 16:0/18:1/18:3 | 180684000 | 230684000 | 236784000 | 242384000 | 220484000 | 312984000 | 284684000 |
| 18:1/17:1/18:2 | 2040932 | 2523932 | 2585932 | 4208932 | 4480932 | 9307932 | 8063932 |
| 18:1/18:1/18:2 | 41067000 | 59897000 | 82277000 | 146257000 | 151157000 | 270257000 | 256057000 |
| 18:1/18:1/18:1 | 57566000 | 82996000 | 97366000 | 176266000 | 148266000 | 264166000 | 236166000 |
| 18:1/18:2/18:2 | 23786000 | 24666000 | 23886000 | 37276000 | 37106000 | 194856000 | 62736000 |
| 18:1/18:2/18:3 | 4033000 | 4218000 | 4060000 | 8135000 | 8378000 | 8587000 | 11959000 |
| 18:0/18:0/18:0 | 874000 | 415000 | 863000 | 16000 | 412000 | 1362000 | 726000 |
| 20:0/16:0/18:1 | 32296500 | 38566500 | 51966500 | 40066500 | 42846500 | 73046500 | 70666500 |
| 18:0/18:1/18:1 | 81152000 | 101912000 | 122712000 | 128612000 | 121612000 | 227012000 | 235612000 |
| 18:0/18:1/20:0 | 4287500 | 2946500 | 5775500 | 5189500 | 6357500 | 10104500 | 8550500 |
| 20:0/18:1/18:1 | 7320500 | 7999500 | 10952500 | 16302500 | 19632500 | 30372500 | 29632500 |
| 20:0/18:1/18:2 | 1844160 | 2363160 | 2575160 | 6299160 | 7283160 | 11603160 | 11413160 |
| 18:0/18:1/20:3 | 10737520 | 11887520 | 15497520 | 12437520 | 13607520 | 20487520 | 20097520 |
| 20:1/18:1/18:2 | 902700 | 1274200 | 2044200 | 4523200 | 6021200 | 8181200 | 7727200 |
| 18:0/18:1/20:4 | 25554100 | 30534100 | 34514100 | 38384100 | 40504100 | 57014100 | 59884100 |
| 18:0/18:1/20:5 | 6982000 | 10821000 | 8221000 | 18731000 | 19941000 | 31471000 | 28641000 |

| | | | | | | | |
|---|---|---|---|---|---|---|---|
| 18:1/18:2/20:4 | 10681000 | 17171000 | 14131000 | 32331000 | 31021000 | 42521000 | 40971000 |
| 16:1/13:0/14:0 | 13329030 | 20259030 | 19019030 | 45249030 | 28799030 | 56029030 | 70829030 |
| 16:0/13:0/14:0 | 6196000 | 10599000 | 11059000 | 36299000 | 23969000 | 32019000 | 49869000 |
| 12:0/14:1/18:3 | 8790000 | 8677000 | 11500000 | 8853000 | 8726000 | 14370000 | 16240000 |
| 16:1/12:0/16:1 | 678033300 | 1046033300 | 1335033300 | 1390033300 | 955133300 | 2383033300 | 2367033300 |
| 16:1/14:1/14:1 | 149165090 | 289265090 | 378165090 | 218965090 | 132165090 | 373365090 | 368365090 |
| 16:0/14:0/14:0 | 150501000 | 206901000 | 227501000 | 317201000 | 269201000 | 517701000 | 517801000 |
| 16:1/14:0/14:0 | 865006000 | 1521306000 | 1564306000 | 1717306000 | 1310306000 | 2807306000 | 2376306000 |
| 16:0/9:0/20:5 | 9265960 | 11568960 | 13068960 | 23668960 | 15348960 | 22308960 | 17968960 |
| 16:1/13:0/16:1 | 40157500 | 59137500 | 68267500 | 62877500 | 63237500 | 92627500 | 88377500 |
| 16:1/12:1/17:1 | 15681520 | 11441520 | 19681520 | 19411520 | 16531520 | 24631520 | 20631520 |
| 16:0/13:0/16:1 | 16147540 | 27777540 | 25897540 | 65397540 | 39867540 | 116777540 | 105977540 |
| 15:0/14:0/16:0 | 2747700 | 5173700 | 5266700 | 10177700 | 11527700 | 16297700 | 19007700 |
| 16:1/12:0/18:3 | 30040190 | 39840190 | 68370190 | 51410190 | 52560190 | 81240190 | 81230190 |
| 16:1/14:1/16:1 | 567743500 | 854043500 | 1023643500 | 754243500 | 774043500 | 1347643500 | 1289643500 |
| 16:1/14:0/16:1 | 1200527000 | 2320527000 | 2475527000 | 2450527000 | 2309527000 | 3902527000 | 4107527000 |
| 16:0/14:0/16:1 | 1199890000 | 2039890000 | 2212890000 | 2472890000 | 2038890000 | 3763890000 | 3703890000 |
| 16:0/14:0/16:0 | 33530000 | 41780000 | 45330000 | 66210000 | 62020000 | 108340000 | 114840000 |
| 18:4/13:0/16:1 | 15020980 | 20390980 | 23860980 | 22120980 | 25580980 | 37290980 | 31310980 |
| 16:1/13:0/18:3 | 12905110 | 25995110 | 23495110 | 20325110 | 15845110 | 39395110 | 30755110 |
| 16:1/13:0/18:2 | 22309630 | 27299630 | 29549630 | 32819630 | 24079630 | 58839630 | 48109630 |
| 15:0/16:0/16:0 | -3774000 | -4006000 | -3577000 | 588000 | -2416000 | 4224000 | 1917000 |
| 15:0/16:0/16:1 | 21870000 | 41550000 | 31210000 | 79930000 | 76170000 | 134650000 | 156050000 |
| 15:0/16:1/16:1 | 12790500 | 19000500 | 21280500 | 58390500 | 37030500 | 72210500 | 87500500 |
| 18:4/14:0/16:0 | 181187000 | 205787000 | 210187000 | 210787000 | 195387000 | 229187000 | 222787000 |
| 16:1/14:1/18:2 | 77313700 | 104483700 | 107483700 | 80713700 | 84323700 | 139483700 | 128883700 |
| 16:1/14:1/18:3 | 18850000 | 24380000 | 19030000 | 24080000 | 18310000 | 28730000 | 18480000 |
| 16:0/16:0/16:0 | 10890000 | 11380000 | 16000000 | 19130000 | 17710000 | 24150000 | 37880000 |
| 16:0/14:0/18:1 | 1462227000 | 2093227000 | 2285227000 | 2493227000 | 2257227000 | 4009227000 | 4207227000 |
| 16:1/14:0/18:1 | 2413634000 | 3721634000 | 4113634000 | 3295634000 | 3620634000 | 6420634000 | 6523634000 |
| 16:1/16:1/16:1 | 1259614000 | 1910614000 | 1894614000 | 1870614000 | 1771614000 | 2733614000 | 2811614000 |
| 18:4/15:0/16:1 | 24866790 | 34216790 | 25226790 | 44996790 | 5740790 | 54936790 | 58736790 |
| 16:1/16:1/17:1 | 29614120 | 53894120 | 53674120 | 58864120 | 52714120 | 94444120 | 104034120 |

| | | | | | | | |
|---|---|---|---|---|---|---|---|
| 16:0/16:0/18:1 | 940998000 | 1337998000 | 1505998000 | 1632998000 | 1397998000 | 2759998000 | 2529998000 |
| 16:1/16:1/17:0 | 19234000 | 26384000 | 25904000 | 82114000 | 53734000 | 105094000 | 122294000 |
| 15:0/16:0/18:1 | 20373000 | 32913000 | 27363000 | 103293000 | 67123000 | 146293000 | 157693000 |
| 16:1/16:1/18:3 | 48716010 | 65426010 | 75796010 | 61616010 | 58326010 | 106266010 | 104066010 |
| 18:0/16:0/16:0 | 2430000 | 3115000 | 3538000 | 2519000 | 4656000 | 7666000 | 9286000 |
| 16:1/16:1/18:1 | 1445819000 | 1048819000 | 1532819000 | 2460819000 | 1112819000 | 1927819000 | 1663819000 |
| 16:0/16:1/18:1 | 2259521000 | 3282521000 | 3769521000 | 3557521000 | 3427521000 | 5693521000 | 6088521000 |
| 16:1/16:1/18:2 | 222845400 | 333245400 | 407745400 | 398745400 | 357645400 | 657445400 | 678045400 |
| 4:0/14:0/16:1 | 4557000 | 3758000 | 7911000 | 6126000 | 6512000 | 9974000 | 10230000 |
| 12:0/12:0/12:1 | 3052000 | 4825000 | 6376000 | 6618000 | 7058000 | 11680000 | 11850000 |
| 4:0/16:1/16:1 | 4847000 | 3396000 | 8107000 | 5018000 | 5778000 | 7704000 | 7573000 |
| 12:0/14:1/14:1 | 82885700 | 97715700 | 173695700 | 64675700 | 97045700 | 135895700 | 101295700 |
| 16:1/12:0/12:0 | 384788700 | 673688700 | 812688700 | 517788700 | 545188700 | 878888700 | 964388700 |
| 12:0/13:0/14:0 | 7012600 | 9015600 | 7736600 | 25022600 | 19612600 | 33282600 | 28552600 |
| 14:1/12:1/14:1 | 5199510 | 12032510 | 18392510 | 5524510 | 10192510 | 18972510 | 7462510 |
| 11:0/14:1/14:1 | 2981000 | 7452000 | 4521000 | 6734000 | 8740000 | 11010000 | 5697000 |
| 12:0/13:0/14:1 | 13711210 | 21751210 | 24651210 | 44951210 | 49221210 | 29041210 | 31341210 |
| 12:0/12:0/14:0 | 295054000 | 487154000 | 597854000 | 534654000 | 443354000 | 959254000 | 877354000 |
| 12:0/12:0/14:1 | 109223650 | 168123650 | 211323650 | 122223650 | 150823650 | 209823650 | 185123650 |
| 6:0/14:1/18:0 | 5382300 | 4312300 | 8269300 | 5289300 | 5407300 | 9215300 | 8442300 |
| 12:0/12:0/13:0 | 6437660 | 12098660 | 12798660 | 9628660 | 10388660 | 14908660 | 15368660 |
| 12:0/12:1/14:1 | 6960950 | 9858950 | 16655950 | 8248950 | 11065950 | 15255950 | 16115950 |
| 12:0/12:0/12:0 | 37670000 | 82170000 | 98680000 | 75030000 | 80380000 | 138180000 | 136280000 |
| 16:1/13:0/14:1 | 42614890 | 53754890 | 58024890 | 55934890 | 48574890 | 69304890 | 70244890 |
| 16:1/11:4/16:1 | 5941000 | 7661000 | 13750000 | 12660000 | 15270000 | 22180000 | 21430000 |
| 14:0/14:0/14:0 | 385915000 | 601715000 | 632015000 | 841015000 | 711715000 | 1287615000 | 1369615000 |
| 14:0/14:0/14:1 | 675182000 | 1052482000 | 1138482000 | 1231482000 | 976882000 | 1697482000 | 1848482000 |
| 16:1/12:0/14:1 | 820078500 | 1081878500 | 1105878500 | 677178500 | 961878500 | 1578878500 | 1143878500 |
| 16:1/12:1/14:1 | 44080000 | 51430000 | 68610000 | 34050000 | 39450000 | 55830000 | 61110000 |
| 14:0/13:0/14:0 | 11909370 | 16269370 | 15669370 | 37449370 | 24689370 | 50449370 | 51789370 |
| 16:1/12:0/13:0 | 39732960 | 57002960 | 61132960 | 55512960 | 79152960 | 82472960 | 76482960 |
| 13:0/14:1/14:1 | 28310000 | 28410000 | 30680000 | 17060000 | 17810000 | 44780000 | 41760000 |
| 12:0/14:0/14:0 | 459324000 | 715924000 | 841324000 | 938724000 | 777924000 | 1409724000 | 1287724000 |

| | | | | | | | |
|---|---|---|---|---|---|---|---|
| sum of all triglyceride values | 2.1588E+10 | 3.1807E+10 | 3.5577E+10 | 3.6082E+10 | 3.2121E+10 | 5.6826E+10 | 5.6153E+10 |